



Tomas Bata University in Zlín
Faculty of Technology

Doctoral Thesis

**Fiber reinforced polymer composites: preparation,
mechanical properties and thermal analysis**

**Vláknny vyztužené polymerní kompozity: příprava, mechanické
vlastnosti a termická analýza**

Author: **Konstantinos Karvanis, M. Sc.**

Degree programme: P3909 Process Engineering

Degree course: 3909V013 Tools and Processes

Supervisor: doc. Ing. Soňa Rusnáková, Ph. D.

Reviewers: doc. Ing. Petr Jonšta, Ph.D.

prof. Dr. Ing. Libor Beneš, IWE

doc. Ing. Michal Sedlačík, Ph.D.

Zlín, 08/2021

© Konstantinos Karvanis

Published by **Tomas Bata University in Zlín** in the Edition **Doctoral Thesis Summary**.

The publication was issued the year 2021

Key words in Czech: *FRP, polymerní kompozit, termální analýza, DMA, TMA, uhlíkové vlákno, skelné vlákno, basaltové vlákno*

Key words: *FRP, polymer composite, thermal analysis, DMA, TMA, TGA, DSC, carbon fiber, glass fiber, basalt fiber, aramid fiber*

Full text of the doctoral thesis is available in the Library of TBU in Zlín.

SHRNUTÍ

V dnešní době se polymerní kompozity široce používají, proto je důležité podrobně zkoumat jejich vlastnosti do hloubky a za různých podmínek. Vlákem vyztužený polymer (FRP-Fiber-reinforced polymer) je kompozitní materiál s polymerním pojivem jako matricí a vlákny jako výztužnou fází. Jak je všeobecně známo, teplota má velký dopad na vlastnosti materiálů, zejména v případě vláknem vyztužených kompozitů, které mají polymerní matrici, protože polymery jsou relativně citlivé na vysoké teploty kvůli své viskoelastické povaze.

V této disertační práci byly pomocí různých výrobních technologií připraveny vláknem vyztužený kompozity s uhlíkovými, aramidovými, skleněnými a čedičovými vlákny. Byly zkoumány různé mechanické vlastnosti, jako je pevnost v tahu a ohybu, zejména byla pozornost věnována termické analýze vláknem vyztužených kompozitů prostřednictvím dynamické mechanické analýzy (DMA), termomechanické analýzy (TMA) a termogravimetrické analýzy (TGA).

Zejména v první experimentální části pojednání k disertační práce byly polymerní kompozity vyztužené skleněnými nebo uhlíkovými vlákny připraveny metodou vakuového lisování s použitím prepregových materiálů. Použitá vlákna jsou ve tkané formě s orientací 0° ($0^\circ/90^\circ$) nebo 45° ($-45^\circ/+45^\circ$) a v jednosměrné formě v podélném nebo příčném směru. V experimentální části tohoto pojednání byl zkoumán optimální typ vláken a jejich orientace prostřednictvím DMA a byla stanovena teplota skelného přechodu (T_g) kompozitů.

Ve druhé experimentální části pojednání disertační práce byly pomocí kombinované metody ruční laminace pod vakuovou fólií připraveny bazaltové vlákny vyztužené polymerní (BFRP) kompozity s epoxidovou matricí, pozůstávající s 20 vrstev a objemovým podílem vláken $V_f = 53,66\%$. Navíc pomocí DMA bylo prozkoumáno jejich viskoelastické chování v teplotním rozsahu $30 - 180^\circ\text{C}$ a frekvenčním rozsahu 1, 5 nebo 10 Hz, zatímco TMA byla zvolena na studium zkoušek creepového zotavení a napěťové relaxace. Kromě toho byla stanovena teplota skelného přechodu (T_g) kompozitů BFRP pomocí píku křivek $\tan\delta$, zatímco rozklad kompozitů BFRP a čedičových vláken ve vzduchu nebo v atmosféře dusíku byl zkoumán TGA. Také mechanické chování kompozitů BFRP bylo experimentálně zkoumáno v tahu a v tříbodovém ohybu.

Je třeba poznamenat, že v rámci zpracování následné disertační práce byly vyrobeny uhlíkové, aramidové nebo uhlík/aramidové hybridní vlákny vyztužené polymerní kompozity, které byly následně vytvrzeny při zvýšených teplotách a bylo zkoumáno jejich tepelné a mechanické chování. Tyto epoxidové kompozity po 7 dnech vytvrzování při pokojové teplotě byly dodatečně vytvrzované podle specifického vytvrzovacího režimu. Vliv dodatečného vytvrzování byl zkoumán

pomocí termické analýzy a tyto experimentálně naměřené výsledky budou prezentovány v rámci disertační práce.

SUMMARY

Nowadays, polymer matrix composites are broadly used, so their properties should be investigated in depth and under various conditions. Fiber-reinforced polymer (FRP) is a composite material which contains polymer as matrix and fibers as reinforcement phase. As it is broadly known, temperature exerts a high impact on materials' properties and especially in the case of the FRP composites which have polymer matrix; due to their viscoelastic nature, polymers are relative sensitive to high temperatures.

In this dissertation, FRP composites, with carbon, aramid, carbon/aramid hybrid, glass or basalt fibers as reinforcement phase were prepared through various fabrication methods. Their various mechanical properties, such as tensile and flexural strength were investigated whereas special attention was given in the thermal analysis of the FRP composites through Dynamic Mechanical Analysis (DMA), Thermomechanical Analysis (TMA), Thermogravimetric Analysis (TGA) experiments, and Differential Scanning Calorimetry (DSC).

In particular, in the first experimental part of this dissertation, glass or carbon fiber-reinforced polymer composites were prepared, through vacuum bag oven method, by using prepreg materials. The used fibers were in woven form, with orientations at 0° ($0^\circ/90^\circ$) or at 45° ($-45^\circ/+45^\circ$), and in unidirectional form, longitudinal or transverse direction. In the experimental study, the optimal fibers' type and orientation were investigated through DMA and the glass transition temperature (T_g) of the composites was determined.

In the second experimental part of the dissertation, basalt fiber-reinforced polymer (BFRP) composites with epoxy matrix, 20 layers, and volume fraction of fibers $\Phi_f = 53.66\%$, were fabricated through a hand lay-up compression molding combined method. Their viscoelastic behavior in the temperature range 30-180 °C and at 1, 5 or 10 Hz was explored by DMA whereas TMA took part in terms of creep recovery and stress-relaxation tests. Moreover, the T_g of the BFRP composites was determined through the peak of the loss modulus and $\tan\delta$ curves while the decomposition of the BFRP composites and basalt fibers, in air or nitrogen atmosphere, was explored through TGA. Also, the mechanical behavior of the BFRP composites was investigated by tensile and three-point bending experiments.

In the third experimental part of the dissertation, carbon, aramid or carbon/aramid hybrid fiber-reinforced polymer composites were fabricated; they were post-cured at elevated temperatures and their thermal and mechanical behavior was explored. After their 7 days curing at room temperature, these epoxy matrix composites were post-cured under specific heating-cooling rates.

Extensive thermal analysis, and also exploration of the mechanical behavior of these composites is taken part, investigating in depth the effect of the post-cure, and the scientific results are presented in the dissertation.

Acknowledgements

I would like to thank my supervisor, doc. Ing. Soňa Rusnáková, Ph.D, and the Department of Production Engineering of Tomas Bata University in Zlin, for their support during my Ph.D. studies.

Also, I would like to thank prof. dr hab. inż. Krzysztof Pielichowski and dr. inż. Tomasz Mariusz Majka for their chance to perform my Erasmus internship in Politechnika Krakowska im. Tadeusza Kościuszki.

CONTENTS

1. INTRODUCTION	11
1.1 Types and classification of composites	11
1.2 FRP composites	12
1.2.1 Type of fibers	13
1.3 Thermal analysis	14
1.4 Production methods for polymer matrix composites	16
1.4.1 Vacuum bag method.....	16
1.4.2 Vacuum injection technique.....	16
1.4.3 Hand lay-up technique	17
1.5 Literature review.....	17
1.6 Objectives of the thesis.....	21
1.6.1 First experimental part	21
1.6.2 Second experimental part.....	21
1.6.3 Third experimental study	22
1.7 Contribution of the thesis to science and practice.....	22
2. FIRST EXPERIMENTAL PART: STUDY ON DYNAMIC MECHANICAL ANALYSIS OF GLASS OR CARBON FIBER/EPOXY COMPOSITES	23
2.1 General information about this research study.....	23
2.2 Materials	25
2.3 Production method.....	25
2.4 Experimental details	27
2.5 Results.....	28
2.5.1 Storage modulus.....	28
2.5.2 Loss modulus.....	30
2.5.3 $\tan\delta$	32
2.5.4 Glass transition temperature (T_g)	34
2.6 Conclusions regarding the GFRP and CFRP composites	35
3. EXPERIMENTAL PART 2: STUDY ON PREPARATION, THERMAL ANALYSIS, AND MECHANICAL PROPERTIES OF BASALT FIBER/EPOXY COMPOSITES	36
3.1 General information about this study	36
3.2 Materials	36

3.3	Experimental	39
3.3.1	General experimental conditions	39
3.3.2	Dynamic mechanical analysis.....	39
3.3.3	Thermomechanical analysis creep-recovery and Thermomechanical analysis stress-relaxation experiments.....	41
3.3.4	Thermogravimetric analysis	41
3.3.5	Mechanical properties.....	42
3.4	Results	43
3.4.1	Displacement sweep test.....	43
3.4.2	Dynamic mechanical analysis.....	44
3.4.3	Thermomechanical analysis creep-recovery and Thermomechanical analysis stress-relaxation	48
3.4.4	Mechanical properties.....	50
3.4.5	Thermogravimetric analysis	56
3.5	Calculation of the volume fraction of the fibers (Φ_f) and volume fraction of the matrix (Φ_m).....	61
3.6	Conclusions regarding the BFRP composites.....	62
3.6.1	Analytical theoretical model for the prediction of the BFRP composites tensile strength	63
4.	EXPERIMENTAL PART 3: PREPARATION, THERMAL ANALYSIS AND VARIOUS MECHANICAL PROPERTIES OF POST-CURED CARBON, ARAMID OR CARBON/ARAMID HYBRID FIBER EPOXY MATRIX COMPOSITES	64
4.1	Purpose of the research study and general information.....	64
4.2	Materials and preparation method.....	65
4.2.1	Materials	65
4.2.2	Preparation of the CFRP, AFRP and ACFRP composites	68
4.3	Experiments.....	74
4.3.1	General experimental conditions	74
4.3.2	DMA, TMA creep-recovery and TMA stress-relaxation experiments	74
4.3.3	Thermogravimetric analysis	75
4.3.4	Differential Scanning Calorimetry (DSC).....	76
4.3.5	Three-point bending on the CFRP and ACFRP composites	76
4.4	Results of the AFRP composites.....	79

4.4.1	Dynamic mechanical analysis	79
4.4.2	TMA creep-recovery and TMA stress-relaxation	82
4.4.3	Thermogravimetric analysis.....	84
4.4.4	DSC	90
4.5	Results of the CFRP and ACFRP composites.....	92
4.5.1	DMA.....	92
4.5.2	T _g of the CFRP and ACFRP composites.....	94
4.5.3	DSC of the CFRP and ACFRP composites	96
4.5.4	TGA of the carbon fibers, aramid fibers, CFRP and ACFRP composites	98
4.5.5	Mechanical properties of the CFRP and ACFRP composites .	103
4.5.6	Hardness Shore D.....	108
4.5.7	Conclusions regarding the CFRP, AFRP and ACFRP composites	109
5.	CONCLUSIONS OF THE DISSERTATION.....	111
6.	RELATING THE SCIENTIFIC RESULTS WITH PRACTICAL APPLICATIONS.....	114
	LIST OF FIGURES	124
	LIST OF TABLES	129
	LIST OF SYMBOLS, ACRONYMS AND ABBREVIATIONS.....	130
	APPENDICES	133
	LIST OF AUTHORS' PUBLICATIONS	134
	PROFESSIONAL CURRICULUM VITAE	135

1. INTRODUCTION

1.1 Types and classification of composites

Composites are materials which are composed of two or more phases which they remain separate and distinct in their final structure. The one phase, called matrix, is usually a low-density material whereas the other one, the reinforcement phase, gives to the composite the upgraded properties. Generally, the role of the matrix is to keep bonded the reinforcement phase and to protect it from harmful environment exposure. The great advantage of composites is that they combine the properties of their individual substances, so that the mechanical behavior of the final composite is better than the one of the initial materials. A broadly used type of composites is the polymer matrix composites (PMC). In particular, the matrix of the PMC can be organic or inorganic polymer and their reinforcing material can be short fibers, continuous fibers, or particles [1].

Classification of composites:

According to the material of the matrix to:

- Polymer matrix composites
 1. Thermosetting
 2. Thermoplastic
- Metal matrix composites
- Ceramic matrix composites
- Carbon matrix composites

According to the type of the reinforcement phase to:

- Fiber-reinforced polymer (FRP) composites

Continuous (long) fiber composites:

1. Unidirectional fiber composite: In this type, all fibers have the same orientation. The principal advantage of this structure is that the composite has excellent properties in the direction of fibers. However, it usually has reduced properties in the other orientations.
2. Woven fiber composite: In this type of composite, the fibers are placed with orientation being balanced in two directions. Remarkably, the composite has good properties in both fiber directions.

Discontinuous (short) fiber composites

Particulate reinforced composites: the reinforcement phase is in particulate form dispersed in the matrix. An example of them is shown in Figure 1.1.

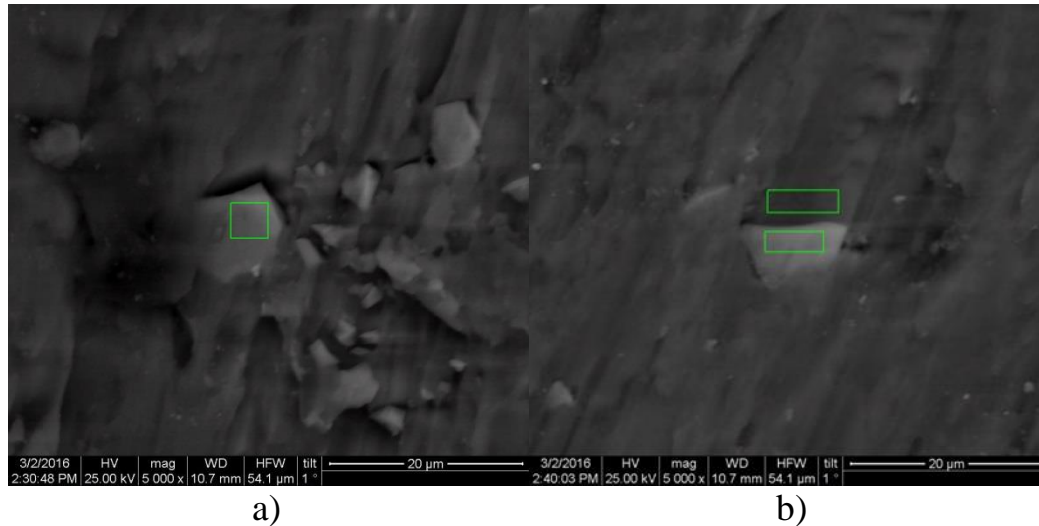


Figure 1.1: a) and b) the structure of an Aluminium matrix\Silicon Carbide particulate 3% composite, as it was observed through scanning electron microscope (SEM). The silicon carbide (SiC) particulates are clearly depicted in the metal matrix.

The hybrid composites have two or more different material kinds as reinforcement phase. In particular, the FRP hybrid composites can be prepared by placement of layers, which have different types of fibers, in the stacking of the laminate, and as well as by using hybrid fiber fabrics.

1.2 FRP composites

FRP composites are widely used given their remarkable characteristics, such as high strength and stiffness to weight ratio, easiness in manufacture, low cost and anti-corrosion resistance. These composites consist of fibers, artificial or natural ones, embedded in a polymer matrix. The matrix provides cohesion and unity to the final material while reinforcement gives physical and mechanical properties to it [2].

Possibly, the most significant advantage of fiber-reinforced polymer matrix materials is tailorability [3]. In detail, FRP composites can be accommodated to meet particular strength and performance demands by an appropriate choice of polymeric resin systems and reinforcements [4]. Viscoelasticity is named the response which combines both liquid-like and solid-like features [5]. A behaviour of both purely elastic solids, at which the deformation is in analogy with the exerted force and of viscous liquids, at which the rate of the deformation is in analogy with the exerted force is described by the term viscoelasticity [6].

The polymer matrix can be thermoset or thermoplastic polymer. Notably, thermosets are transformed irreversibly from viscous liquids to inflexible highly cross-linked polymer solids through a molecular crosslinking process which is named “cure” [7]. Fiber-reinforced thermoplastic polymer composites have great fracture toughness, high damage tolerance, convenience of shape-forming before consolidation, and they can also be reshaped and reused [8].

The term viscoelasticity describes the property of materials to display both viscous and elastic characteristics when they are subjected to deformation [9].

Synthetic fibers are used in applications where remarkably properties as well as high thermal resistance are essential. Nevertheless, it should be mentioned that disadvantages, such as high cost and difficulty in recycling, have limited their usage. Broadly used types of FRP composites, are glass fiber-reinforced polymer (GFRP), carbon fiber-reinforced polymer (CFRP), aramid fiber-reinforced polymer (AFRP) and basalt fiber-reinforced polymer (BFRP) composites. Remarkably, the tensile strength of GFRP bars is up to 5-6 times higher than the one of structural steel [10].

The usual applications of Fiber Reinforced Polymers are in marine, aerospace, automotive and construction industries and also in ballistic armor [11]. Generally, applications of FRP composites include a broad range, such as in automotive, aircraft, marine and space industry and generally in applications where high strength to weight ratio is needed.

1.2.1 Type of fibers

Nowadays, due to environmental concerns, an interest in biodegradable materials and generally the use of natural based materials is constantly growing. Natural fibers are fibers which are plant-based, animal-based and mineral-based ones [12]. Basalt is a type of volcanic rock [13]. Basalt fibers are produced by the melting of finely powdered basalt, at approximately 1500-1700 °C, resulting in a glassy molten liquid, which is then extruded as thin threads [14]. Notably, basalt fibres have higher cost than E-glass fibres but lower than S-glass, aramid or carbon fibres [15]. The development of basalt fiber was realized by the Moscow Research Institute of Glass and Plastic, in the 1953-1954 [16].

Carbon fibers are a kind of synthetic fibers. The carbon fibers have advantages, such as significantly high tensile strength-weight ratio and tensile modulus-weight ratio, high fatigue strengths, high thermal conductivity and very low

coefficient of linear thermal expansion; their disadvantages are low impact resistance, low strain-to-failure and high electrical conductivity [17]. Notably, the carbon fibres have one of the highest, strength to density ratio, out of all types of fibres [18]. Their principal disadvantages are their high cost and difficulties in recycling. Particularly, carbon fibers are classified to high modulus, high strength, and ultra-high modulus fibers.

Aramid fibers are used in high demanding applications where exceptional properties and good thermal resistance are essential characteristics. The Kevlar[®] is an organic fiber of the aromatic polyamide family [19].

Prepregs are usually used for the preparation of FRP composites in high demanding applications. Prepreg is a fiber fabric laminate which has already been pre-impregnated with the polymer matrix and it is ready to be cured under heat and pressure combination. Prepregs are stored in a freezer so as unwanted curing to be prevented. Their principal advantages are excellent quality of the final product, high fibers percentage and exact ratio of matrix-reinforcement percentage. Moreover, due to the solid nature of prepreg, laminates can be easily placed at different orientations, in every layer of the composite structure, so that the properties of the composite are specified according to each particular application. On the contrary, high cost of prepregs and their need for curing under specific heat and pressure conditions are their main disadvantages. Prepreg materials are usually cured in autoclave but the significant cost of autoclave and its high operating cost forced scientists to explore new techniques for a more economic FRP prepreg composites' production.

1.3 Thermal analysis

Due to the fact that FRP composites are broadly used, their properties should be investigated in depth, so as their behavior and overall properties to be absolutely predictable. Since the polymer matrix has generally lower thermal resistance than the reinforcement phase, investigation of temperature effect on properties of FRP composites appears of significant importance; these materials need to be investigated and explored under various temperatures.

Thermal analysis studies the effect of temperature on materials' properties in accordance with time. The thermal analysis sector involves techniques, such as the Dynamic Mechanical Analysis (DMA), Thermomechanical Analysis (TMA), Thermogravimetric analysis (TGA) and Differential Scanning Calorimetry (DSC).

Viscoelastic properties of materials, such as storage modulus, loss modulus and $\tan\delta$ under different temperatures, frequencies or type of loadings can be investigated by DMA. Deformation on samples can be applied in various ways, depending on the instrument, such as 3-point bending, single and dual cantilever bending, tension, compression and shear modes. Information on major thermal transitions and also on secondary or tertiary transitions can be obtained by DMA [20].

Storage modulus counts the stored energy of a viscoelastic material, indicating the elastic part whereas loss modulus counts the energy which was dispersed in the form of heat, indicating the viscous part [21]. Moreover, in the case of a viscoelastic body, a part of the strain energy is stored in it while a part of the strain energy is dispersed as heat [22].

Notably, DMA offers the possibility of determining glass transition temperature (T_g). At T_g , polymers change from a glassy state to a rubbery one. It should be referred that there are many methods for T_g determination through DMA experiments, so that the technique which was followed should be stressed in the results section.

TGA measures thermal decomposition of materials in a specific temperature range. Moreover, due to the fact that every material decomposes in a different temperature, the volume fraction of fibers (Φ_f) in the FRP composites can be determined by TGA. An important point in TGA experiments is the atmosphere at which they are performed and it can be reactive, oxidising or inert [23]. Optimal gases for determination of purely thermal decomposition (pyrolysis) are the inert purge gases, such as helium, nitrogen and argon whereas oxygen and air gases are used for determining thermooxidative decomposition (oxidation) [24].

Nowadays, polymers scientists have been trying to improve thermal resistance of polymers, with relative cheap techniques, such as post-cure process, in order to avoid the autoclave increased cost. Remarkably, epoxies which are cured in high temperatures have much better performance than the ones cured at room temperatures [25]. During post-cure process, PMC, after their curing at room temperature, are exposed at high temperatures, usually in an oven. It should be noted that the following heating-cooling rates are usually provided by the polymers' producer. In addition, post-curing can be implemented in order to enhance the modulus and strength of both polymer and composite and also to decrease residual stresses [26].

Taking into consideration the long-time forces that are exerted on materials during their real-life applications, it is essential for their properties to be explored in relation with time. Familiar time dependent experiments are creep-recovery and stress-relaxation tests. In particular, during a creep-recovery experiment, a force is applied on the specimen and the increasing strain is measured as a function of time whereas in a stress relaxation test, a constant extension is applied on the polymer specimen and the reducing load is measured in relation with time. Polymer-based composites tend to creep and to stress relaxation, because the properties of the matrix are time-dependent [27]. Also, in the creep response of polymeric and polymer composite materials, temperature, time, and stress level are critical parameters [28].

1.4 Production methods for polymer matrix composites

1.4.1 Vacuum bag method

Nowadays, scientists have been trying to develop new or to improve the existing techniques, such as the vacuum bag oven process, without the increased cost of autoclave's use. During the vacuum bag oven technique, a rectangular piece of glass is used as the down part of the mold, where the composite laminate is placed, and then the whole system is airtight, sealed with the vacuum bag. The air is evacuated from the system and the compound cure takes place in laboratory temperature or in an oven. The vacuum bagging technique is a relatively simple but with high efficiency method for PMC production. The advantage of this method is that the produced composite plate has reduced voids, high density and uniform Φ_f in its whole structure.

1.4.2 Vacuum injection technique

This technique is similar to the vacuum bag method but with the difference that the resin is injected to the fabrics. During this method, the structure of the laminate is prepared by placing the fabrics on the mold surface, the laminate stacking is closed by the vacuum bag, and then the vacuum pump is turned on, so as the resin to be infused in the mold.

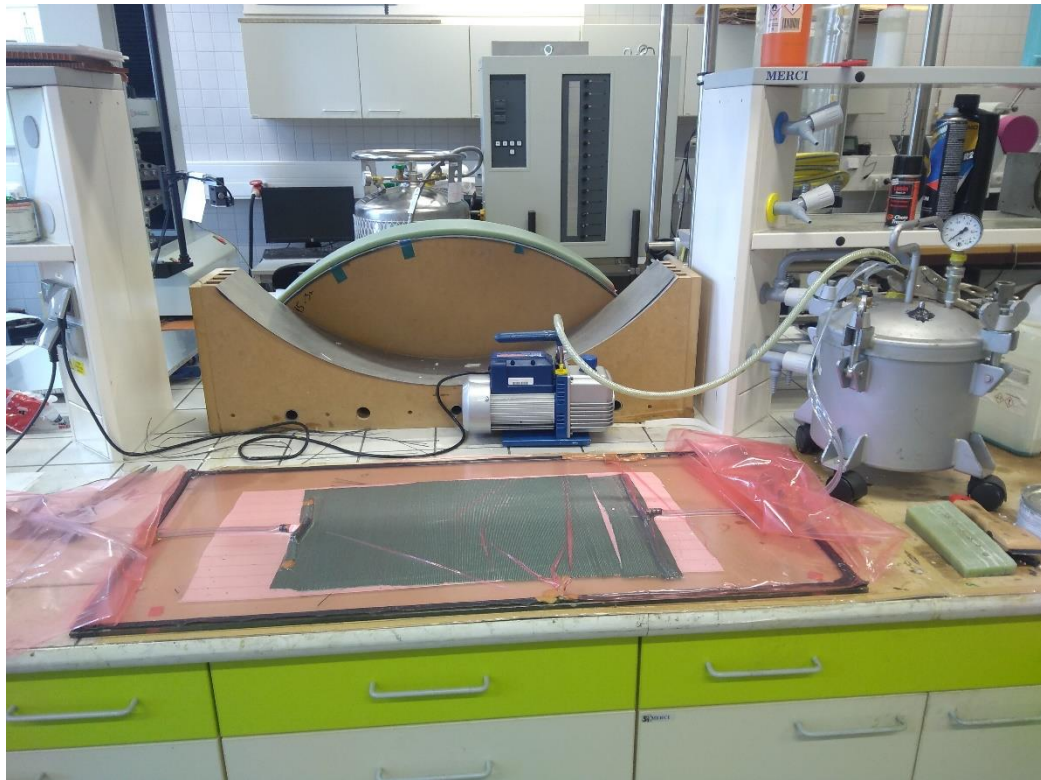


Figure 1.2: Fabrication of composite plate by vacuum injection process (VIP)

1.4.3 Hand lay-up technique

The hand lay-up technique is probably the simplest method for production of FRP composites. In this technique, the laminate, with usually fiber fabric as reinforcement phase, is prepared by placing ply over ply until the desired thickness is achieved. By the use of a roller, as the resin is applied on the fabrics, as the excessive amount of it is removed. The hand lay-up technique has two main disadvantages: it is difficult to achieve uniform distribution of the matrix in the laminate, resulting in non-uniform percentage of fibers/matrix in the composite plate and that during the curing there is no pressure on the laminate, which in turn increases porosity of the composite plate.

1.5 Literature review

Lv et. al. [29] prepared carbon and aramid fibers reinforced polyimide composites and explored the friction and wear behaviour of them in simulated space irradiation environment and start-stop friction process.

By performing static and dynamic three point bending tests, Jia et. al. [30] studied the effect of temperature, in the range from $-100\text{ }^{\circ}\text{C}$ to $100\text{ }^{\circ}\text{C}$, on the

mechanical properties of unidirectional CFRP composites. Notably, the static three-point bending results revealed that CFRP composites had higher flexural strength and flexural strain at break at lower temperatures [30].

Alam et. al. [31] presented a review, including 336 references, on fatigue of carbon fibre reinforced plastics.

The possibility of using carbon fiber and Kevlar[®] fiber woven composites as materials for cryogenic tanks was explored by Islam et. al. [32]. In particular, by Vacuum Assisted Resin Transfer Molding (VARTM) process, carbon fiber and Kevlar[®] woven composites were fabricated; they were then investigated, with and without cryogenic exposure, by tensile, flexural, and short beam shear experiments. The results revealed that tensile strength, tensile chord modulus, flexural chord modulus and flexural strength of carbon and Kevlar[®] fiber composites had not been significantly influenced by cryogenic exposure [32].

Song [33] prepared six types of carbon/glass fiber hybrid composites and six types of carbon/aramid fiber hybrid composites by following VARTM technique and investigated their mechanical properties. In particular, in this study, the correlation between mechanical properties and pairing effects of lamination structures was explored [33].

A study on the effect of thickness on the vacuum infusion processing of aramid/epoxy composites for ballistic applications was conducted by Nunes et. al. [34]. In their work, composites with 5, 8, 13, 18 and 23 plain-weave fiber layers were fabricated and investigated through ultrasonic C-scan inspections, optical microscopy, density and constituent content analyses. Moreover, short beam and flexural tests were performed [34].

Costa et. al. [35] used DMA, DSC, and a rheometer in order to investigate cure kinetics and rheological behavior of a carbon/epoxy prepreg.

Hossain et. al. [36] presented a three-dimensional thermodynamically consistent framework which simulates polymeric materials during their curing. In particular, based on the extension of a one-dimension equation, equations of the three-dimensional finite strain curing framework were evolved. Furthermore, cure-dependent material parameter evolutions and some numerical examples were analysed [36].

A literature review concerning the machining of carbon fiber reinforced plastics/polymers has been presented by Che et. al. [37].

By using the VARTM technique and two types of fibers, namely plain weave carbon fabrics and plain weave aramid fabrics, Wang et. al. [38] produced 12 types of composites and investigated their tensile, flexural, interlaminar shear and damping properties.

The effect of extreme low temperature conditions on the dynamic mechanical properties of carbon fiber reinforced polymers (CFRPs) was investigated by Zaoutsos and Zilidou [39]. In detail, CFRPs were manufactured by the Vacuum Assisted Resin Infusion Molding technique; after their curing they were subjected in extreme low temperatures (-40 °C) for three different periods of time: 30, 45 and 60 days. The CFRPs were then explored by three point bending and DMA experiments. The results revealed that the three point bending strength, three point bending modulus and dynamic storage modulus of the CFRPs were decreased as the time of exposure at 40 °C was increased [39].

Hazer et. al. [40] produced carbon fiber reinforced with poly (lactic acid)/polycarbonate composites, with 5, 10, 15 and 30 % percentage of carbon fibers, and two compositions of poly (lactic acid)/polycarbonate (90/10 and 50/50) blends as matrix. Particularly, these composites were investigated by DSC, TGA, tensile test, DMA, limiting oxygen index, scanning electron microscope and cone calorimeter tests [40].

Joven et. al. [41] used a light radiation method in order to explore the thermal diffusivity and the thermal conductivity of carbon fiber-epoxy composites, which were made with prepregs of different weave fabrics: unidirectional, plain weave and eight-harness weave.

By the VARTM technique, Dong et. al. [42] fabricated carbon fiber/epoxy plain woven composites and they studied, experimentally and numerically, their temperature-dependent thermal expansion behaviors.

The contribution of aramid fibers on the mechanical behavior of a hybrid carbon-aramid-reinforced epoxy composite was explored by Pinchiera et. al. [43]. In particular, in this study, carbon and carbon-aramid fiber reinforced composites were explored by tensile, In-plane shear, out-of-plane compression, charpy and compact tension tests.

The influence of fiber orientation on tensile properties and low cycle fatigue of intraply carbon-Kevlar reinforced epoxy hybrid composite was explored by Hashim et. al. [44].

By implementing the hand lay-up method, Hossain et. al. [45] produced five different types of twill woven Carbon-Kevlar reinforced epoxy composites. The affection of the ply variation, from 1 to 5 plies, on the tensile strength, bending strength, tensile modulus, bending modulus, and impact strength of these composites were studied. Moreover, thermo gravimetric analysis was used for the evaluation of composites' thermal stability whereas the fracture surface of the tensile specimen was investigated by SEM. The results revealed an increasing in the flexural strength of the composites, as the number of the plies was increased while the composite with the three plies achieved the highest tensile and impact strength [45].

Mahnken and Dammann presented a three-scale framework for fibre-reinforced-polymer curing [46].

Nikforooz et. al. [47] explored the effect of the temperature on the static tensile behavior of continuous glass fiber-reinforced thermoplastic laminates. Moreover, the T_g of the E-glass/polyamide composites was determined by DSC, DMA and TMA [47].

The influence of 10 cycles of fatigue (between 100-50000) and then accelerated ageing in tap and artificial seawater for 4, 20 and 40 days on the tensile properties of glass and Kevlar fibers reinforced epoxy composites was investigated by Menail et. al. [48].

Ni et. al. [49] inserted aramid non-woven fabric (ANF), with a thickness of 30 μm and a face density of 16 g/m^2 , into CFRP laminates as interlayers. They investigated the influence of ANF number and arrangement on the dynamic mechanical properties, interlaminar shear strength, flexural modulus, flexural strength, compression after impact, type I interlaminar fracture toughness, and type II interlaminar fracture toughness of the composites. Remarkably, it was found that the CFRP with 1ANF had a higher flexural strength than the control CFRP composite; in comparison with the control CFRP composite, the CFRP samples with 3 or 7 ANF had approximately the same or slightly lower flexural strength, respectively [49].

Cecen et. al. [50] studied temperature dependence of heat capacity and thermal conductivity of polyester and epoxy-based composites, reinforced with non-crimp stitched glass, carbon and aramid fabrics by heat-flux DSC [50].

1.6 Objectives of the thesis

1.6.1 First experimental part

The properties of PMC, with continuous fibers as reinforcement phase, depend to a great extent on the orientation of fibers. As an example, unidirectional FRP composites exhibit high tensile strength in the longitudinal fiber direction but contrastively low tensile strength in the transverse direction whereas the woven FRP composites present good properties in both directions of fibers. In the current knowledge of the author, a research study exploring the dynamic mechanical properties of glass fiber/epoxy composites which have unidirectional fibers in the longitudinal or transverse direction or woven at 0° or 45° has not been performed so far. It should be pointed that, due to the viscoelastic nature of the matrix of CFRP and GFRP composites, these need to be explored in a broad range of temperature, for their dynamic mechanical properties to be absolutely predictable.

In this study, a comparison between the viscoelastic properties of GFRP composites, which contain unidirectional fibers, in longitudinal or transverse direction, and woven fibers at 0° or 45° took place. Specifically, by using prepreg materials and vacuum bag method, GFRP and CFRP composites were fabricated, and their dynamic mechanical properties were investigated, in order to determine the optimal fibers' type and orientation at elevated temperatures. Moreover, the T_g of these composites was determined by two different methods: peak of loss modulus and $\tan\delta$ curves.

1.6.2 Second experimental part

The natural origin fibers, like the basalt, when they are embedded in a polymer matrix composite, in percentage over 50%, provide to it biodegradable characteristics. The latter is nowadays becoming more and more important due to environmental concerns. Furthermore, in order to gain a better understanding of FRP composite, due to its viscoelastic matrix, several thermal analysis techniques should be employed, in order to study and characterize it. Based on the literature review, a research study on BFRP composites, with volume fraction of fibers (Φ_f) over 50%, with adequate experimental results, both on mechanical and thermal behavior of these compounds, appears to be lacking. In the present study, BFRP composites, consisting of 46.4% epoxy and 53.6% of basalt fibers, in 20 layers, were successfully prepared by a hand lay-up compression molding combined technique and by DMA; their storage modulus, loss modulus, $\tan\delta$, and T_g were determined. TMA creep-recovery and TMA stress-relaxation tests were also performed whereas decomposition of basalt fibers and BFRP composites as well as weight fraction of the basalt fibers and epoxy matrix were determined by TGA,

in air and N₂ atmosphere, respectively. Moreover, the mechanical behavior of BFRP composites was explored following tension and three-point bending experiments.

1.6.3 Third experimental study

The post-cure process is a cheap method for improving thermal behaviour of cold-cured polymer matrix composites. Moreover, due to their viscoelastic nature, post-cured FRP composites need to be explored by many thermal analysis techniques, so as valid conclusions on their thermal resistance to be drawn. In terms of performance, carbon and aramid fibers are ranked top on synthetic fibers' classification and they are used in high demanding applications. It needs to be noted that in case the properties of FRP composites are compared, it is essential these composites to have same Φ_f , and to consist of reinforcement phase which has the same weave, weight, and thickness. For this purpose, in this study CFRP, AFRP and (aramid/carbon fiber reinforced polymer) ACFRP composites were prepared by using 161 g/m² twill 2/2 aramid fibers fabric and 160 g/m² twill 2/2 carbon fibers fabric. Similarity of both fabrics, in terms of weight, weave and thickness, allows for a direct comparison between the properties of the composites, so that valid conclusions regarding advantages of each composite structure to be drawn.

1.7 Contribution of the thesis to science and practice

In this dissertation, various types of fibers are combined with epoxy matrices so as the positive and negatives of each composite structure combination to be determined. Special attention is given on thermal analysis of FRP composites, with the target to be potential composite materials for applications in airspace industry. Also, as the mechanical behavior of FRP composites is always a critical factor, various mechanical properties of them are determined.

2. FIRST EXPERIMENTAL PART: STUDY ON DYNAMIC MECHANICAL ANALYSIS OF GLASS OR CARBON FIBER/EPOXY COMPOSITES

This study has been presented in the following journal:

KARVANIS, Konstantinos, Soňa RUSNÁKOVÁ, Milan ŽALUDEK and Alexander ČAPKA. Preparation and Dynamic Mechanical Analysis of Glass or carbon Fiber/Polymer Composite. International Conference on Smart Engineering Materials (ICSEM 2018), *IOP Publishing IOP Conf. Series: Materials Science and Engineering* [online], 2018, 362, 012005, doi:10.1088/1757-899X/362/1/012005. Available from: <https://doi.org/10.1088/1757-899X/362/1/012005>

2.1 General information about this research study

In this study, by using prepreg materials and vacuum bag oven technique, GFRP and CFRP composites were prepared while their dynamic mechanic properties, such as the storage modulus, loss modulus, $\tan\delta$ and glass transition temperature were determined by DMA. The main objectives of this study are to investigate the influence of the orientation of glass unidirectional fibers, when they are placed in the longitudinal or transverse direction, and to provide some details concerning the viscoelastic behavior of CFRP composites; the latter demonstrate different thicknesses, so that their properties cannot be compared. Moreover, the T_g of GFRP and CFRP composites was determined based on the peak of loss modulus and $\tan\delta$ curves. Epoxy is one of the most widely used matrices in FRP composites industry. Notably, in aerospace applications, epoxy is used as matrix in a percentage more than two-third out of all polymer matrices [51].

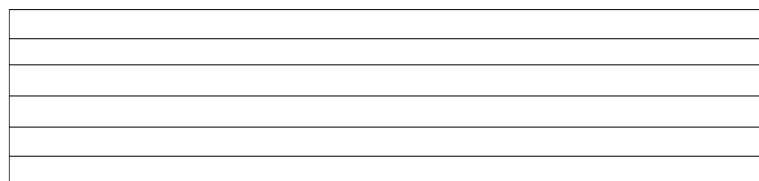


Figure 2.1: base of orientation: unidirectional fibers in longitudinal direction (0°)

Table 2.1 Prepared GFRP and CFRP composites

Symbol of composite	Type of prepreg-fabric name	Type of fibers and orientation	Percentage of matrix	Thickness of composite +- 0.1 (mm)
GF-UD-L-34%	VV430U-DT806R-34	Glass fiber, unidirectional, longitudinal, (0°)	34%	2.35
GF-UD-TR-34%	VV430U-DT806R-34	Glass fiber, unidirectional transverse, (90°)	34%	2.35
GF-UD-L-39%	VV430U-DT806R-39	Glass fiber, unidirectional longitudinal, (0°)	39%	2.85
GF-UD-TR-39%	VV430U-DT806R-39	Glass fiber, unidirectional transverse, (90°)	39%	2.85
GF-W-0°-37%	VV320P-DT806R-37	Glass fiber, woven, 0°, (0°/90°)	37%	2.35
GF-W-45°-37%	VV320P-DT806R-37	Glass fiber, woven, 45°, (-45°/+45°)	37%	2.35
CF-UD-L-38%	IMP503Z/GV420U	Carbon fiber, unidirectional longitudinal, (0°)	38%, +-1%	3.7
CF-UD-TR-38%	IMP503Z/GV420U	Carbon fiber, unidirectional, transverse, (90°)	38%, +-1%	2.85
CF-W-0°-38%	IMP503Z/GG630T	Carbon fiber, woven 0°, (0°/90°)	38%, +-1%	3.15
CF-W-45°-38%	IMP503Z/GG630T	Carbon fiber, woven 45°, (-45°/+45°)	38%, +-1%	1.3

2.2 Materials

During the preparation of GFRP and CFRP composites, the prepregs were placed in the moulds in various layers numbers, so as the thickness of the compounds to be variable. In detail, the carbon and glass fibers were in unidirectional or woven fabric type. The glass fiber epoxy prepregs, both the unidirectional and woven types, were fabricated by the Delta-Preg S.p.A. by the resin DT 806R while the carbon fiber prepregs were prepared by Impregnatex Compositi S.r.l. by using the resin IMP 503Z. In Table 2.1 the specifications of the prepregs and fibers' type are presented. The unidirectional prepreg were placed in longitudinal (Fig. 2.1) or transverse direction and the woven prepreg were oriented at 0° (fibers at $0^\circ/90^\circ$) or at 45° (fibers at $-45^\circ/+45^\circ$). Specifically, the following composites were fabricated:

- GFRP composites consisted of unidirectional fibers in longitudinal direction.
- GFRP composites consisted of unidirectional fibers in transverse direction.
- GFRP composites consisted of woven fiber fabrics at 0° , (fibers $0^\circ/90^\circ$).
- GFRP composites consisted of woven fiber fabrics at 45° , (fibers $-45^\circ/+45^\circ$).
- CFRP composites consisted of unidirectional fibers in longitudinal direction.
- CFRP composites consisted of unidirectional fibers in transverse direction.
- CFRP composites consisted of woven fiber fabrics 0° , ($0^\circ/90^\circ$).
- CFRP composites consisted of woven fiber fabrics 45° , ($-45^\circ/+45^\circ$).
- Two more GFRP composites (UD fibers in longitudinal or transverse direction), with different percentage of matrix, compared to the other type of GFRP composite, were produced.

The produced composites are presented analytically in Table 2.1.

2.3 Production method

The GFRP and CFRP composites were produced by vacuum bag oven method. Firstly, the vacuum bag system was prepared. In detail, the prepreg laminates were cut in the desired dimensions and they were placed in the moulds in various layers numbers. In the next step, a release film and a breath cloth were placed over the laminate of the prepreg. Then, the system was sealed and closed by a vacuum bag which was stuck in the perimeter of the mould by sticky tape; the bag was connected with the vacuum pump by the vacuum valve. After the sealing of the system, air leak was tested, since it is one of the most critical problems in these processes. Finally, the vacuum bag system was placed in the oven where the composites were cured under the following thermal cycle: the temperature was

increased slowly up to 65 °C in which it was held for 30 minutes; next the temperature was raised to 120 °C where it was maintained for 60 minutes; and finally it was slowly reduced up to ambient temperature. It should be mentioned that this process lasted totally about 4 hours. Then, the composites were let to solidify for one day at room temperature and then samples were mechanically cut in the desired dimensions.

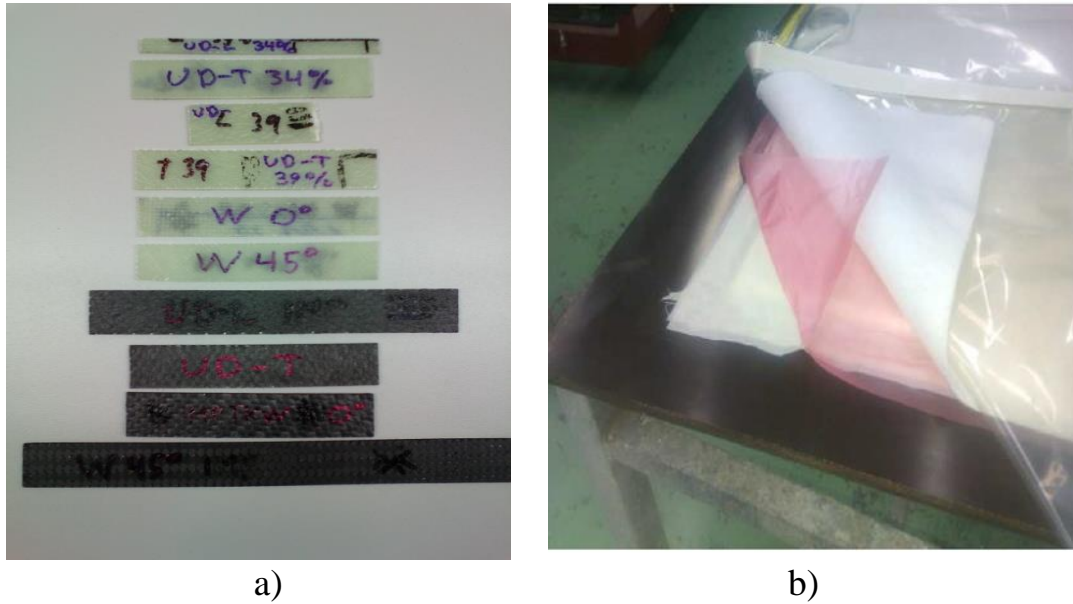


Figure 2.2: a) Produced GFRP and CFRP composite plates and b) materials of the vacuum bag system

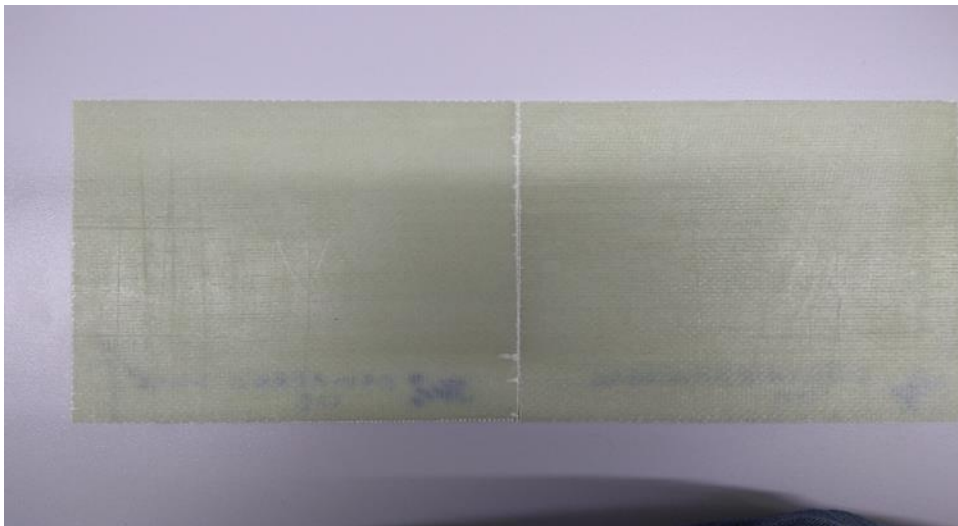


Figure 2.3: GFRP composite plates

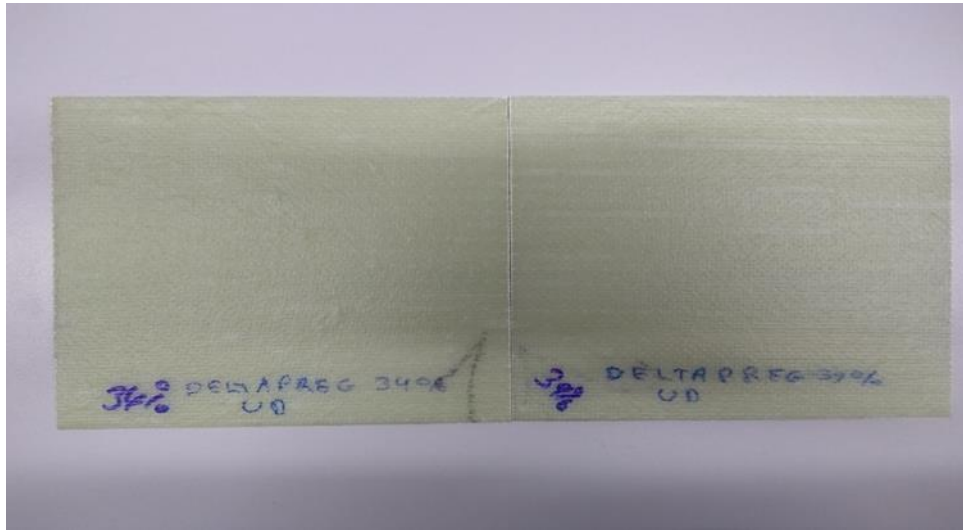


Figure 2.4: The other side of the GFRP composite plates

2.4 Experimental details

The DMA measures the viscous and elastic responses of a material, as a function of temperature, frequency or time, under a periodic stress. In detail, a sinusoidal stress is exerted on the specimen and the generated strain is measured.

The complex modulus [52], which consists of both the elastic part (E') and the viscous part (E''), is described by the equation:

$$E^* = E' + iE''$$

Where E' = elastic (storage) modulus and E'' = viscous (loss) modulus.

A perfect elastic solid has phase lag $\delta = 0^\circ$ and a perfect viscous solid has phase lag $\delta = 90^\circ$; The viscoelastic materials have $0^\circ < \delta < 90^\circ$ [52].

In this study, the DMA experiments were exhibited by the METTLER TOLEDO instrument (Figure 2.5), under three-point bending configuration, with specimens of dimensions of 40 mm x 7 mm with the span length between the supports to be 30 mm. The thickness of the GFRP and CFRP composites is presented in Table 2.1. In detail, the DMA experiments were performed by scanning in the temperature range 30-200 °C, with a heating rate of 2 °C/min at a steady frequency of 1 Hz. Moreover, the displacement amplitude adjustment was 20 μ m whereas a force of 1 N was used as preload.

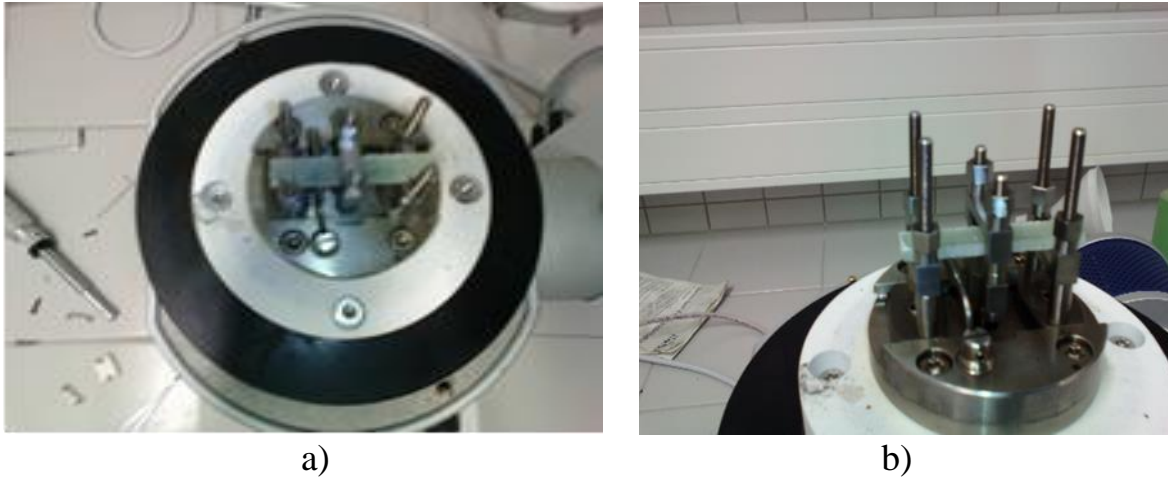


Figure 2.5: a) and b) GFRP composite on the three-point bending configuration on the instrument DMA 1 METTLER TOLEDO



Figure 2.6: GFRP and CFRP composites specimens after the DMA experiments

2.5 Results

2.5.1 Storage modulus

The storage modulus of the GFRP and CFRP composites, in the temperature range 30-200 °C, is illustrated in Figures 2.7 and 2.8, respectively. As can be seen, except for a slightly increase in the low temperatures in some of the composites, the storage modulus decreases as the temperature increases. As regards polymer matrix composites, the usual middle transition region is depicted as a sharp decrease in storage modulus curves and this phenomenon is correlated with T_g ; this sharp fall usually defines the maximum operating temperature of

materials. Remarkably, the GFRP composites with 34% percentage of matrix and with unidirectional fibers in the longitudinal or transverse direction exhibited much higher storage modulus than the same type GFRP composites with 39% matrix, despite their relatively small thickness. This fact indicates that even a small increment in the percentage of glass fibers can significantly contribute to composite demonstrating higher storage modulus. Furthermore, a comparison between the GFRP composites with unidirectional fibers in longitudinal orientation and in transverse one revealed that the placement of unidirectional fibers in longitudinal direction, is much more effective than when they are placed in transverse direction. Furthermore, the GFRP sample with woven fabric at 0° exhibited higher storage modulus than the GFRP with woven fabric at 45°.

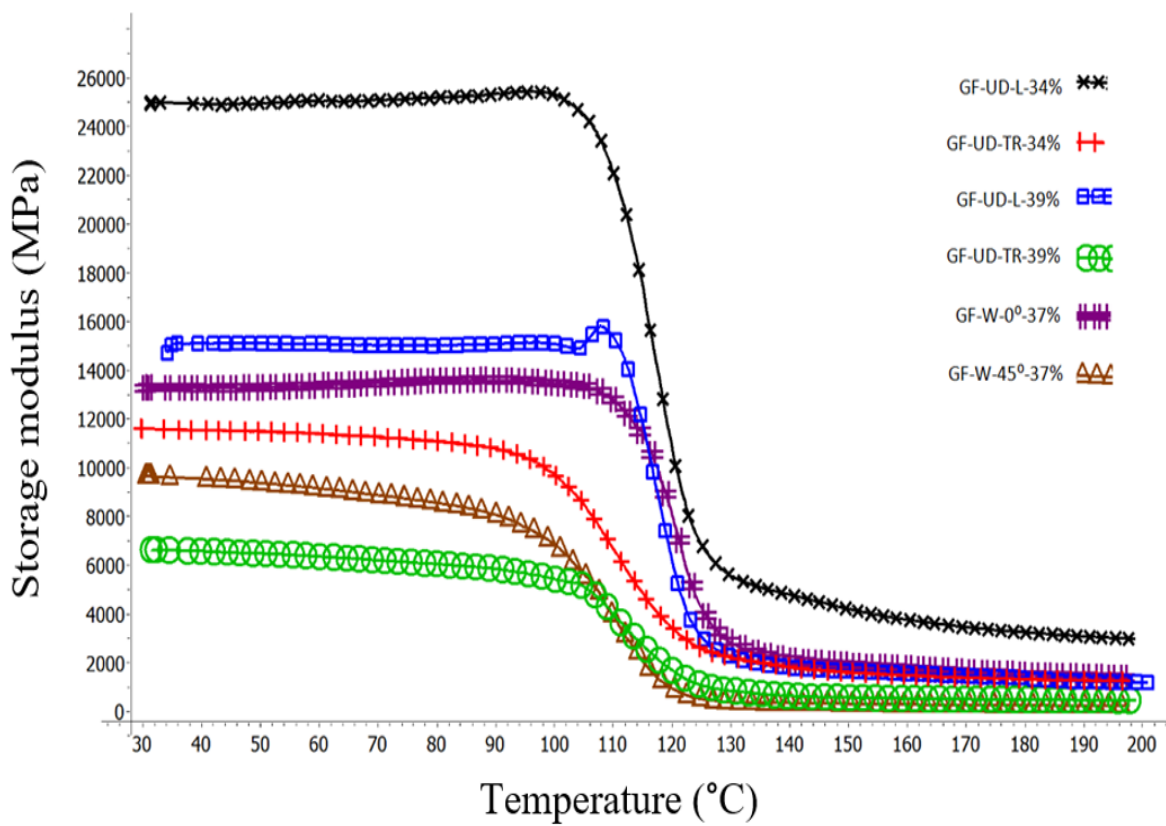


Figure 2.7: Storage modulus of the GFRP composites as a function of the temperature in the range 30-200 °C

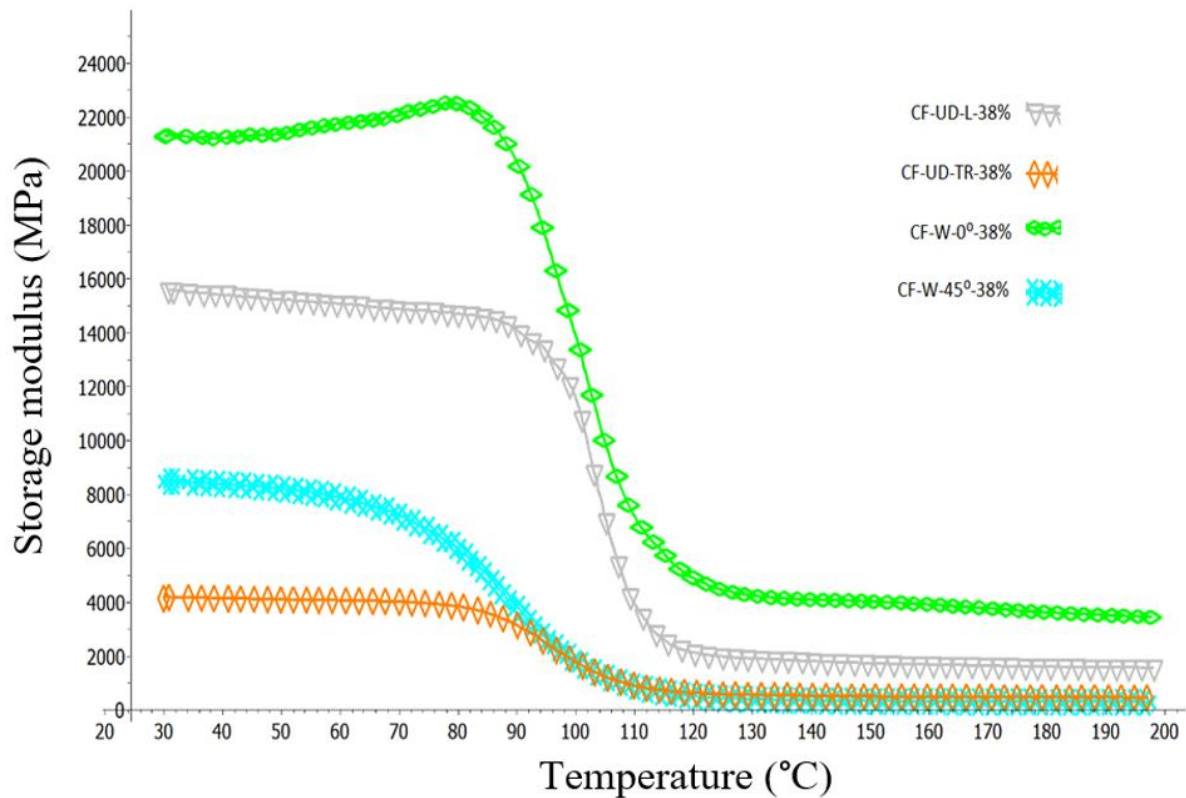


Figure 2.8: Storage modulus of the CFRP composites as a function of the temperature in the range 30-200 °C

2.5.2 Loss modulus

The loss modulus of the GFRP and CFRP composites, in the range 30-200 °C, is presented in Figures 2.9 and 2.10, respectively. It can be seen that the loss modulus values are almost stable at low temperatures while after about the 70-80 °C a steep increase is observed until a peak value. Then, a sharp decrease is obtained until very low values which are maintained up to the final 200 °C. The same trend which was noticed in the storage modulus graph appears also in this case: the GFRP composites consisting of unidirectional fibers in the longitudinal direction exhibit much higher loss modulus than the ones with unidirectional fibers in the transverse direction. Furthermore, the placement of glass fiber woven fabric at 0° seems to be much more effective than in the occasion it is placed at 45°.

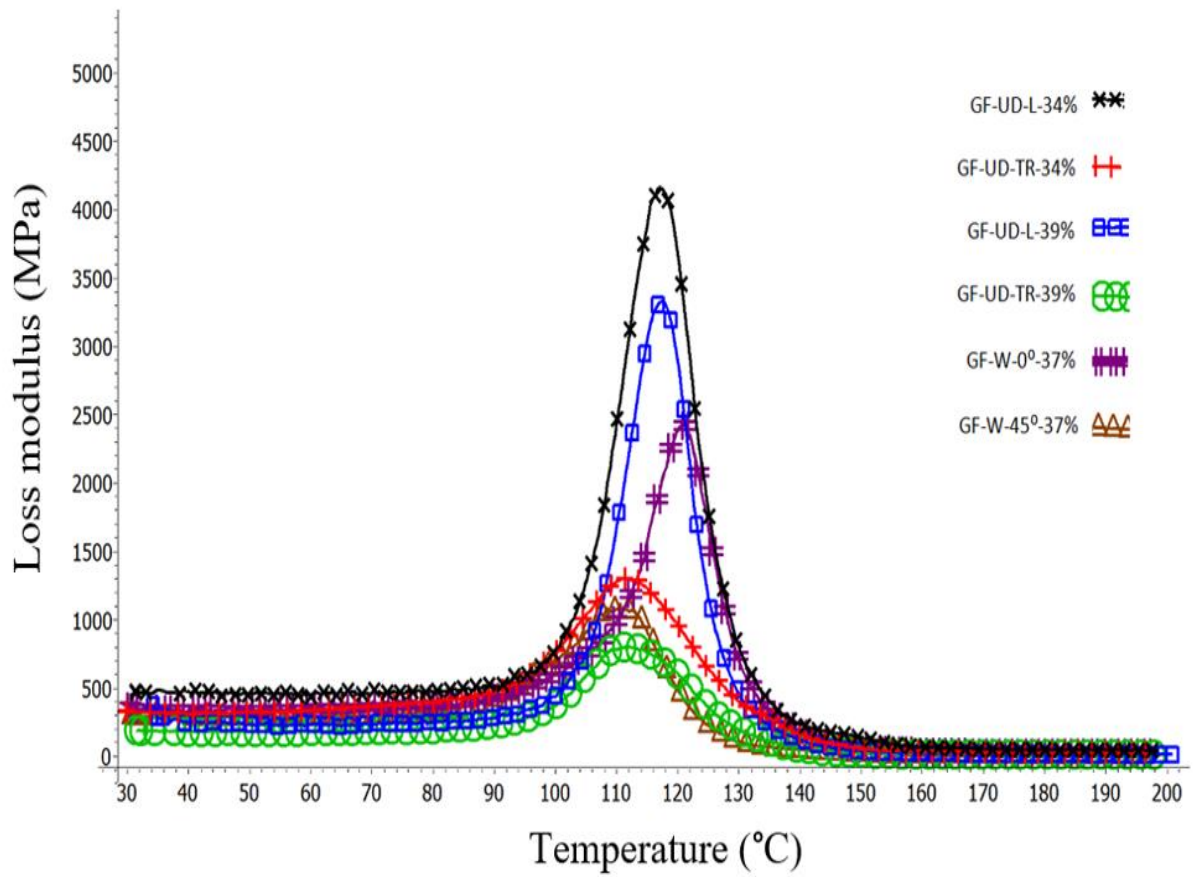


Figure 2.9: Loss modulus of the GFRP composites as a function of the temperature in the range 30-200 °C

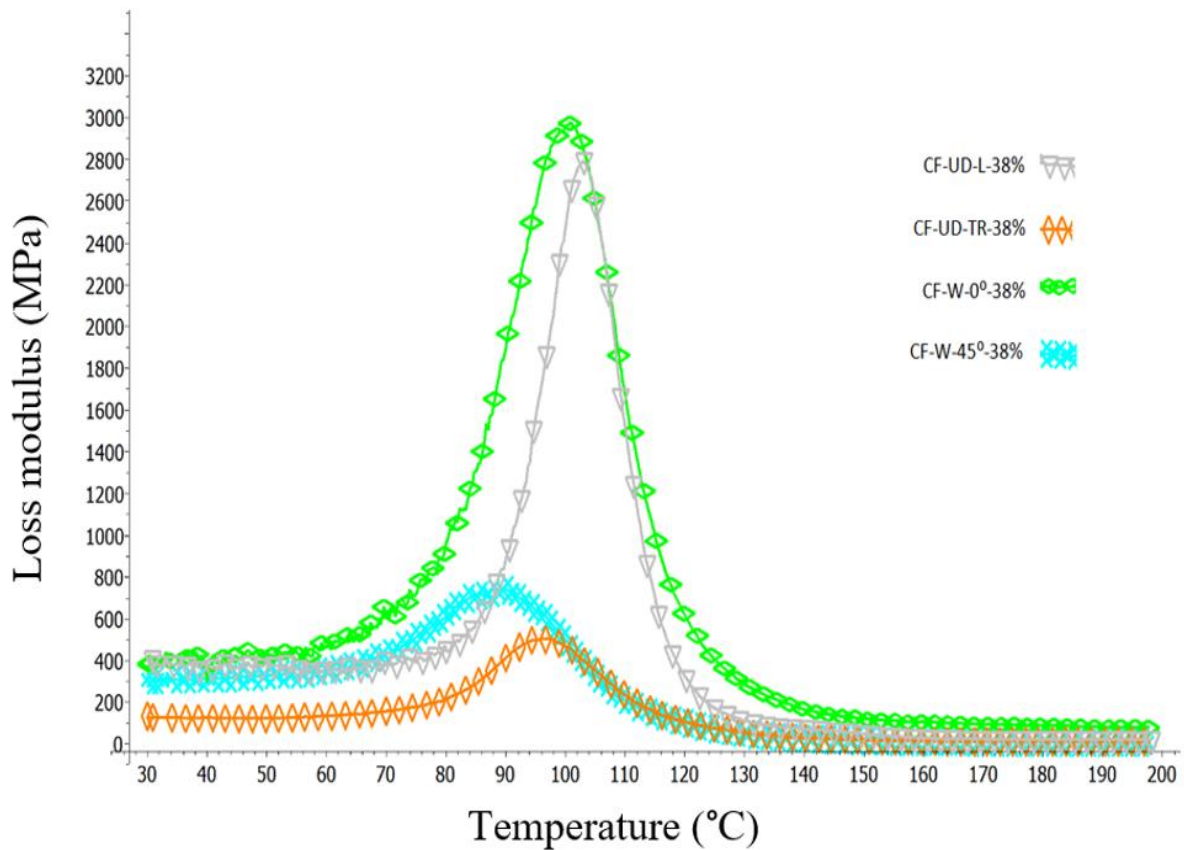


Figure 2.10: Loss modulus of the CFRP composites as a function of the temperature in the range 30-200 °C

2.5.3 $\tan\delta$

The ratio of loss modulus to storage modulus is the $\tan\delta$ and it is a specification of the materials' damping. Figures 2.11 and 2.12 depict the $\tan\delta$ curves of the GFRP and CFRP composites in the range 30-200 °C. It is observed that at about 90 °C, the $\tan\delta$ increases sharply, achieving maximum values whereas then it falls steeply. Remarkably, the $\tan\delta$ curve of the CF-W-45°-38% composite follows a nonlinear decrease after the peak. This is caused due to deflection of the specimen at high temperatures under the three-point bending configuration, because of its relatively small thickness. It should be referred that a second specimen of this type of composite was tested and the same nonlinearity was observed.

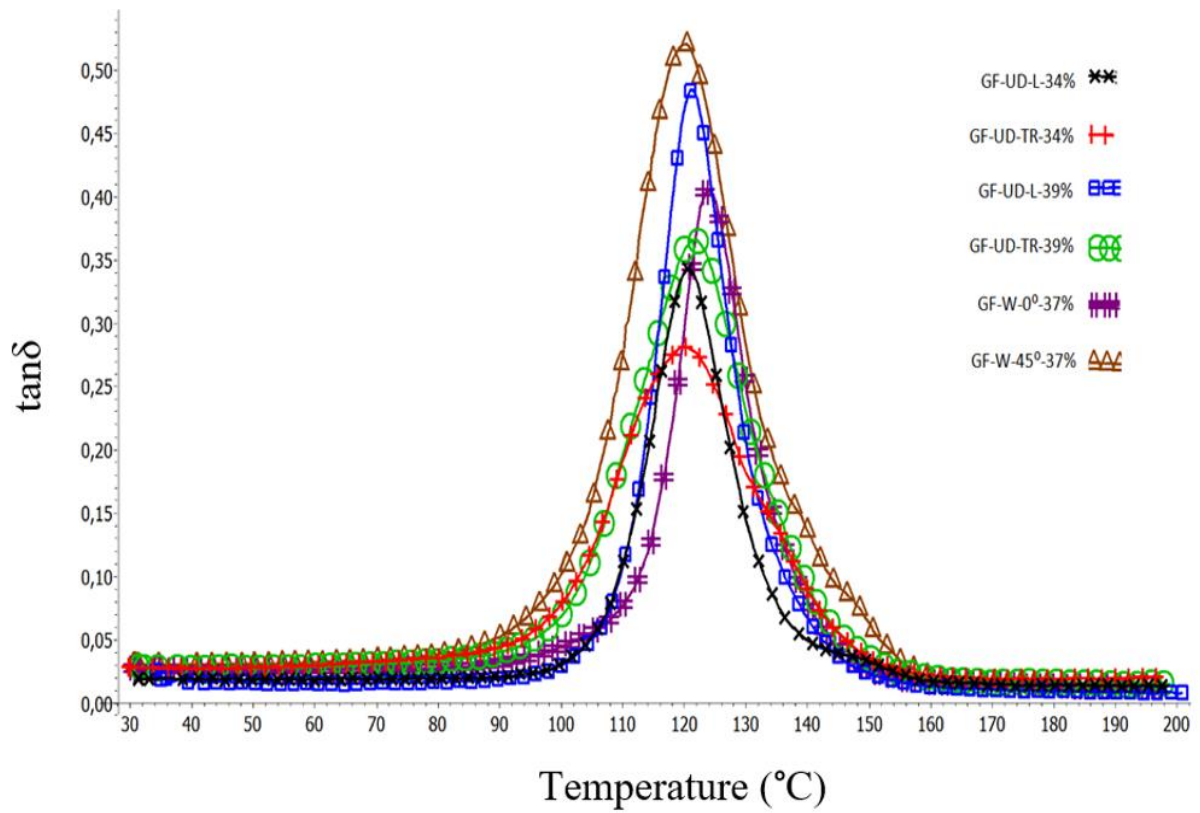


Figure 2.11: $\tan \delta$ of the GFRP composites as a function of the temperature in the range 30-200 °C

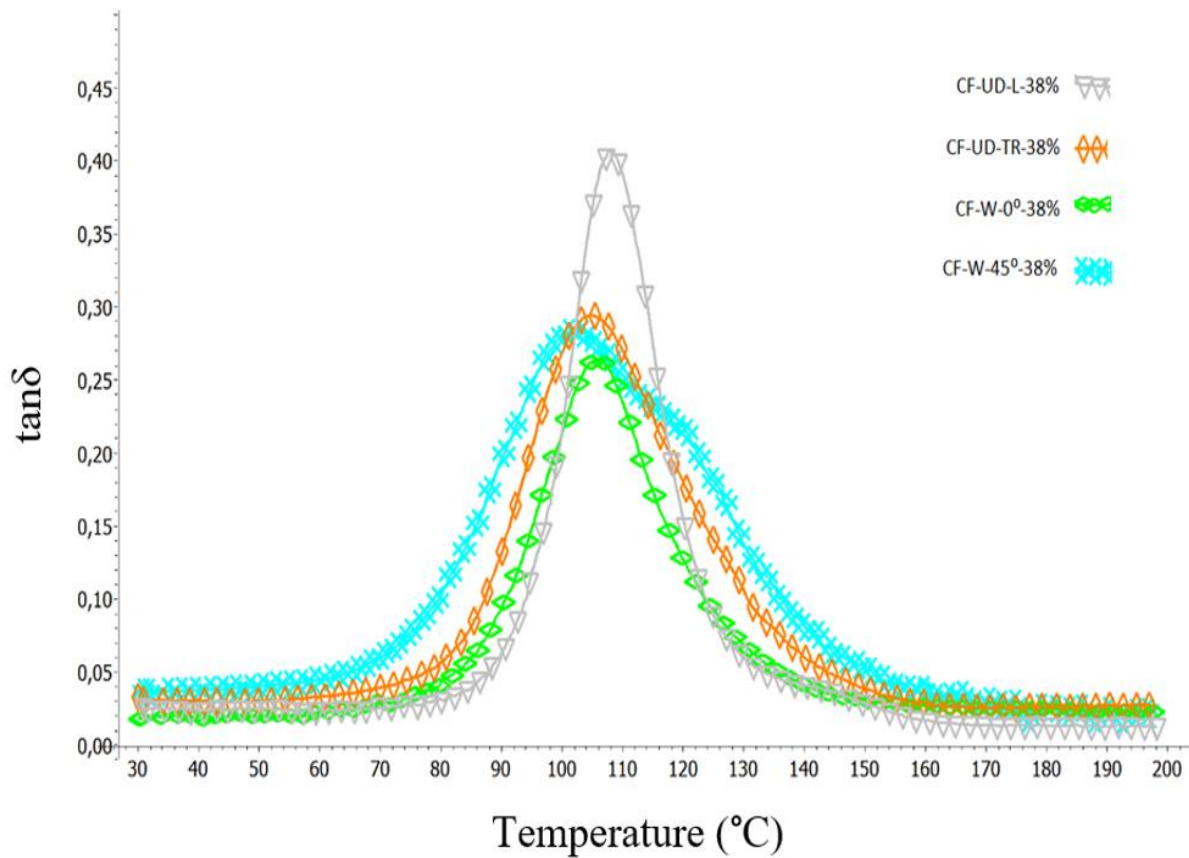


Figure 2.12: $\tan \delta$ of the CFRP composites as a function of the temperature in the range 30-200 °C

2.5.4 Glass transition temperature (T_g)

In this research, the T_g of the GFRP and CFRP composites were obtained by the peak of the loss modulus and $\tan \delta$ curves; these are illustrated in Table 2.2. A comparison of the two methods revealed that the T_g acquired by the corresponding temperature of the $\tan \delta$ peak is a little higher than the T_g calculated from the loss modulus curves. Notably, the GFRP and CFRP composites achieved significantly high T_g , which stresses their high quality, broadening their applications in advanced composites industry. Moreover, in both methods, the composite composed of woven (0°/90°) glass fibers exhibited the highest T_g .

Table 2.2 T_g of the GFRP and CFRP composites

	T_g values obtained by loss modulus peak (°C)	T_g values obtained by $\tan\delta$ peak (°C)
GF-UD-L-34%	116.91	120.54
GF-UD-TR-34%	111.69	119.85
GF-UD-L-39%	117.47	121.27
GF-UD-TR-39%	111.68	121.83
GF-W-0°-37%	120.79	123.66
GF-W-45°-37%	110.46	120.01
CF-UD-L-38%	103.08	107.54
CF-UD-TR-38%	96.27	104,96
CF-W-0°-38%	100.97	106.56
CF-W-45°-38%	88.93	101.42

2.6 Conclusions regarding the GFRP and CFRP composites

The overall conclusions of this research study are the following:

1. The principal research finding of this study is that when placed in the longitudinal direction, the glass fibers contribute towards to epoxy matrix composite exhibiting much higher storage modulus and loss modulus than if they are placed in the transverse direction.
2. As the volume fraction of the glass fibers in an epoxy matrix composite increases, the composites exhibit higher storage and loss modulus.
3. In DMA experiments under three-point bending configuration, the low thickness of CFRP composites is a restrictive factor.
4. The vacuum bag oven method is characterized as a cheap and efficient method for fabrication of GFRP and CFRP composites. In particular, by this method, the increased cost of autoclave is avoided while the produced composites display remarkably dynamic mechanical properties.
5. The GFRP and CFRP composites exhibited remarkably high T_g , fact which classifies them as potential materials in high demanding applications, such as in aircraft industry, and generally in cases thermal resistance is a critical factor.

3. EXPERIMENTAL PART 2: STUDY ON PREPARATION, THERMAL ANALYSIS, AND MECHANICAL PROPERTIES OF BASALT FIBER/EPOXY COMPOSITES

This research study has been published in the journal *Polymers*: KARVANIS, Konstantinos, Soňa RUSNÁKOVÁ, Ondřej KREJČÍ and Milan ŽALUDEK. Preparation, Thermal Analysis, and Mechanical Properties of Basalt Fiber/Epoxy Composites. *Polymers* [online], 2020, vol. 12, iss. 8. 1785. Available from: <https://doi.org/10.3390/polym12081785>

3.1 General information about this study

In this study, BFRP composites, with epoxy matrix and twill 2/2 weave basalt fibers fabric, in 20 layers, were prepared by a hand lay-up compression molding combined technique. In the experimental part, DMA was exhibited in the range 30-180 °C and at 1, 5 or 10 Hz and based on corresponding temperatures of the peak of loss modulus and $\tan\delta$ curves, the T_g of these composites was determined. Moreover, TMA was performed in the modes of creep recovery and stress-relaxation experiments whereas thermal decomposition of the basalt fibers and BFRP composites in air and nitrogen atmosphere, respectively was investigated by TGA experiments. Based on TGA experiments, it was calculated that $\Phi_f = 53.66\%$. Also, tensile and flexural characteristics of the BFRP composites were determined by tension and three-point bending experiments.

3.2 Materials

The epoxy matrix of the BFRP composites, is a mixture of the Epoxy resin Epidian[®] 652 CIECH Sarzyna S.A (Cieszyn, Poland) and the hardener TFF CIECH Sarzyna S.A (Cieszyn, Poland), in a mixing ratio of 100:27 parts per weight and the reinforcement phase is a fabric of basalt fibers 235 g/m², in twill 2/2 weave, supplied by Havel Composites (Cieszyn, Poland) (Figure 3.3). It needs to be noted that the specific weight of the used basalt fibers is 2.67 g/cm³. The steps followed for the preparation of the BFRP composites are described below. By the hand lay-up technique, a laminate, composed of 20 layers of polymer fibers, was prepared; then it was placed between two rectangular metal plates forming a mold. It should be mentioned that the polymer matrix was applied on the fiber's fabric through a roller. In the next step, this laminate was placed in a compression machine, where it was pressed under 20 MPa for 24 h, at a laboratory temperature of 24 °C. Then, the composite plate was left for curing at room

temperature for a week, and finally specimens were cut in the desired dimensions by water jet and mechanical cutting.



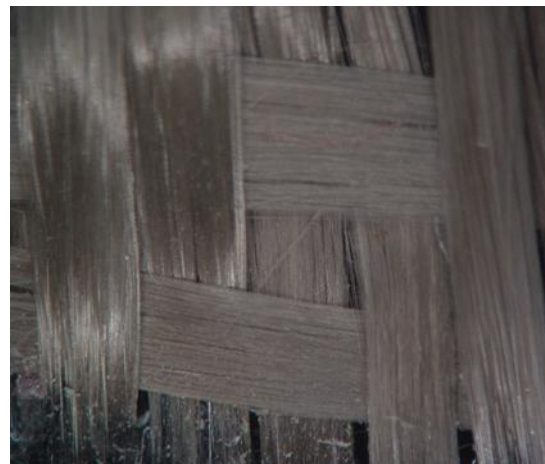
Figure 3.1: Preparation of the BFRP composites by the hand lay-up compression molding combined method



Figure 3.2: The produced BFRP composite plate. The compression machine pushed the excessive resin in the edges of the mold, contributing towards so as the composite structure to achieve high Φ_f . Moreover, some small white pieces on the surface of the composite plate are just cook paper from the mold.



a)



b)

Figure 3.3: a) and b) Photos of the used Basalt fibers fabric. The photos were taken with the Carl Zeiss Stemi 2000C Microscope (Jena, Germany) from the edges of the BFRP composite structure.

3.3 Experimental

3.3.1 General experimental conditions

Before the experiments of both thermal analysis and mechanical behavior, the specimens were in storage in a laboratory environment at 24 °C, for not less than 40 h prior the tests. During the experiments, the conditions in the laboratory were at a temperature of 23 °C and humidity of approximately 50%. The fact that all experimental data, both of thermal analysis and mechanical properties, were acquired directly from the software of the according instrument should be stressed.

3.3.2 Dynamic mechanical analysis

The DMA experiments were performed with the DMA 1 instrument, from METTLER TOLEDO (Schwerzenbach, Switzerland) (Figure 3.4) by using the STARe Software and under single cantilever configuration (Figure 3.5). The dimensions of the rectangular shape specimens were 25 mm × 5.7 mm × 2.1 mm (length × width × thickness) (Figure 3.6).



Figure 3.4: DMA 1 METTLER TOLEDO instrument

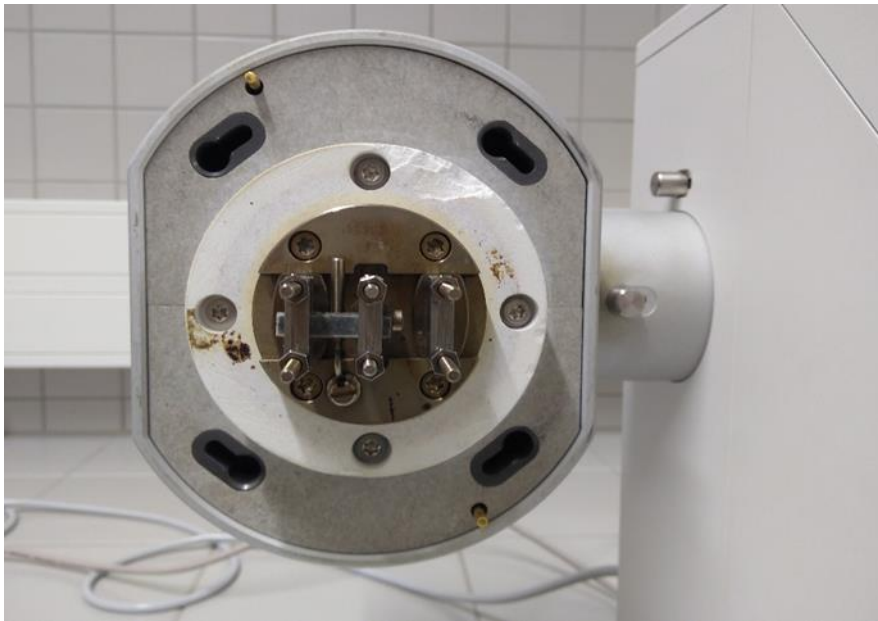


Figure 3.5: BFRP sample on the single cantilever configuration



Figure 3.6: DMA specimens

In DMA, it is important the experiments to take part in the linear viscoelastic region of materials. Initially, strain sweep tests over the displacement range 1–31 μm were performed at 25 °C and at 1 Hz frequency.

Then, DMA temperature sweep tests were conducted over the temperature range of 30–180 °C, with a heating rate of 2 K/min while the frequency was 1, 5 and 10 Hz with a displacement amplitude of 8 µm. Based on these results, the T_g of the BFRP composites were identified by the corresponding temperatures of the peak of loss modulus and $\tan\delta$ curves; T_g values are shown in Table 3.1.

3.3.3 Thermomechanical analysis creep-recovery and Thermomechanical analysis stress-relaxation experiments

The creep recovery and stress-relaxation tests were carried out by the METTLER TOLEDO DMA 1 (Schwerzenbach, Switzerland) instrument, using the STARe Software, under TMA mode and three-point bending configuration. In particular, in both types of experiments, namely the TMA creep recovery and TMA stress-relaxation, the specimens were of rectangular shape with dimensions 40 mm × 5.7 mm × 2.1 mm (length × width × thickness) with a span length of 30 mm between the supports. The specifications of these tests are described below.

Creep recovery tests

In the first type of the TMA creep-recovery experiments, at isothermal 25 °C, a force of 1, 3, and 5 Newton was applied on the specimens for 30 min; then their recovery behavior was recorded under 0 N for 120 min.

In the second type of the TMA creep-recovery tests, at a temperature of 25, 50, and 75 °C, 1 N was applied on the BFRP composite specimens for 30 minutes; then the force was released and the recovery of the composite structure, under 0 N, was recorded for 120 min.

Stress-relaxation tests

During the TMA stress-relaxation tests experiments, 20 µm extension was applied on the specimens, at a temperature of 25, 50 or 60 °C, and their time-dependent stress was being measured for 60 min. It should be pointed that the experiments were performed at 75 °C, but they failed due to the small resistance of the BFRP sample in deformation at this temperature; the force was always reaching negative values.

3.3.4 Thermogravimetric analysis

The TGA experiments were carried out by the TGA Q50 Thermogravimetric Analyzer, from the TA Instruments (New Castle, Delaware, USA), using the Thermal Advantage Release 5.4.0 software whereas the results were evaluated with the TA Instruments Universal Analysis 2000 version 4.5A program. In

particular, in this kind of experiments thermal decomposition of the BFRP composites was explored in the temperature range 30–900 °C, with a heating rate of 10 °C/min, in air and nitrogen atmosphere, respectively. The samples had weight approximately 60 mg, as the complex composite structure requires enough mass during TGA experiments, and they were placed in an alumina crucible. Moreover, the total flow was set at 100 mL/min; balance purge flow 40 mL/min, and sample purge flow 60 mL/min.

3.3.5 Mechanical properties

The three-point bending experiments were carried out at room temperature with the testing machine Zwick/Roell 1456 (Ulm, Germany), by using the software testXpert® II V2.1. In particular, the rectangular shape specimens were of dimensions 75 mm × 10 mm × 2.1 mm (length × width × thickness), with span length-to-depth ratio of 20:1, whereas the crosshead speed was set to 1 mm/min. Specifically, in each side, the specimen overhanged the support of the three-point bending configuration by approximately 16.5 mm, so as to avoid slipping of the specimen whereas the force was applied in the center of them. Moreover, for reliability purposes, four samples were tested for determination of flexural characteristics of the BFRP composites; these results are presented in Table 3.2. Particularly, since the specimens did not break under the bending force in any of the four tests, these were performed until sufficient deformation of them (more than 5%) to be achieved.

The tensile tests were exhibited at room temperature, with the testing machine Vibrophore 100, from Zwick/Roell Company (Ulm, Germany) using the software TestExpert III. In particular, the tensile characteristics of the BFRP composites were measured with rectangular shape specimens with dimensions 150 mm × 13 mm × 2.1 mm (Figure 3.7 a) with each gripping section being 40 mm (Figure 3.7 b) whereas the length of the extensometer was 50 mm. For reliability purposes, five samples of this kind of experiments were tested; their values are presented in Table 3.3. Furthermore, the crosshead speed was set at 1 mm/min.

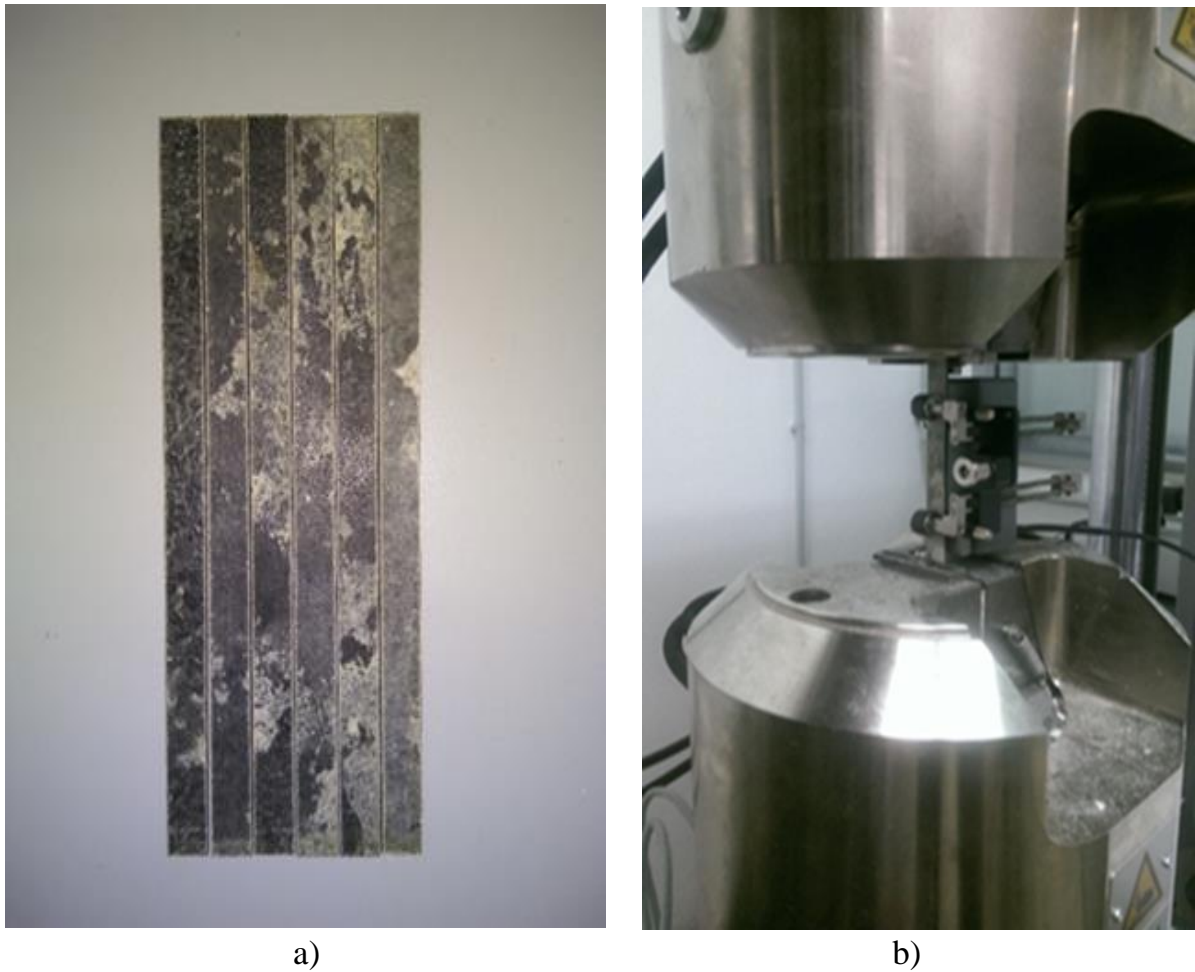


Figure 3.7: (a) Tensile specimens and (b) tensile specimen on the tension grips

3.4 Results

3.4.1 Displacement sweep test

Figure 3.8 shows the displacement sweep curve of the BFRP composite. As can be seen, the initial storage modulus value does not change remarkably at the chosen $8 \mu\text{m}$; thus, it is assumed that the DMA experiments take part in the linear viscoelastic region of the materials.

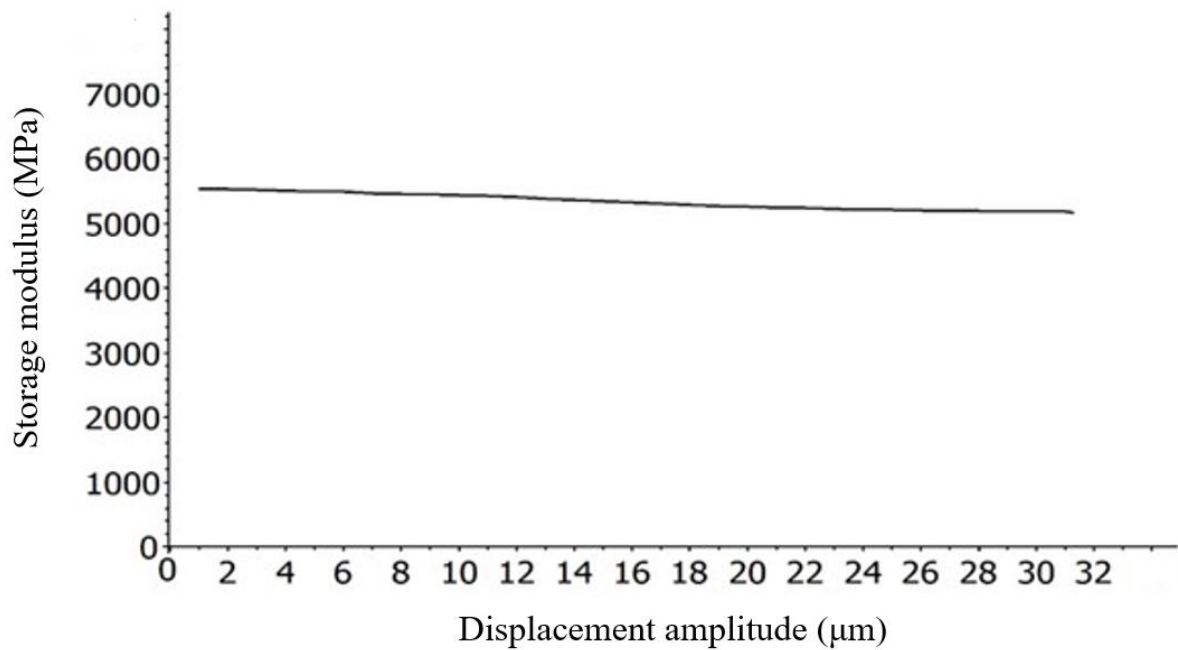


Figure 3.8: Displacement sweep test

3.4.2 Dynamic mechanical analysis

Figure 3.9 illustrates the storage modulus of the BFRP composites, in the temperature range 30-180 °C, at 1, 5 and 10 Hz. In this graph, it is observed that as the temperature increases, the storage modulus of the BFRP composites decreases. In detail, the storage modulus curves are divided in three regions: from about 30-55 °C is the glassy state, from 55-85 °C is the middle transition region, which is associated with T_g , and from 85-180 °C is the rubbery region. One significant observation is that as the frequency is raised, the middle transition region becomes less abrupt and of longer duration.

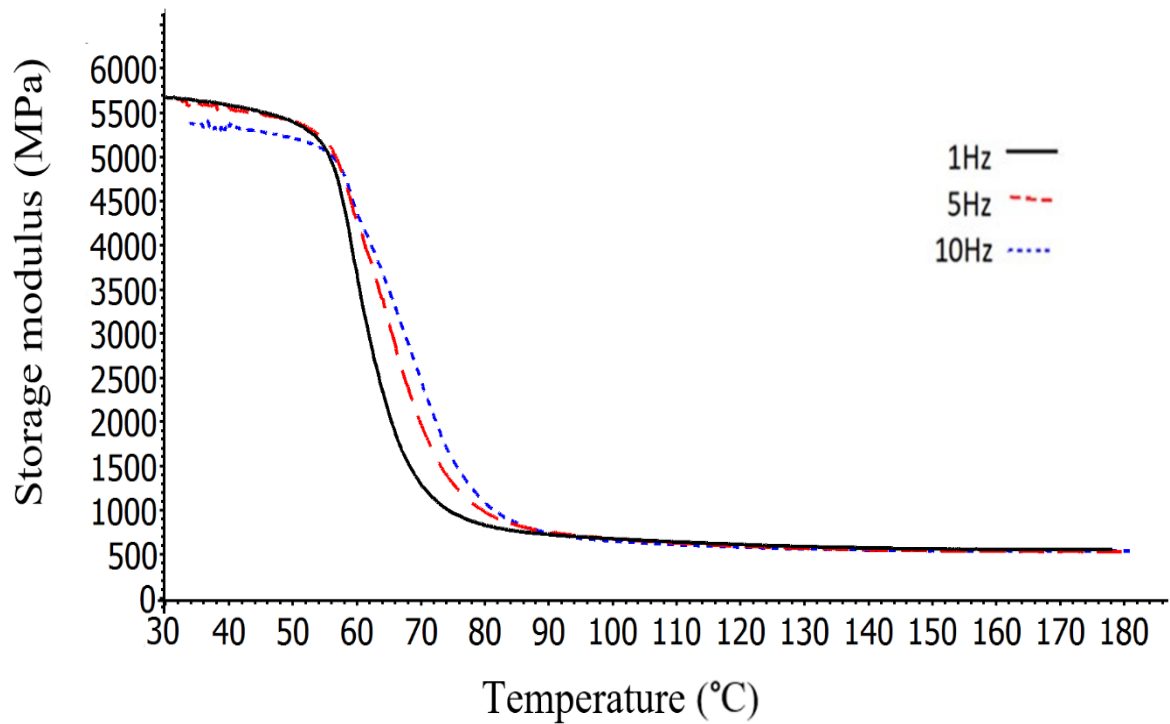


Figure 3.9: Storage modulus of the BFRP composites, as a function of the temperature, at 1, 5 and 10 Hz

The E'' is correlated with lost energy, in the form of heat, in DMA tests. The loss modulus of the BFRP composites, in the range 30-180 °C, at 1, 5 and 10 Hz is depicted in Figure 3.10. As it can be seen, the loss modulus, after approximately 50 °C exhibits a sharp rise, achieving peak values; then a steep fall is observed until almost zero values which are maintained up to the final 180 °C. Furthermore, it seems that higher frequencies exert a negative impact on the loss modulus maximum values.

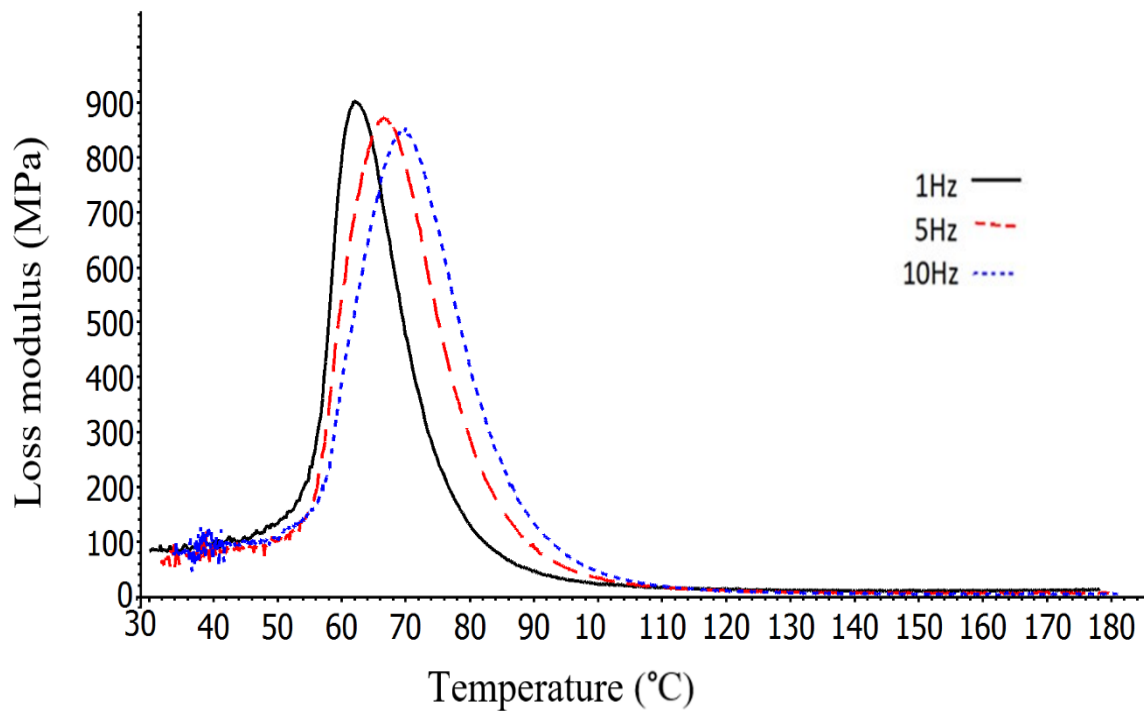


Figure 3.10: Loss modulus of the BFRP composites, as a function of the temperature, at 1, 5 and 10 Hz

Figure 3.11 presents the $\tan\delta$ curves of the BFRP composites, over the temperature range 30–180 °C, at 1, 5, and 10 Hz. As observed in this graph, $\tan\delta$ values remain almost stable at low temperatures, whereas after approximately 50 °C, they follow a steep upward trend, achieving peak values; then they fall steeply until zero values which are maintained up to the final 180 °C.

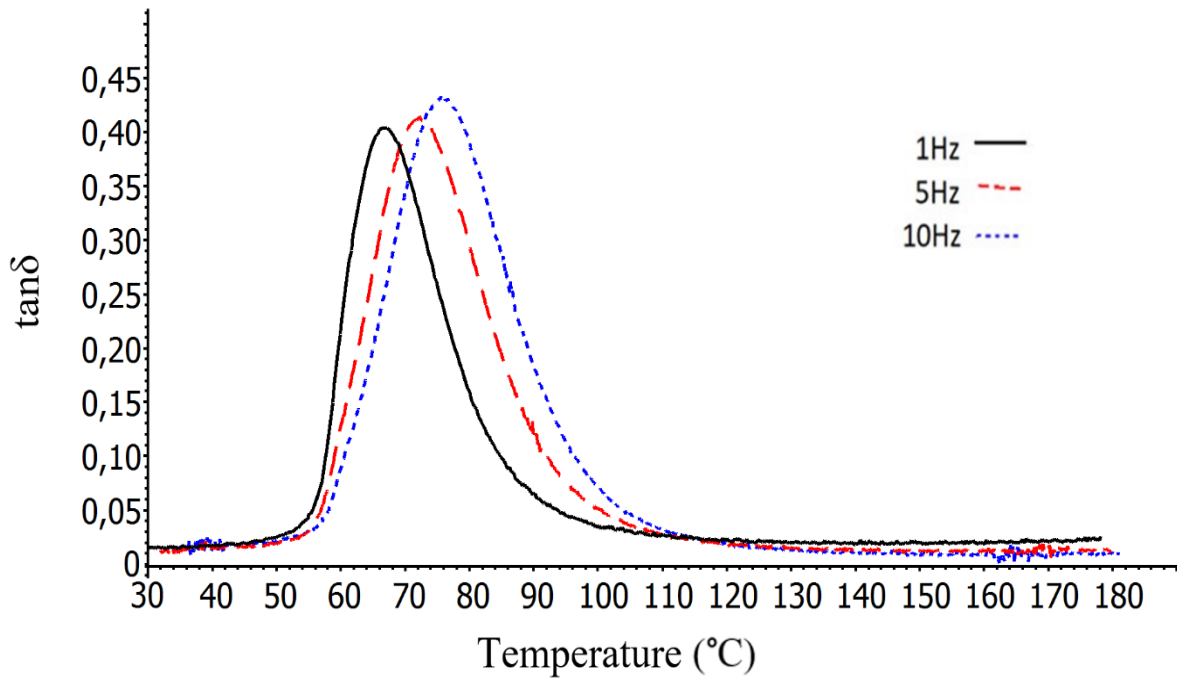


Figure 3.11: $\tan\delta$ of the BFRP composites as a function of the temperature at 1, 5, or 10 Hz

The T_g of the BFRP composites, which was identified by the corresponding temperatures of the peak of $\tan\delta$ and loss modulus curves, are depicted in Table 3.1. In this table, it can be noticed that as frequency increases, the BFRP composite exhibits higher T_g ; based on the $\tan\delta$ the T_g is higher than the $\tan\delta$ acquired from the loss modulus. The same trend was also noticed in the study of the GFRP and CFRP composites. Thus, it seems that in epoxy matrix composites, it is a rule the $\tan\delta$ results in higher T_g than the loss modulus. Moreover, it could be concluded that the BFRP composites exhibit high T_g regarding cold-cured polymer composites.

Table 3.1 T_g of the BFRP composites

Frequency	1 Hz	5 Hz	10 Hz
T_g (peak of $\tan\delta$)	67.1 °C	72.1 °C	75.4 °C
T_g (peak of loss modulus)	61.8 °C	66.5 °C	69.2 °C

3.4.3 Thermomechanical analysis creep-recovery and Thermomechanical analysis stress-relaxation

The creep-recovery behavior of the BFRP composites, under an initial force of 1, 3 and 5 N, at 25 °C, is illustrated in Figure 3.12. As it can be seen, the creep behavior of the BFRP composites increases very slightly during the exertion of force whereas their structure recovery appears immediately after the force release. Moreover, the 3 and 5 N forces provoked the highest final plastic deformation on the structure of the composites.

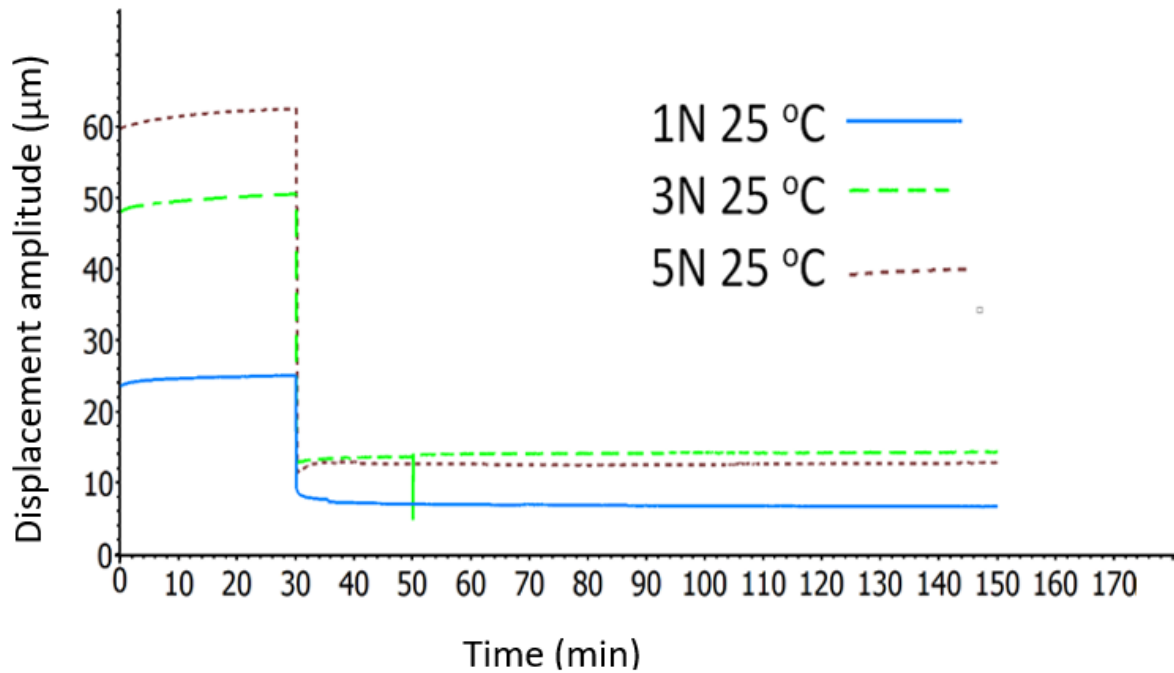


Figure 3.12: The creep-recovery curves of the BFRP composites, at 25 °C, and under 1, 3 and 5 N

The effect of 25, 50 and 75 °C, on the creep-recovery behavior of the BFRP composites is shown in Figure 3.13. As expected, as the temperature is raised, the resistance of the BFRP composite to deformation is reduced. Notably, in higher temperatures the viscoelasticity of the BFRP composites' structure becomes more evident in the very first minutes of the experiments.

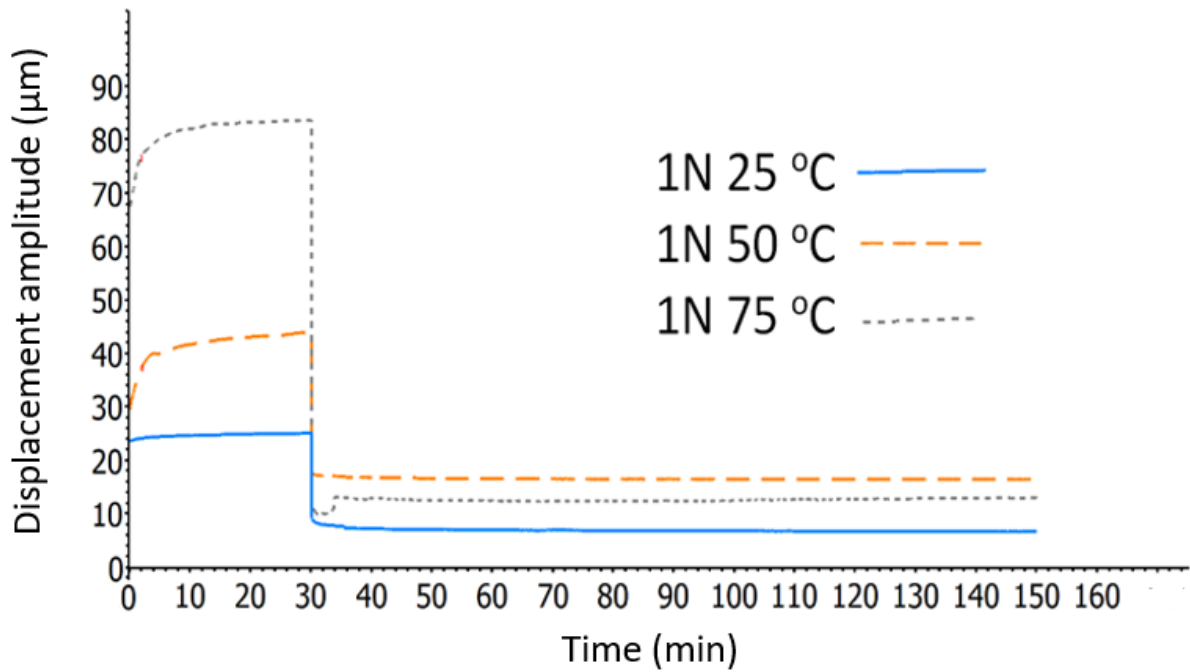


Figure 3.13: The effect of 25, 50 and 75 °C on the creep-recovery of the BFRP composites, under initial force of 1 Newton

The effect of 25, 50 and 60 °C, on the stress-relaxation behavior of the BFRP is illustrated in Figure 3.14. As it can be observed, in the first minutes of these experiments, the BFRP composites show relaxation and their viscoelastic behavior whereas then the curves become almost flat.

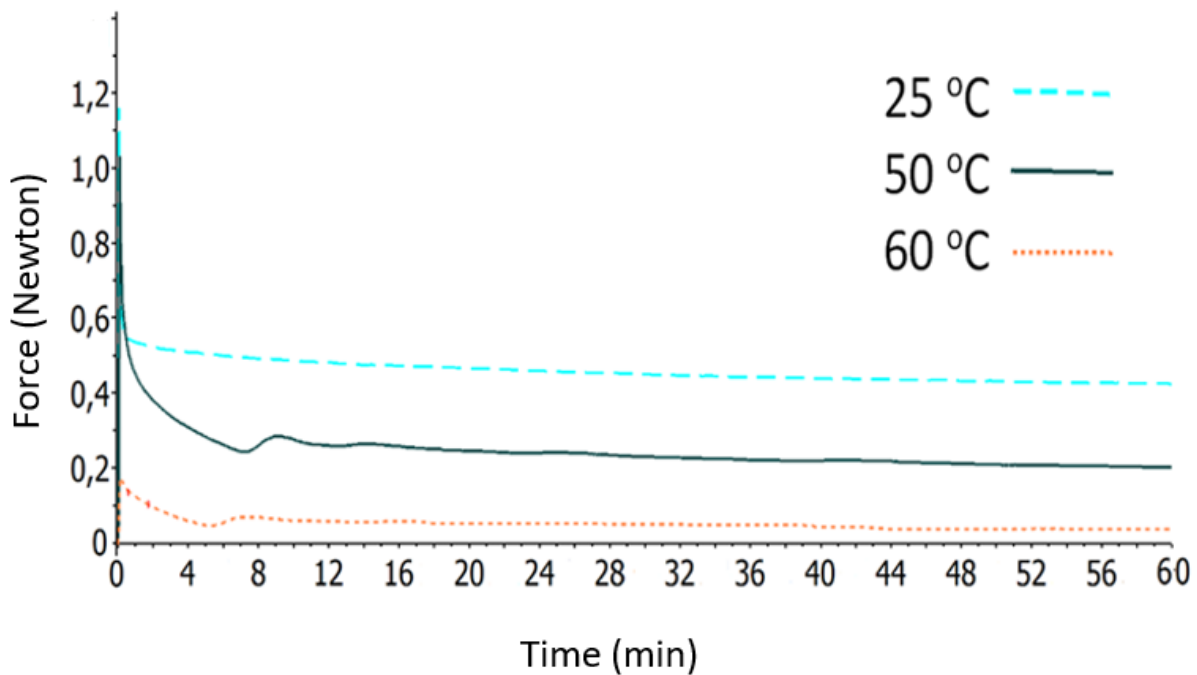


Figure 3.14: Stress-relaxation curves of the BFRP composites at 25, 50 and 60 °C

3.4.4 Mechanical properties

During the investigation of FRP composites, identification of their flexural strength is of significant importance, as this property is in strong correlation with the quality of the matrix-fiber interface. Moreover, a strong interfacial adhesion contributes to the load being effectively transferred from the soft organic matrix to the stiff fibers, thus improving the whole load bearing capacity of the composite structures [53]. Table 3.2 presents the three-point bending experiments results in detail and Figure 3.15 depicts the flexural stress (σ_f) versus flexural strain (ϵ_f) curves. It should be noted that the BFRP composite specimens did not break under the bending forces, so the experiments were performed until a relative high deformation of the specimens is achieved. In Table 3.2, it can be observed that the BFRP composite specimens exhibited relatively high σ_f , indicating thus that a very good interfacial bond between fibers-epoxy has been achieved.

σ_{fmax} = maximum flexural stress

δ = deformation

ΔL = displacement

W = work

Table 3.2 Three-point bending results

	Flexural modulus (MPa)	σ_{fmax} (MPa)	ΔL at σ_{fmax} (mm)	Upper yield point (N)	δ at upper yield point (mm)	W at max force (Nmm)
1	19500	283	2.3	195	2.3	240.84
2	18600	248	2.6	171	2.6	269.1
3	18500	262	2.4	177	2.4	225.78
4	20100	335	2.9	237	2.9	377.71
Average value	19200	282	2.5	195	2.5	278.35

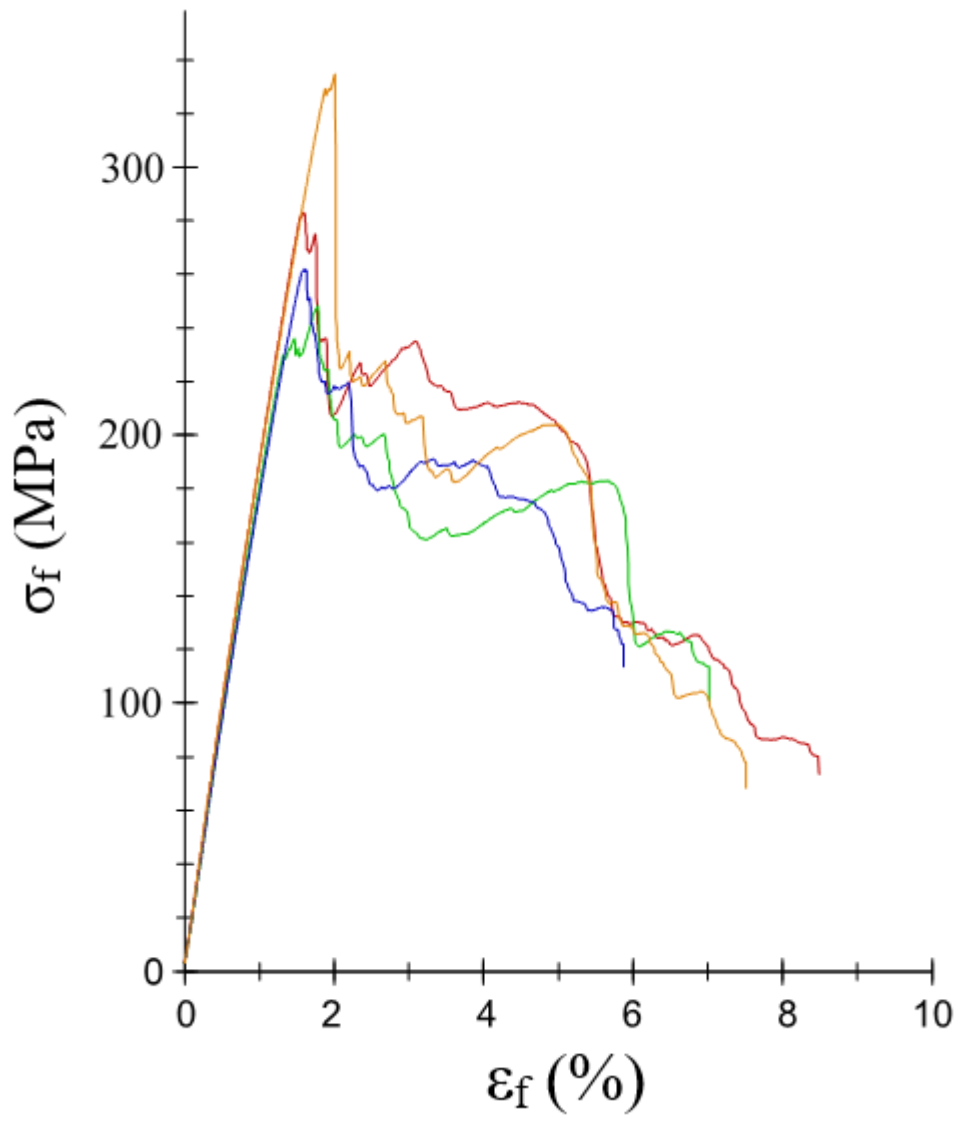


Figure 3.15: The four $\sigma_f - \epsilon_f$ curves of the BFRP composites

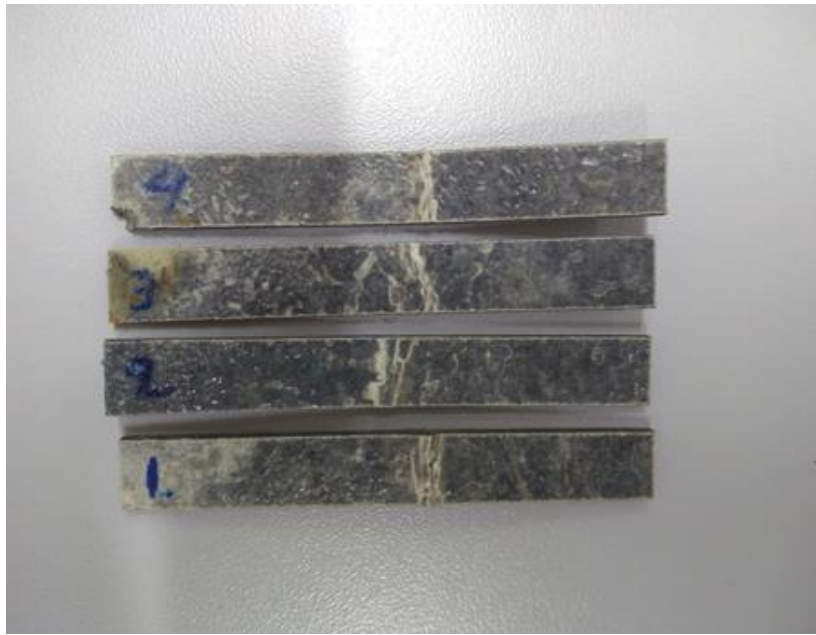


Figure 3.16: The three-point bending specimens after the experiments

In uniaxial tests, the stress (σ) is defined as the ratio of the force to the cross-sectional area in which the force is applied. Moreover, it has value in SI the Pascal. Critical parameter is the strain (ϵ), which is the ratio of the change in length (ΔL) to the primary length, and the tensile tests are presented in σ - ϵ graphs.

$$\sigma = \frac{F}{A} \text{ Pascal (3.1),}$$

where F = force (N) and A = cross-sectional area (mm)

$$\epsilon = \frac{L-L_0}{L_0} \text{ mm or \% (3.2) where } L = \text{final length and } L_0 = \text{primary length}$$

E = young modulus

The ratio of stress to strain (stiffness), that a material exhibits at the elastic stage of a tensile experiment, is the Young Modulus [54]. The exact point where the material starts to acquire permanent deformation is named ‘elastic limit’; if the stress is relieved before this point, the material recovers to its primary size and shape. Furthermore, the amount of stress which causes a material to have plastic strain of 0.2% is the 0.2% offset yield strength [55]. The symbol of the 0.2% offset yield strength is the $\sigma_{0.2}$.

Figure 3.17 illustrates the five σ - ϵ curves of the BFRP composites whereas their tensile characteristics are presented in detail in Table 3.3. As it can be revealed, the σ - ϵ curves after the elastic limit, about $\sigma = 80$ MPa, follow a linear trend, pointing out that there are not early microcracks in the composite structure. Thus, a uniform and strong adhesion interface has been formed between basalt fibers-epoxy matrix. Moreover, a relatively good reliability can be obtained, with the assumptions of the simple hand lay-up fabrication method. The composite heterogeneous structure, as three tensile specimens exhibited identical curves whereas the other two follow in general the same general trend, even though they exhibited lower maximum values. In comparison with the σ_f , the σ of the BFRP composite is significantly lower. Overall, the BFRP composites exhibited high maximum stress (σ_{max}) confirming hence their high quality.

Table 3.3 Tensile experimental results of the BFRP composites

	Young modulus (MPa)	$\sigma_{0.2}$ (MPa)	σ_{max} (MPa)	ϵ (%)
1	26500	2640	520	4.8
2	25800	2470	439	4.3
3	26900	2630	526	5
4	26400	2550	473	4.5
5	26600	2610	514	4.8
Average value	26400	2580	494	4.7

Table 3.4 Tensile experimental results of the BFRP composites (continue of Table 3.3)

	ΔL at breakage (mm)	W at force (Nmm)	W at fracture (Nmm)
1	2.4	15406.3	15868.5
2	2.1	11839.5	11884.7
3	2.5	16315.3	16432
4	2.5	13152.4	15403.5
5	2.4	15439.6	15485.6
Average value	2.4	15014.9	15014.9

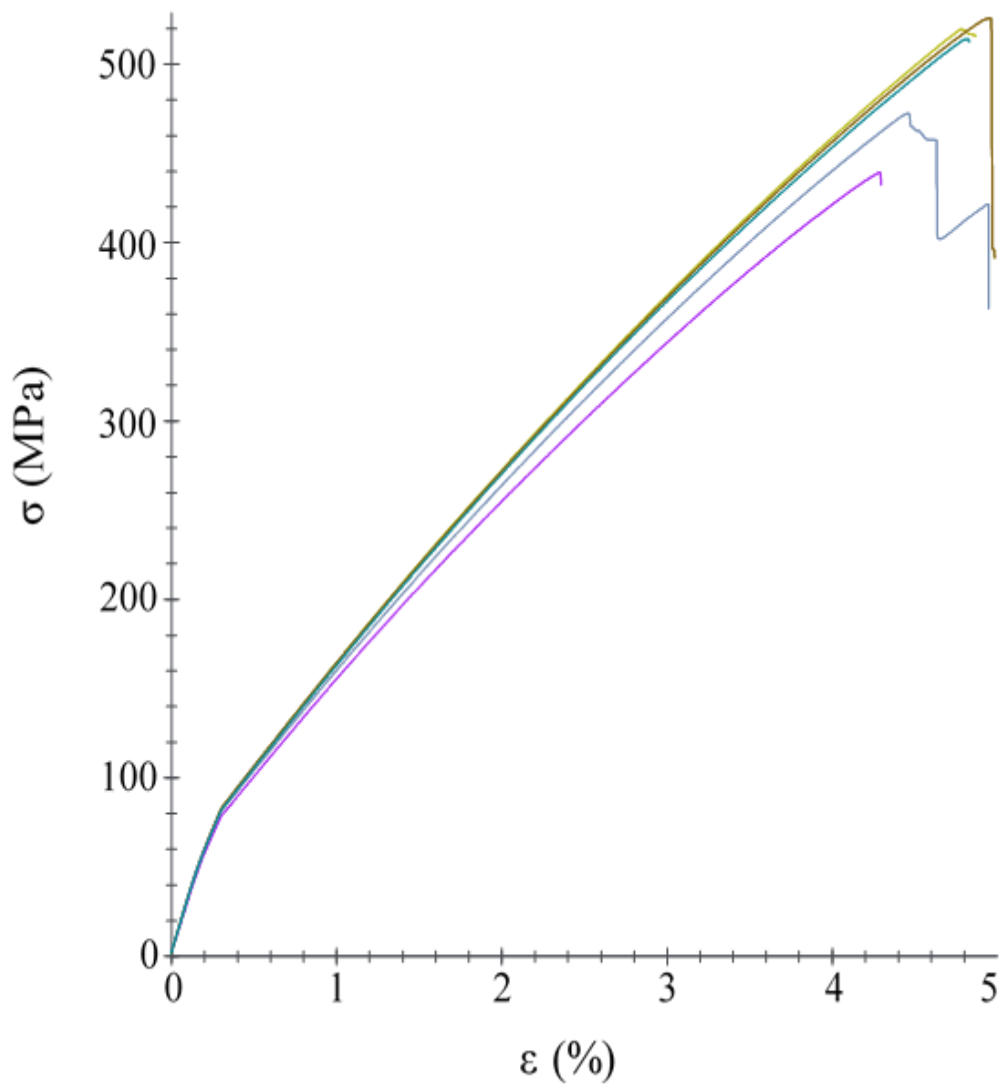


Figure 3.17: σ - ϵ curves of the five tension experiments



Figure 3.18: tension specimen on the grips after the breakage

3.4.5 Thermogravimetric analysis

Figures 3.19, 3.20 and 3.21 depict the thermal decomposition of the BFRP composites, in the range 30-900 °C, under nitrogen and air atmosphere, respectively. As can be seen, under both atmospheres, the main weight loss of the BFRP composites starts approximately above 250 °C; this is attributed to decomposition of the epoxy matrix. Moreover, it is revealed that oxygen atmosphere is more harmful during the thermal decomposition of the matrix than nitrogen, as in the former atmosphere the epoxy has completely decomposed up to the 550 °C, whereas in the latter atmosphere, its decomposition appears continuous, with a slow rate up to the 900 °C; the following graphs show that the basalt fibers are not thermally affected in this temperature range. A remarkable point in DTG graphs is maximum peaks which correspond to the maximum

degradation rate of the investigated materials. In the case of TGA in N_2 environment, one peak appears at about $341\text{ }^\circ\text{C}$, attributed to matrix degradation whereas in air atmosphere, two maximum heating rates are presented, at $336.4\text{ }^\circ\text{C}$ and $458.6\text{ }^\circ\text{C}$. Furthermore, in N_2 atmosphere, two samples, taken from different places of the BFRP composite plate, were TGA tested, so as to check the reliability of the composites' production method. These results are shown in Figures 3.19 and 3.20. It is clear that both curves are very identical, confirming thus that a steady Φ_f and uniform mixture of basalt fibers/epoxy has been formed in the composite structure. The hand lay-up compression molding method is qualified as highly efficient and reliable method for the production of FRP composites.

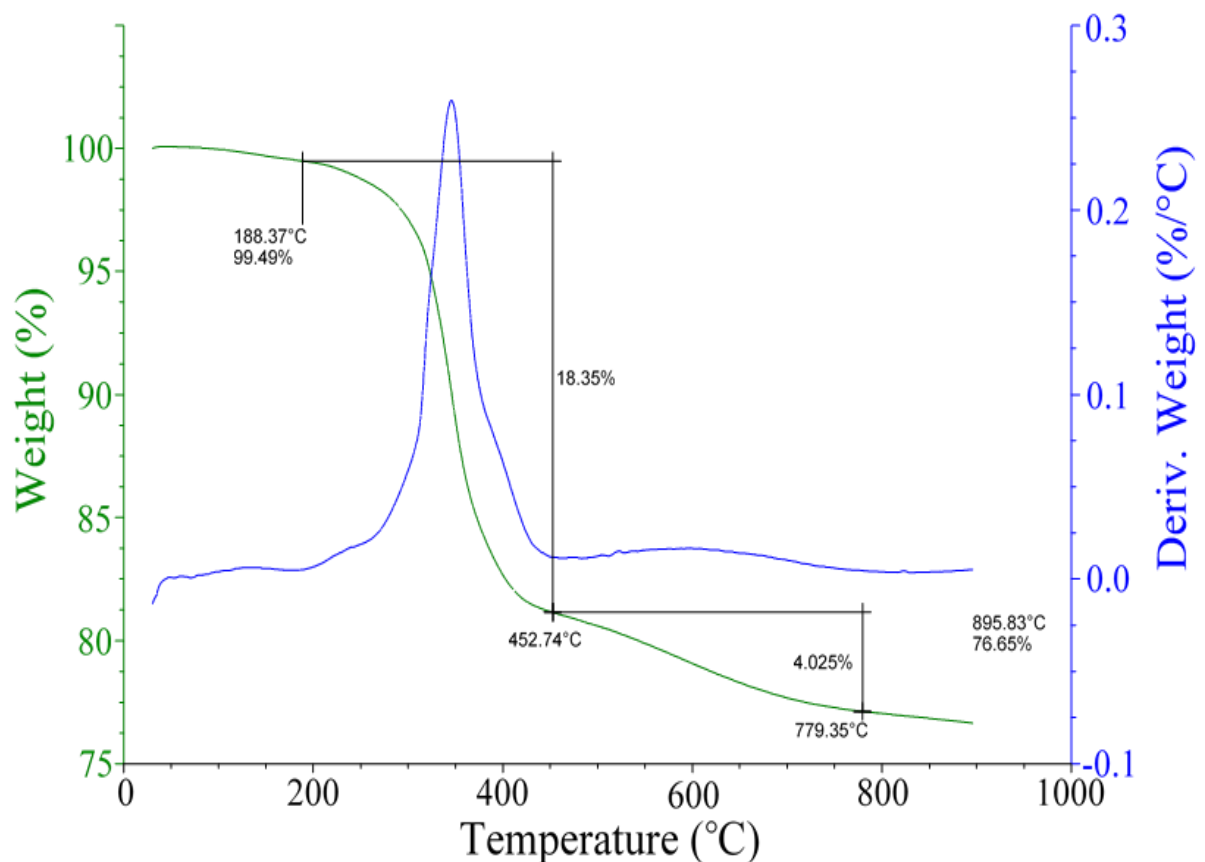


Figure 3.19: TGA results showing the weight (%) and weight loss rate (DTG) of the BFRP composite as a function of the temperature in N_2 atmosphere (first sample)

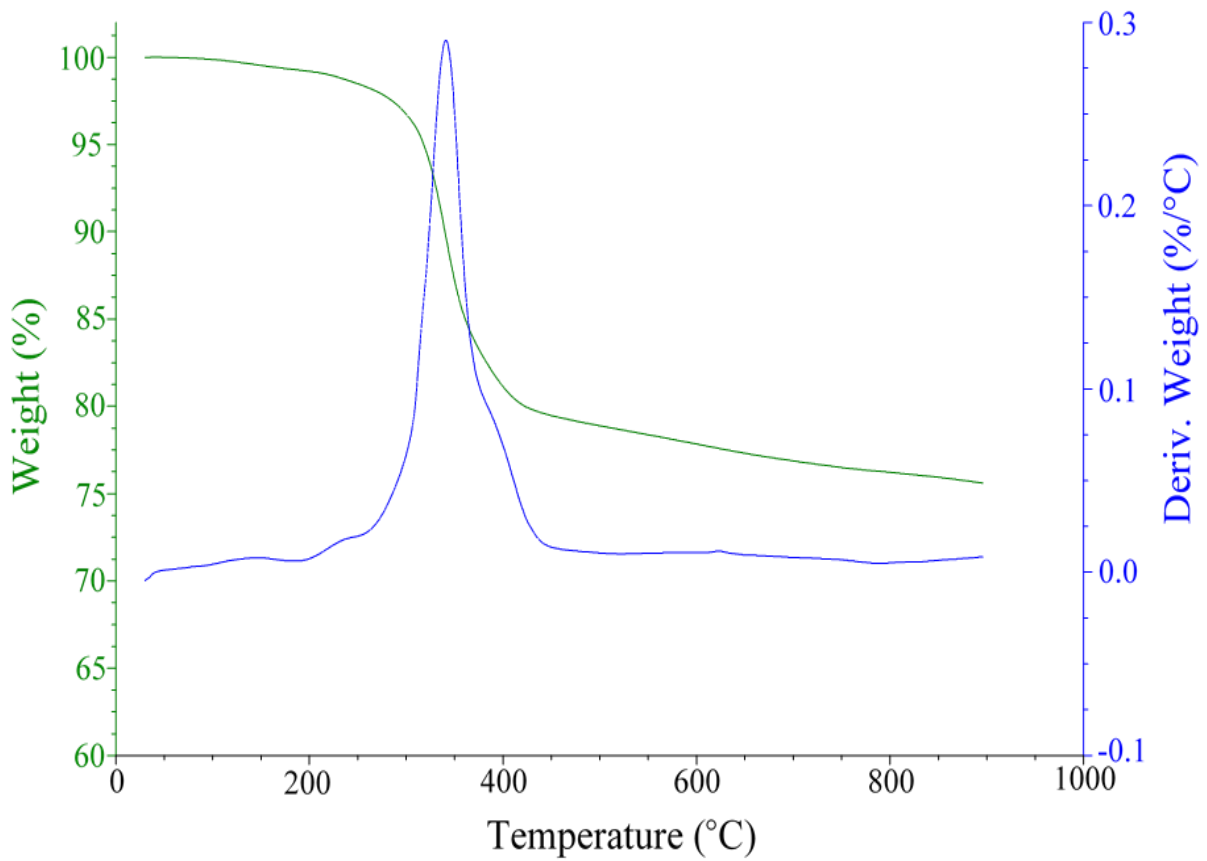


Figure 3.20: TGA results showing the weight (%) and weight loss rate (DTG) of the BFRP composite as a function of the temperature in N₂ atmosphere (second sample)

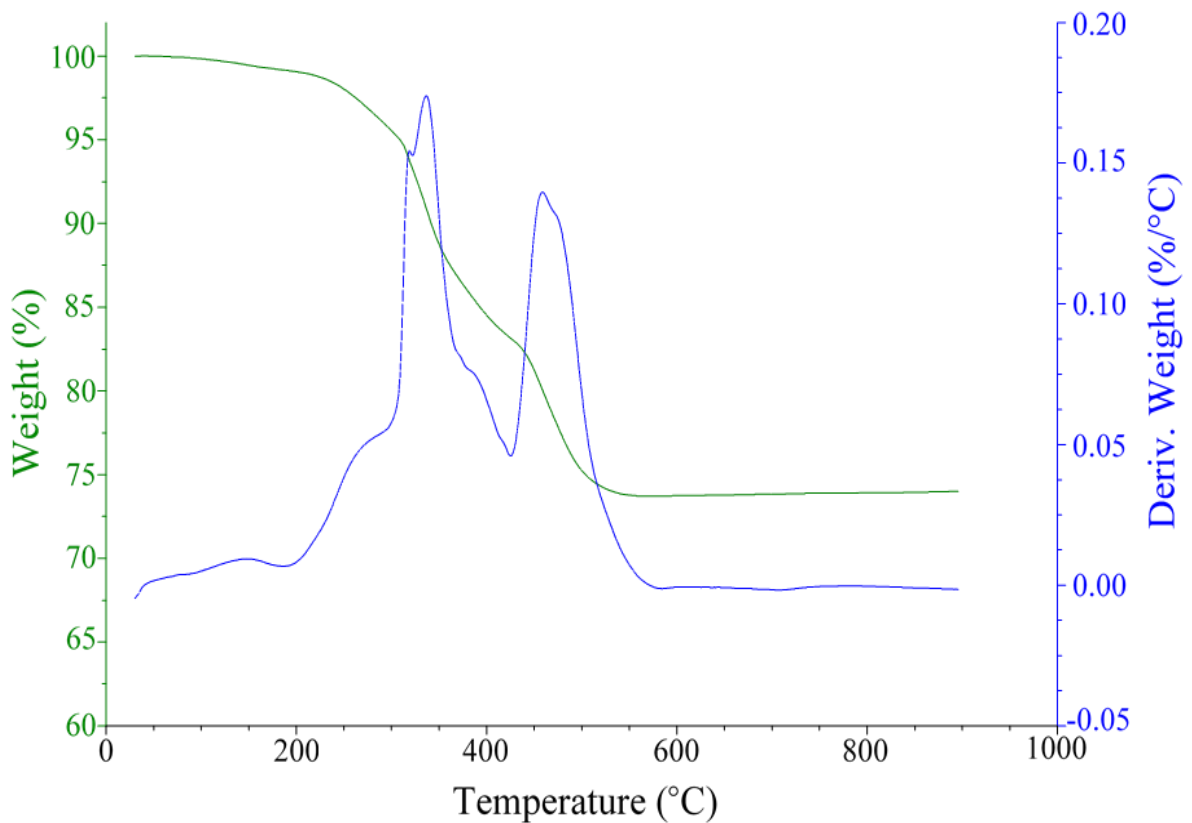


Figure 3.21: TGA results showing the weight variation and weight loss rate (DTG) of the BFRP composite as a function of the temperature, in air atmosphere

Figures 3.22 and 3.23 depict thermal decomposition of the basalt fibers, in the range 30 – 900 °C, in N₂ and air atmosphere, respectively. From these graphs, it is revealed that the basalt fibers have excellent thermal resistance, as they are not thermally affected up to the final 900 °C in both atmospheres. For sure, the basalt fibers are highly recommended in applications where high thermal resistance is a required factor.

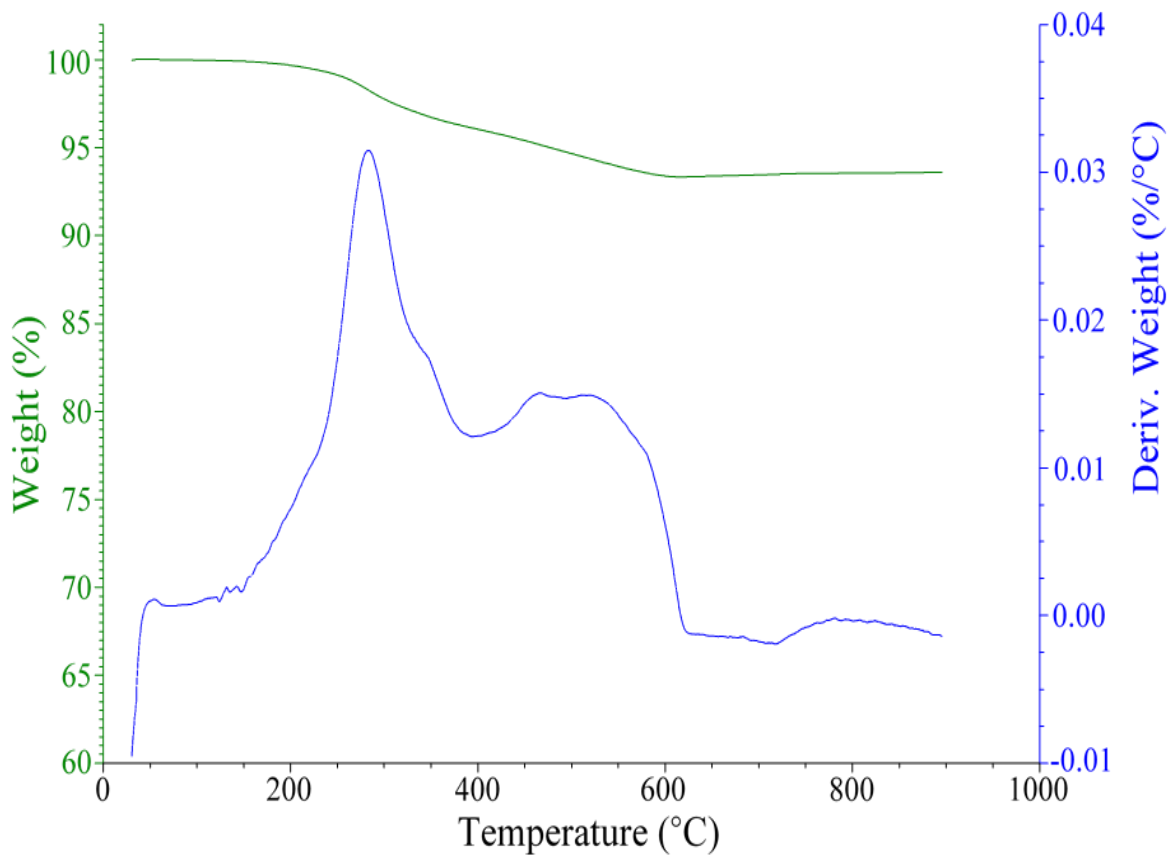


Figure 3.22: TGA results presenting the weight (%) variation and weight loss rate (DTG) of the basalt fibers* in N₂ atmosphere.

*The basalt fibers were taken from the edges of the BFRP composite plate, so they were not absolutely pure. The approximately 6% weight reduction which takes part in temperature range 200–600 °C is attributed to thermal decomposition of a very small part of epoxy which was stuck on the basalt fibers during the composites' production. This is also verified by the fact that after the approximately 600 °C, the basalt fibers were not thermally affected.

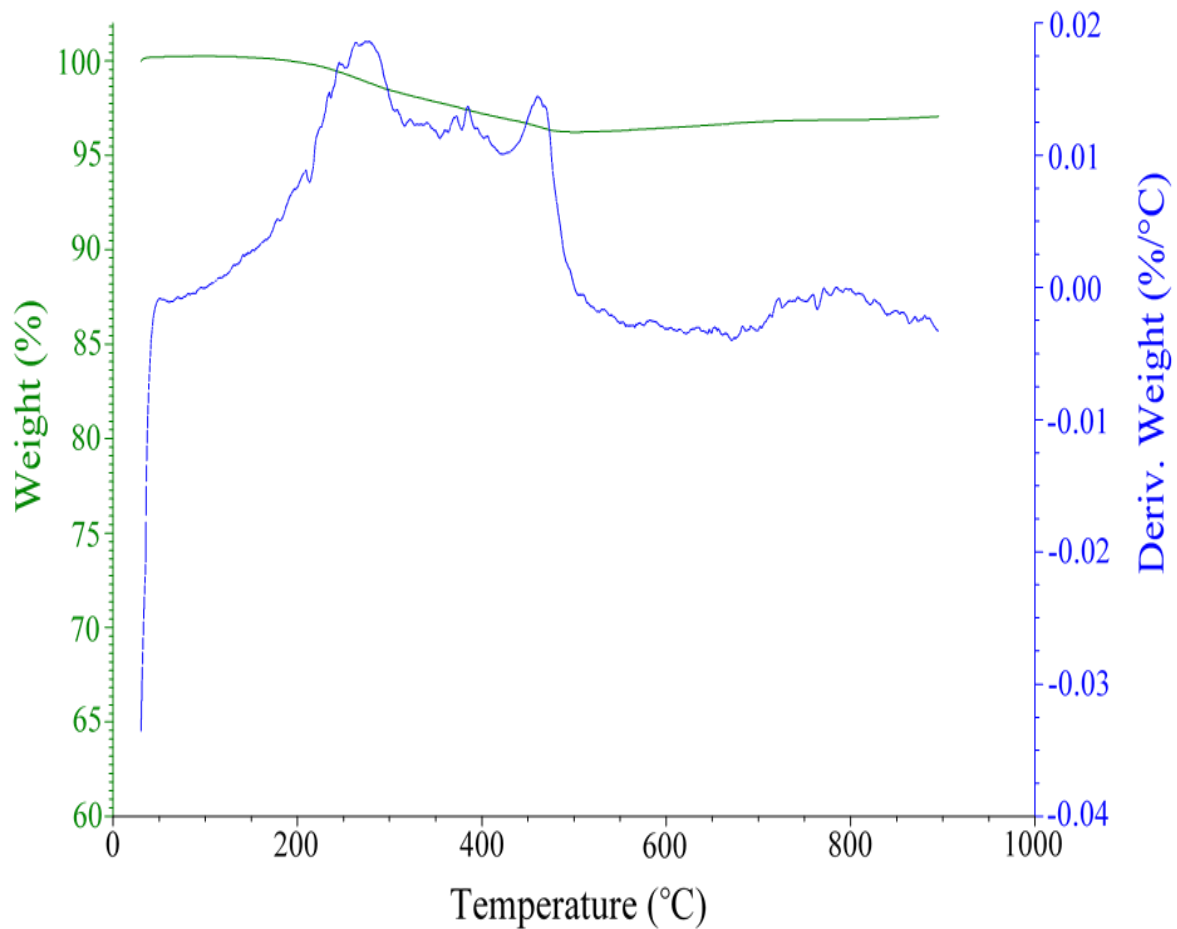


Figure 3.23: TGA results showing the weight (%) variation and weight loss rate (DTG) of the basalt fibers* in air atmosphere

*The basalt fibers were taken from the edges of the BFRP composite plate, so they were not absolutely pure. The approximately 4% weight reduction which takes part in the temperature range 200–500 °C is attributed in thermally decomposition of a very small part of epoxy which was stuck on the basalt fibers during the composites' production. This is also verified from the fact that after approximately the 500 °C the basalt fibers are not thermally affected.

3.5 Calculation of the volume fraction of the fibers (Φ_f) and volume fraction of the matrix (Φ_m).

The TGA results of the BFRP composite in air atmosphere (Figure 3.21) demonstrates that the thermal decomposition curve of the BFRP composite after 550 °C becomes steady and flat, pointing thus that the epoxy matrix has been

completely decomposed whereas at the same time the basalt fibers were not thermally affected. At 550 °C, the weight of the BFRP composite is 73.76 %, including only the basalt fibers. So, by using the appropriate equation and the known densities of the basalt fibers and epoxy matrix, Φ_f was calculated.

$$W_f = 73.76\% \text{ and } W_m = 26.24 \%$$

$$\Phi_f = \frac{1}{1 + \frac{\rho_f}{\rho_m} \left(\frac{1}{W_t} - 1 \right)} = 53.66\% \quad (3.3) \quad [56]$$

Where: ρ_m = density of matrix = 1.10 g/cm³, ρ_f = density of reinforcement phase = 2.67 g/cm³, W_t = weight proportion of the reinforcement phase

So, finally, $\Phi_f = 53.66\%$ and $\Phi_m = 46.34\%$.

3.6 Conclusions regarding the BFRP composites

Based on experimental results, the following conclusions can be drawn. The BFRP composites exhibited high T_g , with the assumption of the cold-curing production method, which was followed. This characteristic classifies them as potential materials in a broad range of applications. Additionally, in temperatures over T_g , the composites reduced their resistance in deformation forces, fact confirming that T_g is a critical point in the behavior of FRP composites.

Based on DMA results, it was revealed that as frequency is increased the BFRP composites achieve higher T_g and that T_g based on $\tan\delta$ is higher than T_g acquired from the loss modulus curves.

One of the significant outputs of this research is the thermal resistance of basalt fibers, as these were not thermally influenced, in oxygen or N₂ atmosphere, up to the final 900 °C of TGA experiments. This characteristic of the basalt fibers can be attributed to their origin from the earthquake lave. Moreover, due to the basalt fibers' relative low density, the combination of them in a polymer matrix results in a composite with low weight, attributing thus to very important materials' characteristics, such as high strength-to-weight and high stiffness-to-weight ratios. These characteristics, in conjunction with the relative low price of the basalt fibers and their natural origin, classifies them as a very promising material in FRP composites industry.

Generally speaking, the BFRP composites exhibited high tensile and flexural strength, verifying a very good interfacial bond formed between basalt fibers-

epoxy; the FRP composites demonstrate a low mechanical behavior in the case of a poor bond between matrix-fibers. In addition, the BFRP composite plate has a stable thickness through its entire structure (+0.1 mm). So, the novel hand lay-up compression molding method is characterized as a highly efficient and reliable technique for the preparation of FRP composites with significantly high Φ_f .

3.6.1 Analytical theoretical model for the prediction of the BFRP composites tensile strength

In order to achieve the optimal design and modelling of the FRP composites, scientists have been using analytical theoretical models. In particular, these tools offer a deep investigation of the composites' mechanical behavior as well as significant saving in time and materials.

Hirsch's model

The x can be in the range 0-1, so as to be chosen in the most accurate fit [57]. For the case of the particular BFRP composite, their tensile strength is predicted quite accurate for $x = 0.22$.

σ_{fiber} = tensile strength of fibers

σ_m = tensile strength of matrix

$\sigma_{\text{fiber}} = 4200 \text{ MPa}$, $\sigma_m = 45 \text{ MPa}$, $\Phi_f = 0.5366$ and $\Phi_m = 0.4634$

$$[57] \sigma = x \cdot (\sigma_m \cdot \Phi_m + \sigma_{\text{fiber}} \cdot \Phi_f) + (1-x) \frac{\sigma_{\text{fiber}} \cdot \Phi_m}{\sigma_m \cdot \Phi_f + \sigma_{\text{fiber}} \cdot \Phi_m} \Rightarrow (3.4)$$

$$\sigma = 0.22 \cdot (4200 \cdot 0.5366 + 45 \cdot 0.4634) + (1-0.22) \cdot \frac{4200 \cdot 0.4644}{45 \cdot 0.5366 + 4200 \cdot 0.4644} \Rightarrow$$

$$\sigma = 501.18 \text{ MPa}$$

The Hirsch model equation predicted with high accuracy the σ of the BFRP composites.

4. EXPERIMENTAL PART 3: PREPARATION, THERMAL ANALYSIS AND VARIOUS MECHANICAL PROPERTIES OF POST-CURED CARBON, ARAMID OR CARBON/ARAMID HYBRID FIBER EPOXY MATRIX COMPOSITES

The research about the AFRP composites has been published in the following journal:

KARVANIS, Konstantinos, Soňa RUSNÁKOVÁ, Ondřej KREJCI and Alena KALEDOVÁ. Thermal analysis of post-cured aramid fiber/epoxy composites. *Reviews on advanced materials*, 2021, volume 60. DOI: 10.1515/rams-2021-0036

4.1 Purpose of the research study and general information

In this research work, applying the vacuum infusion process (VIP), eight layered CFRP, ACFRP and AFRP composites, with twill 2/2 weave fibers fabric and epoxy matrix, were prepared and then post-cured under specific heating/cooling rates. The important point is that both fiber fabrics, carbon and aramid, have the same weave, thickness and dry weight; in this sense, the properties of composites can be compared and the advantages of each composite structure are revealed. The results are presented in two result parts: in the first part, the AFRP composites are investigated in depth with various thermal analysis techniques, so as the effect of the post-cure process on them to be deeply explored; in the second part, a comparison between thermal behavior and mechanical properties of the CFRP and ACFRP composites is taking part.

It should be mentioned that most of the research works on thermal analysis of CFRP, AFRP and ACFRP composites, concentrate mostly on no more than two techniques in this sector whereas post-cured FRP composites, due to viscoelastic matrix, need to be explored by several thermal analysis techniques, in order for their T_g , dynamic mechanical properties and thermal decomposition to be investigated in depth. So, despite the fact that many research studies have been presented on thermal analysis of post-cured FRP composites, there are many points requiring further investigation.

4.2 Materials and preparation method

4.2.1 Materials

For the preparation of the CFRP, AFRP and ACFRP composites, carbon and aramid fiber fabrics, both produced by the company C. Cramer & Co, were used. These have the same characteristics, namely 160 sqm weight, twill 2/2 weave and thickness around 0.36 mm. In particular, the carbon fabric is the product code Style 442, composed of the fibers Pyrofil™ TR30S T-Size 3K 200tex (Mitsubishi Chemical), while the aramid fabric is the product code Style 502 (C. Cramer & Co) with fibers Kevlar49 T965 (1580dtex) (DuPont). The epoxy matrix is a mixture, parts by weight 100:30, of the epoxy Biresin® CR80 (Sika®) (Figure 4.1) and the hardener Biresin® CH80-2 (Sika®) which was gently stirred until homogeneity was achieved. The laminate structure of the hybrid ACFRP composite is composed of four aramid fiber fabric layers in the middle and of two carbon fiber fabric layers in up and down outer sides, respectively.



Figure 4.1: Biresin® CR80

Table 4.1 Materials used for the fabrication of the CFRP, AFRP and hybrid ACFRP composites

Epoxy matrix	Biresin[®] CR80 + Biresin[®] CH80-2
Reinforcement phase (fiber fabrics)	<p>1. Carbon fiber fabric Style 442 produced by C. Cramer & Co [58]</p> <ul style="list-style-type: none"> ➤ Weave: Twill 2/2 ➤ Thickness approximately 0.36 mm ➤ Dry weight 160 g/m²
	<p>2. Aramid fiber fabric Style 502 produced by C. Cramer & Co [59]</p> <ul style="list-style-type: none"> ➤ Weave: Twill 2/2 ➤ Thickness approximately 0.40 mm ➤ Dry weight 161 g/m²

Table 4.2 Physical data of the resin and the hardener [60]

	Biresin[®] CR80	Biresin[®] CH80-2
Viscosity, 25 °C, mPa.s	~ 900	~ 45
Density, 25 °C, g/ml	1.13	0.99

Table 4.3 Typical thermal properties of fully cured neat resin [60]

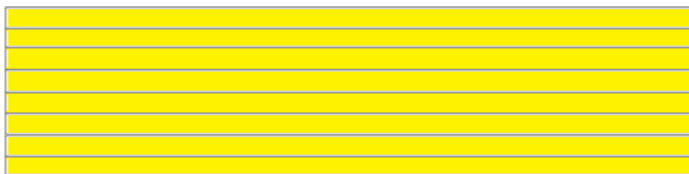
Biresin[®] CR80 plus Biresin[®] CH80-2	
Heat distortion temperature ISO 75A	89 °C
Glass transition temperature ISO 11357	93 °C

Table 4.4 Typical Mechanical properties of Fully Cured Neat Resin [60]

Biresin[®] CR80 plus Biresin[®] CH80-2	
Tensile strength ISO 527	88 MPa
Tensile E-Modulus ISO 527	2,900 MPa
Tensile elongation (at break) ISO 527	6.0 %
Flexural strength ISO 178	125 MPa
Flexural E-Modulus ISO 178	3,100
Compressive strength ISO 604	104 MPa
Density ISO 1183	1.16 g/cm ³
Shore hardness ISO 868	D 86
Impact resistance ISO 179	67 kJ/m ²



a)



b)



c)

Figure 4.2: The three types of the eight-layered composites (a) CFRP, (b) AFRP and (c) hybrid ACFRP

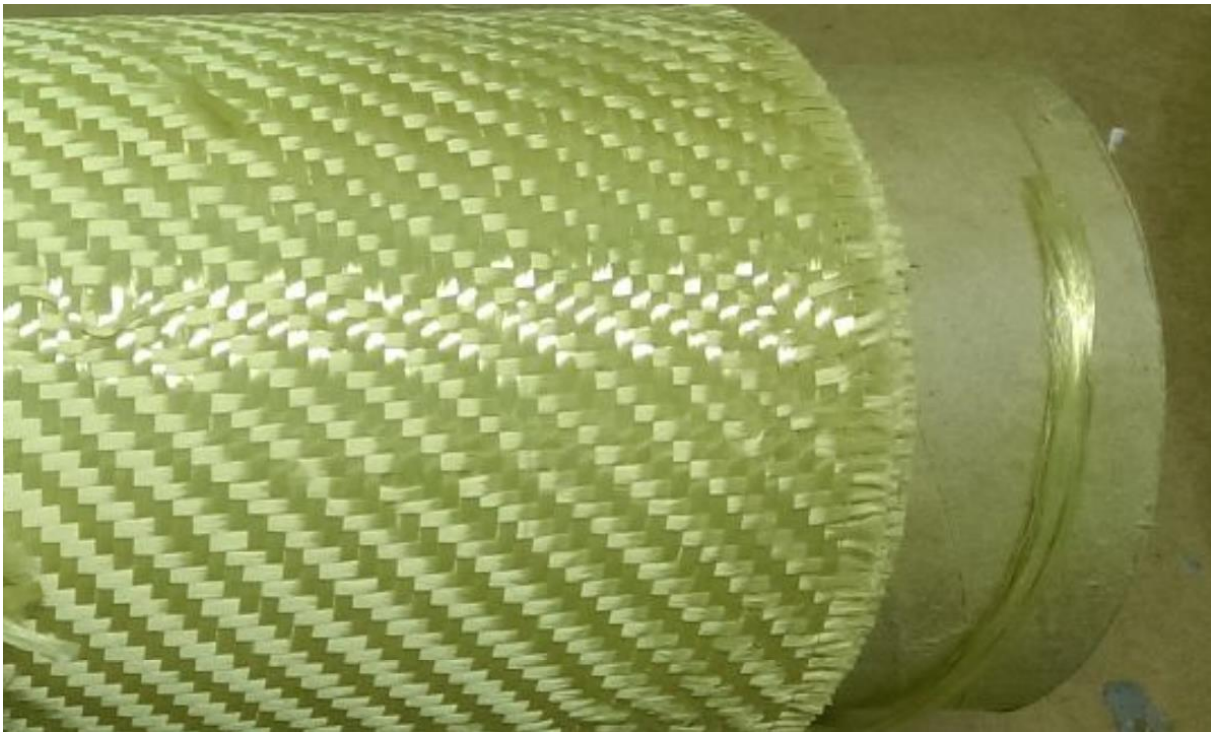


Figure 4.3: Zoom on the twill 2/2 aramid fiber fabric roll.

4.2.2 Preparation of the CFRP, AFRP and ACFRP composites

For the production of FRP composites, there are many variations of the VIP, with the differences between them been indistinguishable and based on the experience and preference of the according researcher. In order to avoid confusion, the CFRP, AFRP and ACFRP composites' production method in this study is simply named VIP while special attention is given on its accurate description.

In details, a rectangular plate of glass, with dimensions 90 mm × 62 mm × 10 mm (length x width x thickness) was used as the base of the vacuum system. In order to ensure a smooth surface, the upper part of this glass was polished three times with a wax. Next, eight layers of the reinforcement phase were cut, with dimensions 50 mm x 30 mm, and placed on the polished surface. In the next step, a peel ply and a perforated release film were placed over the fabrics' stacking and then a resin flow medium was used, so as to cover all of them.

Next, near and across the vertical sides of the fabrics, the resin distribution channels were placed; these included the infusion spiral medium flow and the two t-fittings, one connected with the vacuum pump and the other one with the resin supply. Finally, the whole system was closed by the vacuum bag, which was stuck

across the glass perimeter with sealant tape and an air leak test took part. Then, the vacuum pump was turned on and the resin, which was previously gently stirred until homogeneity, was infused in the mold with the supply tube. The composite plates were let for solidification, in laboratory environment, at 23 °C for 7 days, and then they were post-cured in an electric oven, modified with a PID controller, under the heating–cooling rates, suggested [60] by the resin producer (Figure 4.4). It should be referred that curing for 7 days at 23 °C was chosen, according to an example from the resin datasheet [60].

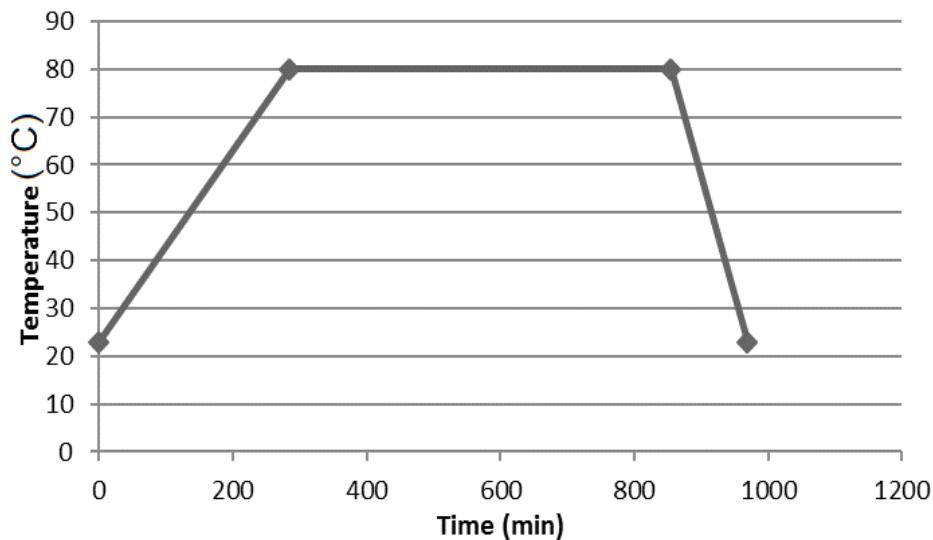


Figure 4.4: post-cure temperature diagram

During the post-cure process, firstly, the temperature was increased, with a heating rate of 0.2 °C/min, from 23 °C to 80 °C followed by an isothermal hold at 80 °C for 9.5 hours. Then, cooling of the composites plates took place, from 80 °C up to 23 °C, with a cooling rate of 0.5 °C/min. Finally, the specimens were cut in the desired dimensions with water jet tool. It is significant that during the AFRP composite plate preparation, the 8 layers of the aramid fibers fabric weight was measured and then compared with the final weight of the composite plate. It was found that the weight of the aramid fibers fabric is the 54% of the whole AFRP composite plate.

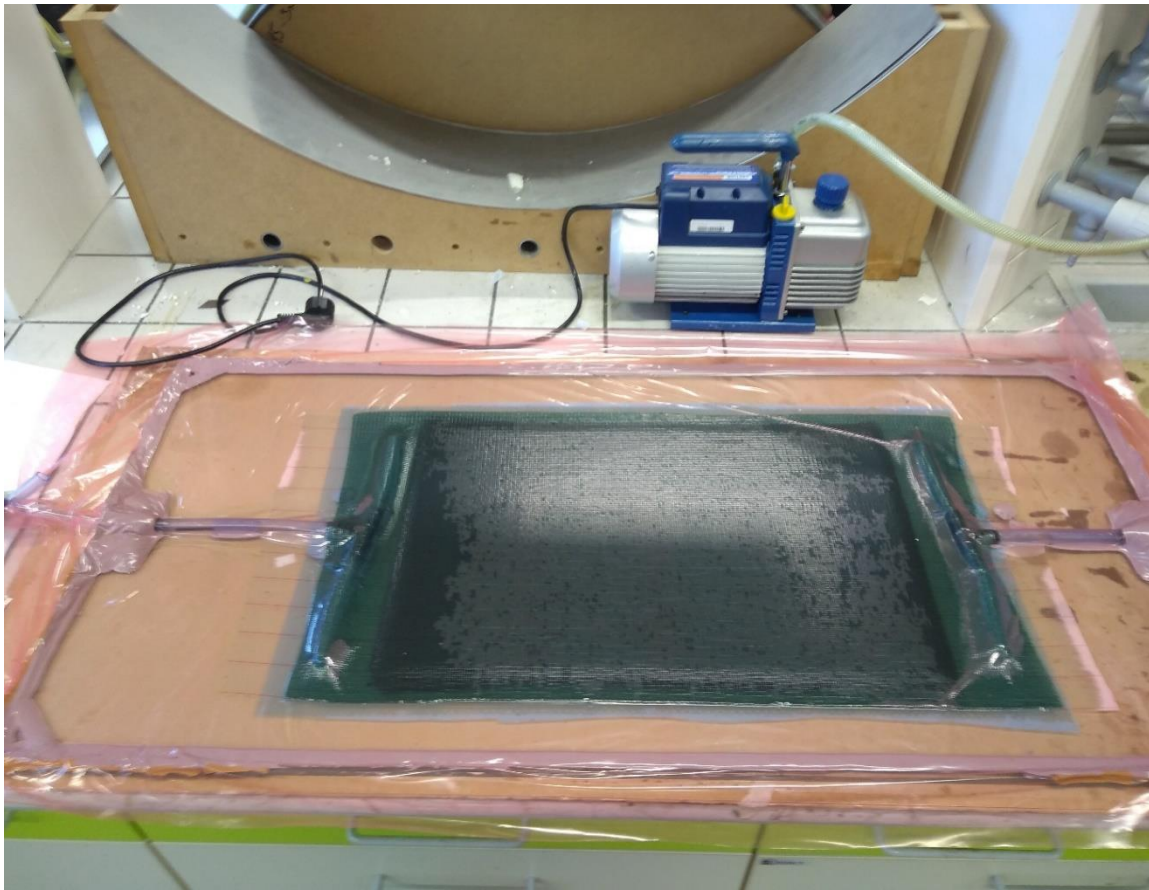


Figure 4.5: Preparation of the CFRP composite with the Vacuum Infusion Process. The photo was taken hours after the resin infusion.



a)



b)

Figure 4.6: a) and b) the two sides of the CFRP composite plate.

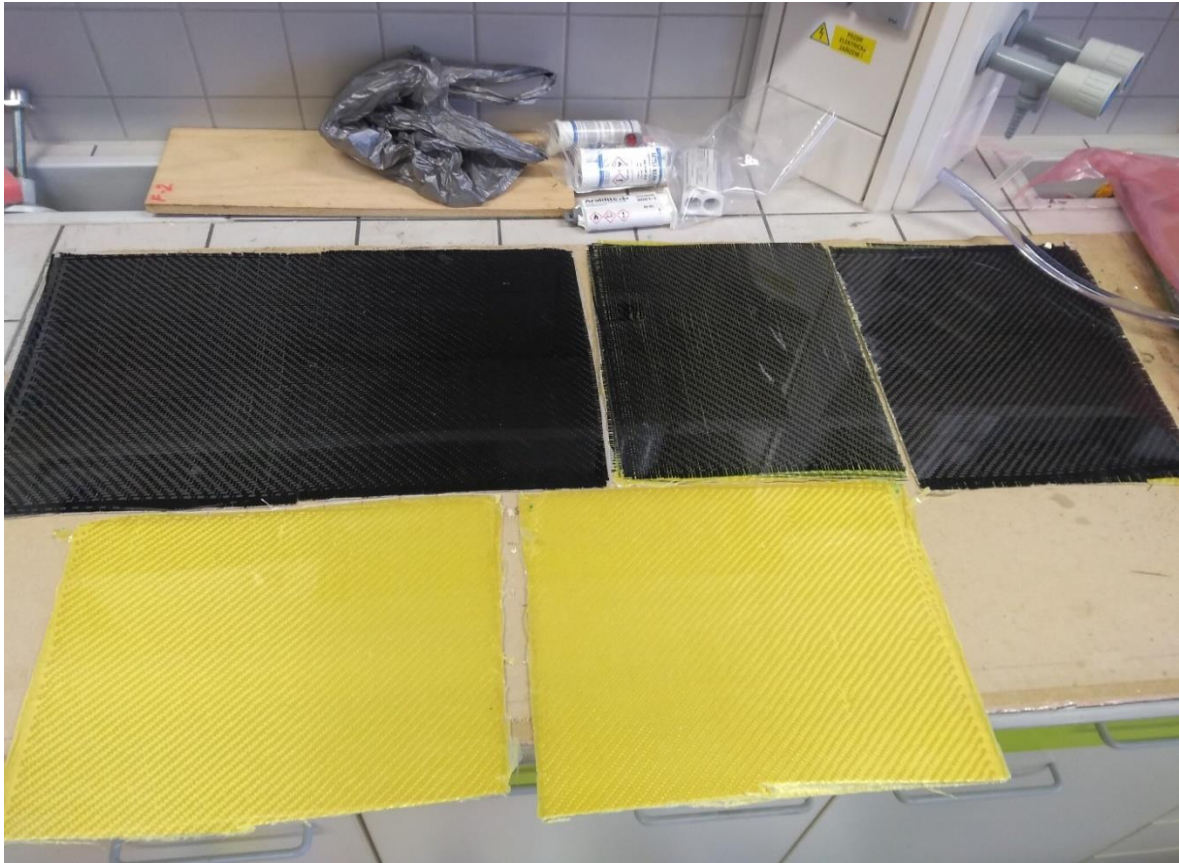


Figure 4.7: The prepared CFRP, AFRP ACFRP and composite plates. The laminates were cut in the half, through mechanical cutting, so as to be put in the oven.



Figure 4.8: Zoom view of the AFRP composite plate

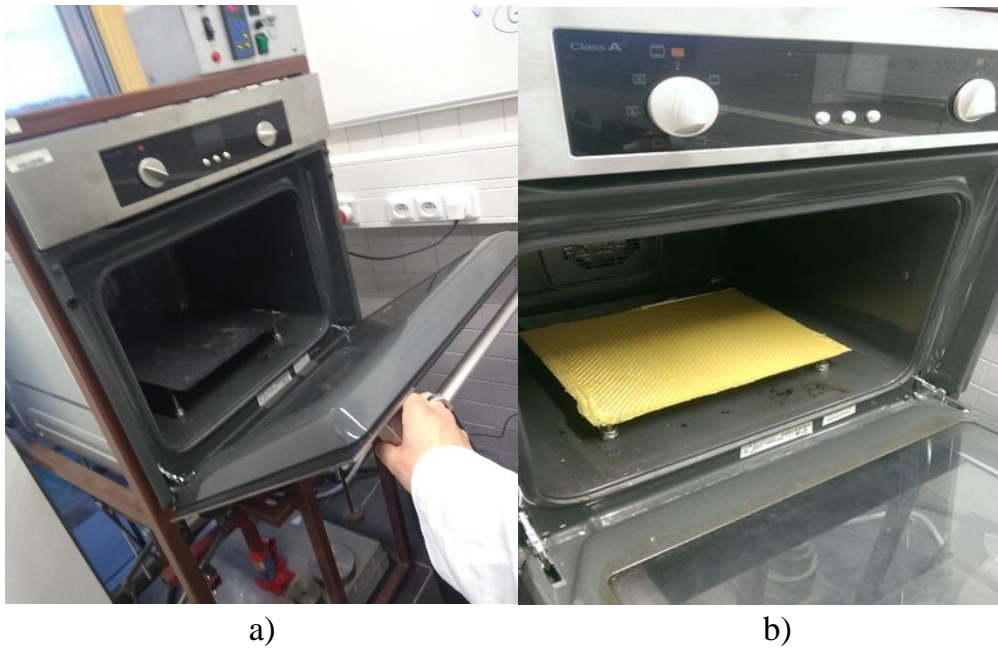


Figure 4.9: The post-cure process of the (a) CFRP and (b) AFRP in the oven. Down of the composites plates there is a metal plate for support.

4.3 Experiments

4.3.1 General experimental conditions

In all experiments of both thermal analysis and mechanical properties, the specimens were stored in laboratory environment, at 23 °C, for not less than 40 h prior the tests and experimental data were directly calculated by the according instrument software. Also, during the experiments, the conditions in the laboratory were at a temperature of 23 °C and humidity of approximately 50%.

4.3.2 DMA, TMA creep-recovery and TMA stress-relaxation experiments

The DMA, TMA creep-recovery and TMA stress-relaxation experiments were performed by the instrument DMA 1 METTLER TOLEDO (Schwerzenbach, Switzerland), under three-point bending configuration, using the STARe Software. In particular, the specimens were of rectangular shape with dimensions 40 mm x 5 mm x 1.75 mm. (length x width x thickness) (Figure 4.10) with a span length of 30 mm between the supports.

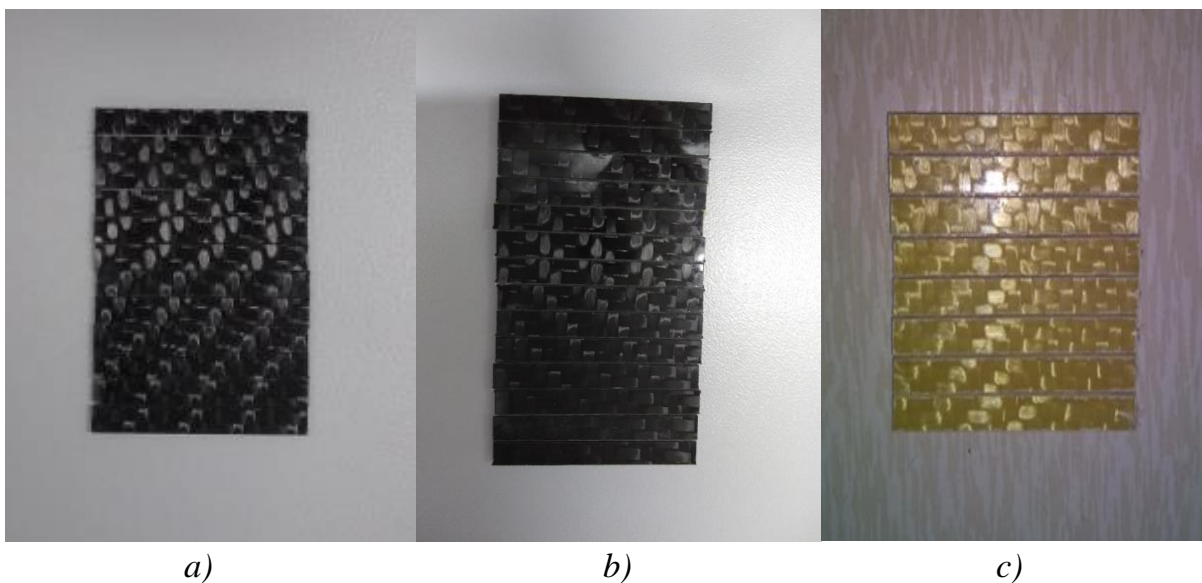


Figure 4.10: Part of the DMA, TMA creep-recovery and TMA stress-relaxation specimens of the (a) CFRP, (b) ACFRP and (c) AFRP composites.

In particular, the DMA took place by scanning in the range 30 °C to 200 °C, with a heating rate of 2 °C/min, under 1, 5 and 10 Hz, with the displacement been 15 µm whereas 1 Newton force was used as preload. Moreover, the temperature range was chosen based on the assumption that T_g of epoxy is about 90 °C, so

that the final 200 °C of the DMA experiments is enough for determination of the behaviour of the composites above their T_g .

The TMA creep-recovery experiments were exhibited at isothermal 25 °C, with a force of 1, 3 or 5 Newton applied on the specimens for 30 minutes and then their recovery was recorded under 0 N for 120 minutes; one more experiment of this type was carried out at 50 °C with initial force of 1 N. During the TMA stress-relaxation tests, 12 μm extension was applied on the AFRP composite specimen, at 25 °C and its time-dependent stress was measured for 48 minutes.

4.3.3 Thermogravimetric analysis

The TGA experiments were performed with the instrument TGA Q50 (Figure 4.11) from TA Instruments (New Castle, Delaware, USA). It should be noted that the TGA tests were set and performed with the Thermal Advantage Release 5.4.0 software while results were evaluated with the TA Instruments Universal Analysis 2000 version 4.5A program. Due to the fact that the TGA is of significant importance in the thermal analysis sector, various such experiments were undertaken. In detail, the following were evaluated by the TGA:

1. Thermal decomposition of pure post-cured epoxy, carbon fibers, aramid fibers and CFRP, AFRP and ACFRP composites, in the range of 30-900 °C, with heating rate of 10 °C/min, in air and nitrogen atmosphere, respectively. In the latter atmosphere, two samples taken from different places of the AFRP composite plate were tested, so as to check the production method reliability.
2. Thermal stability of aramid fibers, CFRP, AFRP and ACFRP composites and pure post-cured matrix, in N_2 atmosphere, at isothermal 350 °C for 240 minutes.
3. In order to determine the maximum temperature at which aramid fibers are not thermally affected, TGA isothermal scans, in nitrogen atmosphere, were exhibited in the range 360 – 380 °C with every 60 minutes step of 10 °C.
4. Carbon fibers were TGA tested at isothermal 450, 460, 470 °C, with every 60 minutes step of 10 °C.

In all TGA scans, an alumina crucible was used for placing the specimens and the totally flow rate was adjusted at 100 ml/min; balance purge flow 40 ml/min

and sample purge flow 60 ml/min. It needs to be mentioned that the composites were TGA tested with samples of 35 mg, since their complex composite structure requires enough mass during its TGA exploration. Meanwhile, carbon fibers, aramid fibers and pure post-cured epoxy matrix were TGA tested with samples of approximately 14-20 mg.

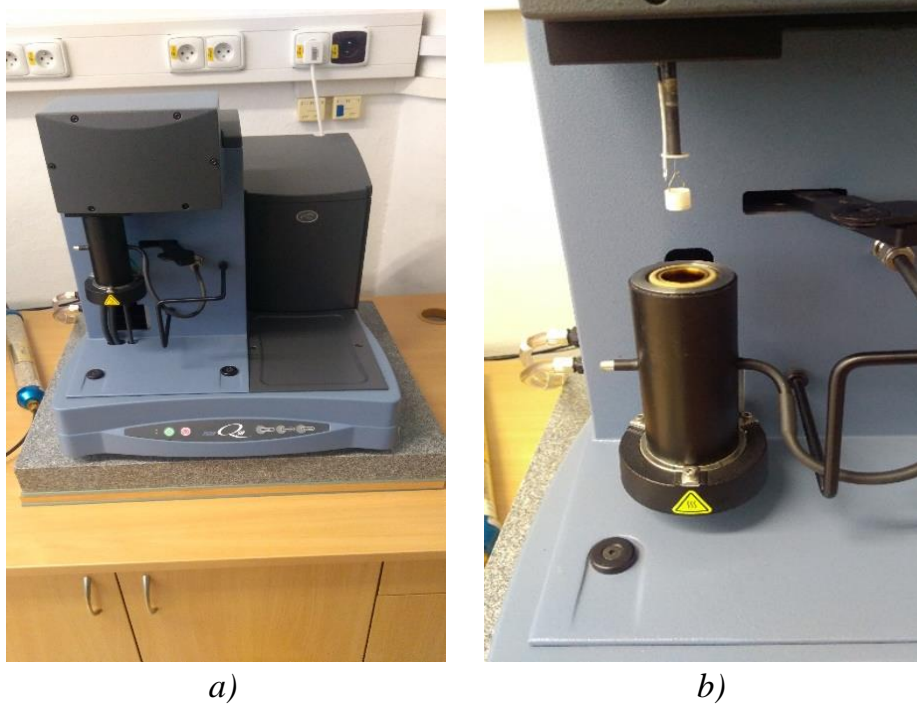


Figure 4.11: a) and b) TGA Q50 TA instruments

4.3.4 Differential Scanning Calorimetry (DSC)

The DSC experiments were carried out with the DSC 1 METTLER TOLEDO (Schwerzenbach, Switzerland), by scanning in the temperature range 30-600 °C, with a heating rate of 20 °C/min, in nitrogen atmosphere, using the software STARe SW 14.00. In this kind of experiment, the approximately 23 mg sample was placed in an aluminium sample holder of 40 ul and then it was heated and cooled twice.

4.3.5 Three-point bending on the CFRP and ACFRP composites

The flexural strength of the CFRP and ACFRP composites was determined by the testing machine Zwick/Roell 1456 (Ulm, Germany) (Figures 4.12, 4.13 and 4.14) with the software testXpert® II V2.1. In details, the specimens were of dimensions 100 mm x 14 mm x 1.86 mm (length x width x thickness) whereas the span length was 40:1. Specifically, in each side, the specimen was over hanged

the support of the three-point bending configuration by approximately 12.8 mm, so as to avoid specimen slipping while the force was applied in the specimen center. Moreover, the crosshead speed was set at 1mm/min and the tests were performed until breakage of the samples.

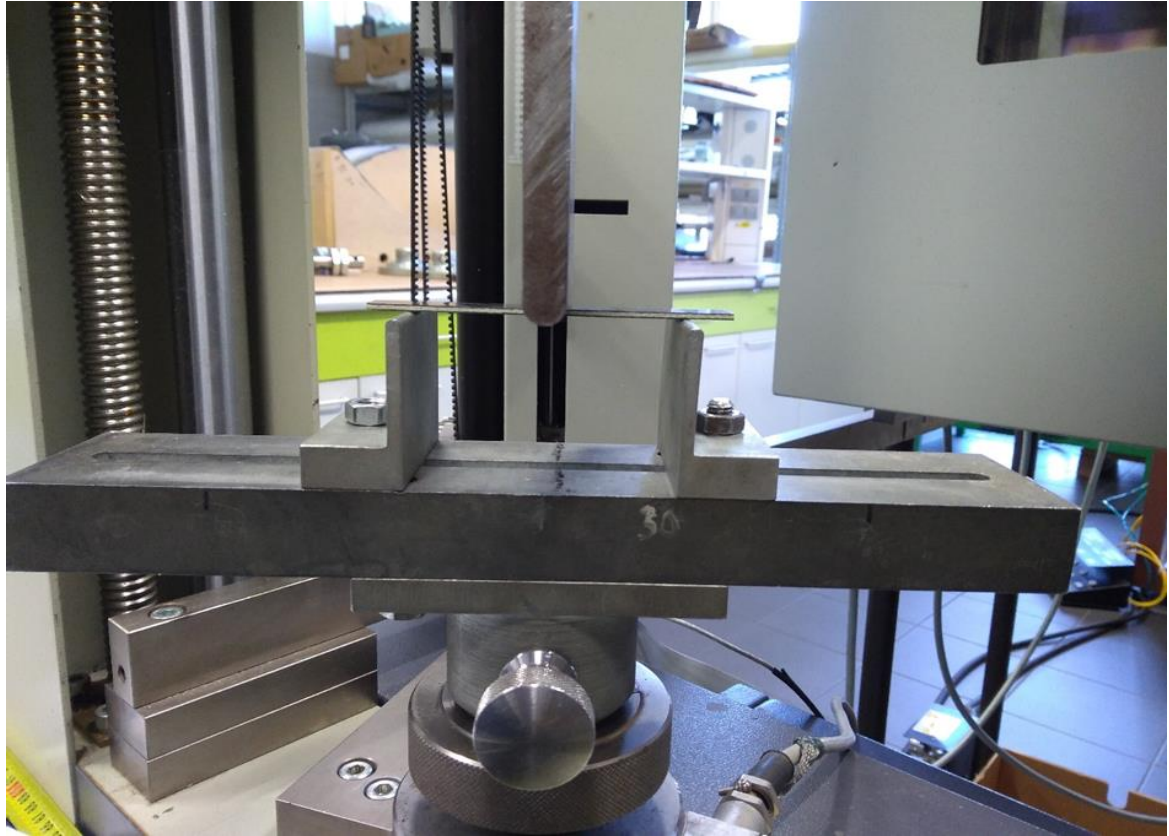


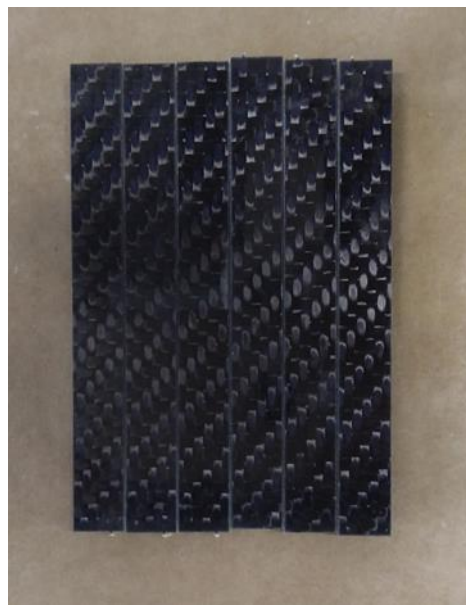
Figure 4.12: ACFRP composite specimen on the three-point bending configuration



Figure 4.13: ACFRP composite specimen on the three-point bending configuration



a)



b)

Figure 4.14: a) CFRP and b) ACFRP three-point bending specimens

4.4 Results of the AFRP composites

4.4.1 Dynamic mechanical analysis

Figure 4.15 shows the storage modulus of the AFRP composite, in the temperature range 30-200 °C, at 1, 5 and 10 Hz. In this graph, it is revealed that the storage modulus curves are separated in three regions: 30-80 °C is the glass state, where the polymer molecules are rather frozen and the composite exhibits high storage modulus, 80-110 °C is the middle transition region, correlated with the T_g , and 110-200 °C is the viscous region. Moreover, at 1 and 5 Hz, the storage modulus is slightly reduced as the temperature increases; contrastively, it is almost stable in the glassy state region, at 10 Hz. This can be attributed to the fact that, at higher frequencies, the elastic behavior dominates over the viscous behaviour in the polymer matrix, thus the AFRP composite exhibits better thermal stability. Moreover, as the frequency is increased, the initial values of the storage modulus are reduced.

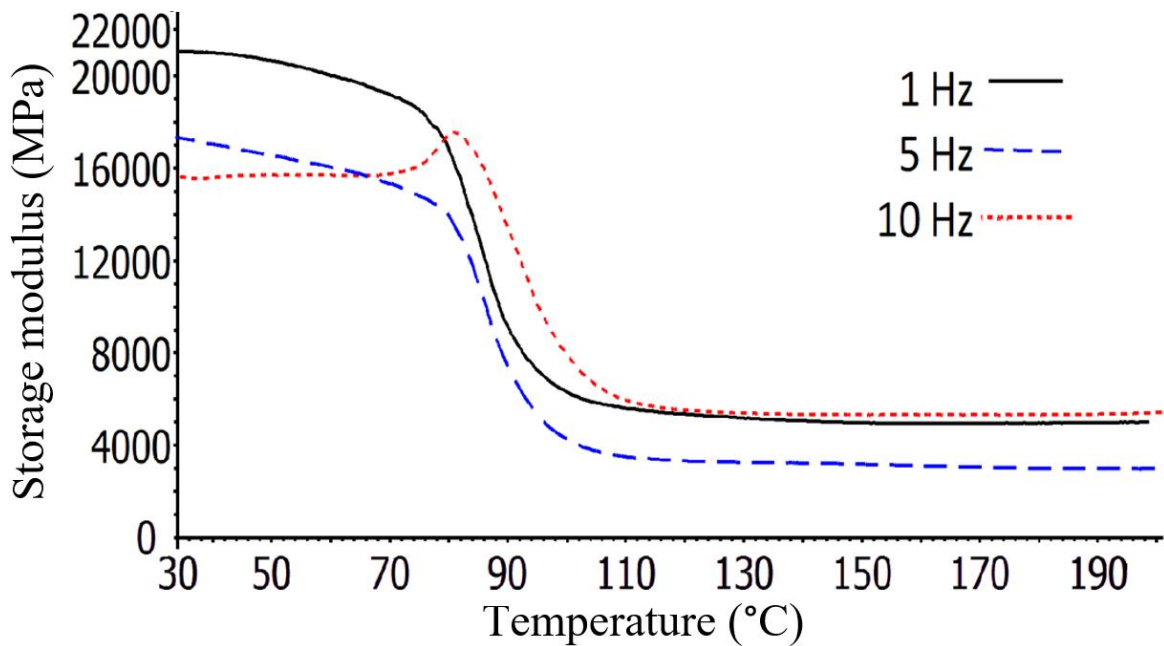


Figure 4.15: Storage modulus of the AFRP composite in the range 30-200 °C, at 1, 5 and 10 Hz

The Figure 4.16 illustrates the loss modulus (E'') of the AFRP composites in the range 30-200 °C and at frequency 1, 5 and 10 Hz. As it can be seen, at about 70 °C, the loss modulus curves depict an abrupt increase, achieving maximum values; then they fall sharply to almost zero. It is worthy of mentioning that in the

temperature range where the loss modulus achieves peak, the storage modulus is reduced.

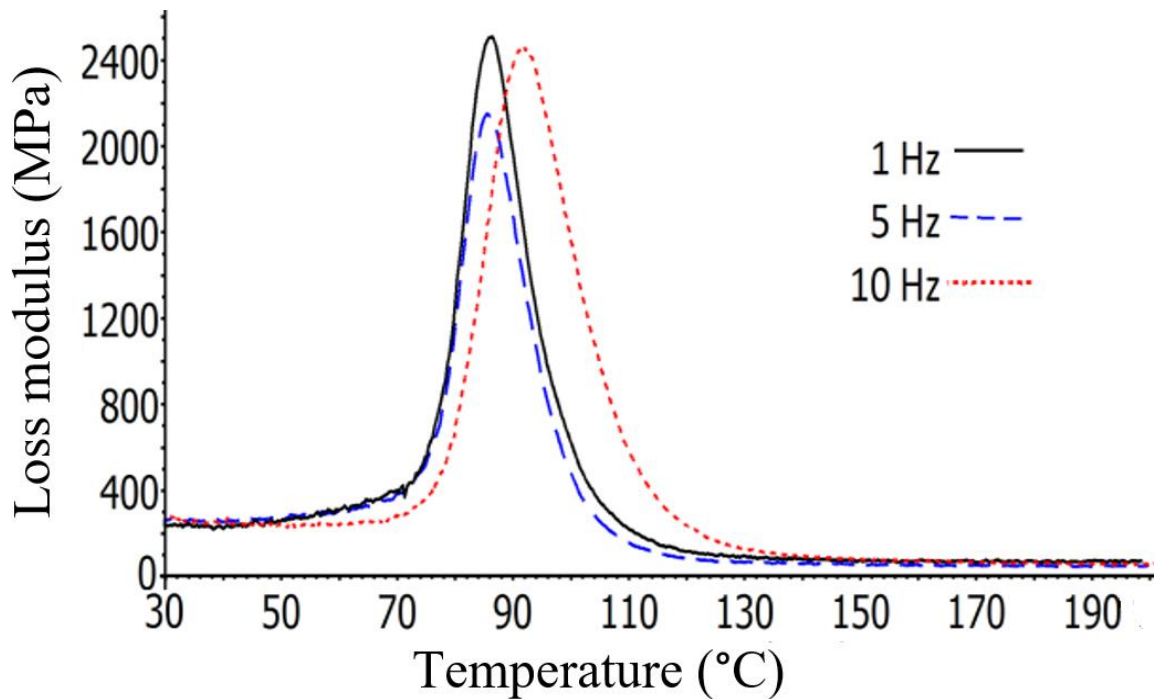


Figure 4.16: Loss modulus of AFRP composite in the range 30-200 °C, at 1, 5, and 10 Hz

Figure 4.17 depicts the $\tan\delta$ of the AFRP composite, in the temperature range 30-200 °C and at 1, 5 or 10 Hz. As it is showed, the $\tan\delta$ values are relatively low, so it can be concluded that the elastic (solid-like) behavior dominates over the viscous one. Moreover, the same trend which was noticed in the previous experimental studies of this dissertation can be also noticed here: as the frequency is increased, the peak of the $\tan\delta$ curves moves to higher temperatures. Furthermore, the adhesion between fiber/polymer can be qualified by the $\tan\delta$. Probably, the composite under continuous cyclic loading will dissipate energy at the fiber/matrix interface and the amount of it relies on the adhesion degree [61]. In that way, a weak fiber/polymer adhesive bond is expected to contribute to more energy loss, thus resulting to a higher damping coefficient [61]. The AFRP composite exhibits $\tan\delta = 0,22 - 0,23$, so it can be assumed that a very good interfacial bond between aramid fibers/epoxy has been formed.

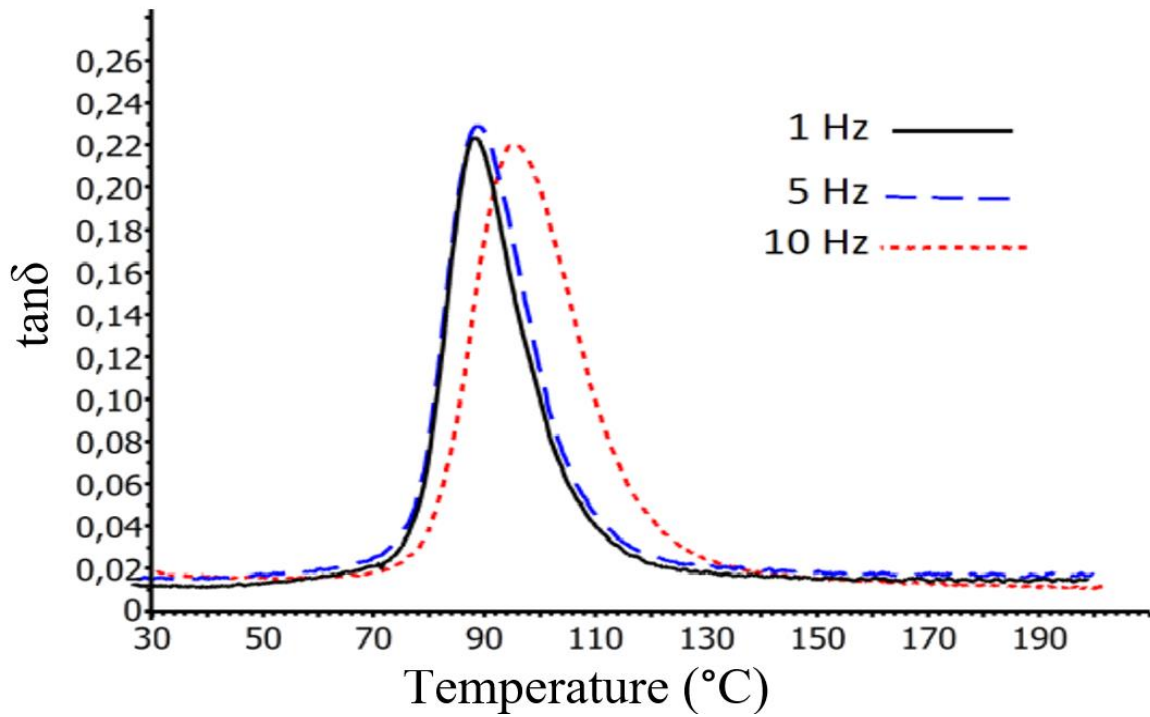


Figure 4.17: $\tan\delta$ variation of the AFRP composite in the range 30-200 °C, at 1, 5 and 10 Hz

Table 4.5 T_g of the AFRP composites (based on the DMA)

AFRP composite	1 Hz	5 Hz	10 Hz
T_g (peak of loss modulus)	86.40 °C	85.52 °C	92.29 °C
T_g (peak of $\tan\delta$)	88.07 °C	88.39 °C	95.10 °C

Table 4.5 shows the T_g of the AFRP composites, which are based on the corresponding temperatures of the loss modulus peaks and $\tan\delta$ curves, at 1, 5 and 10 Hz. The datasheet [62] of the resin/hardener producer refers for the combination, Biresin[®] CR80 and Biresin[®] CH80-2, $T_g = 92$ °C in the chapter “Detailed information: infusion and RTM systems”. Hence, the cure-postcure process followed can be characterized as highly effective for production of the particular materials.

Moreover, T_g remains almost stable or reduces very slightly between 1 Hz and 5 Hz while it is highly increased at 10 Hz. Also, the T_g acquired from the $\tan\delta$ is higher than the one determined by the loss modulus curves; the same fact was also

found in the BFRP composites study, so it seems that it a rule the $\tan\delta$ curves to give higher T_g .

4.4.2 TMA creep-recovery and TMA stress-relaxation

The creep-recovery curves of the AFRP composite are shown in Figure 4.18. Remarkably, the final deformation (plastic), caused by the forces on the end of these experiments, on the composites' structure, is very small. A perfectly elastic material will recover to its primary dimension after the release of the force so it is concluded that the elastic behaviour prevails entirely over the viscous behaviour in the structure of the AFRP composite. Even in the 5 Newton stress tests, in which primarily high initial deformation was obtained in the structure of the specimens, the elastic recovery after the release of the force is remarkably high. Moreover, in all cases the recovery occurred immediately after the release of the force.

As can be seen, between a comparison of the creep-recovery tests at 25 °C and 50 °C the high resistance in deformation forces at elevated temperatures, of the AFRP composites can be obtained. The 1 N caused the same initial displacement at both temperatures and both curves are very similar.

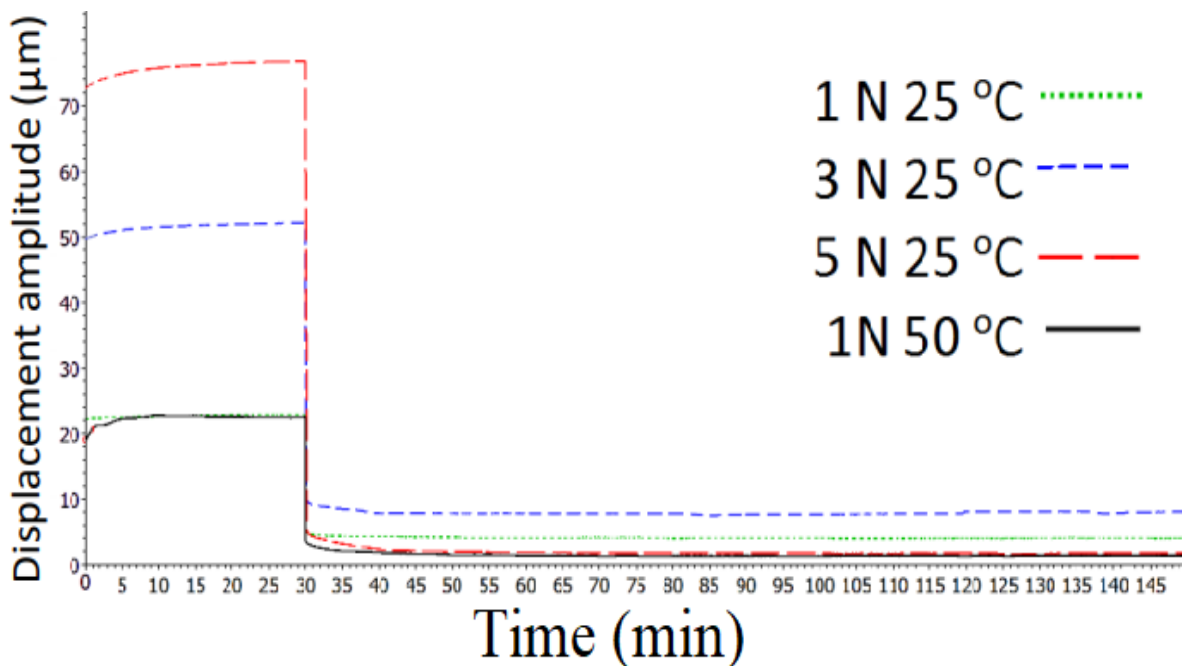


Figure 4.18: TMA creep-recovery of the AFRP composite

Figure 4.19 illustrates the stress-relaxation curve of the AFRP composite. In this graph, the viscoelastic behavior of the composite structure can be seen in the first minutes of the experiment as then the stress-relaxation curve becomes flat and almost stable.

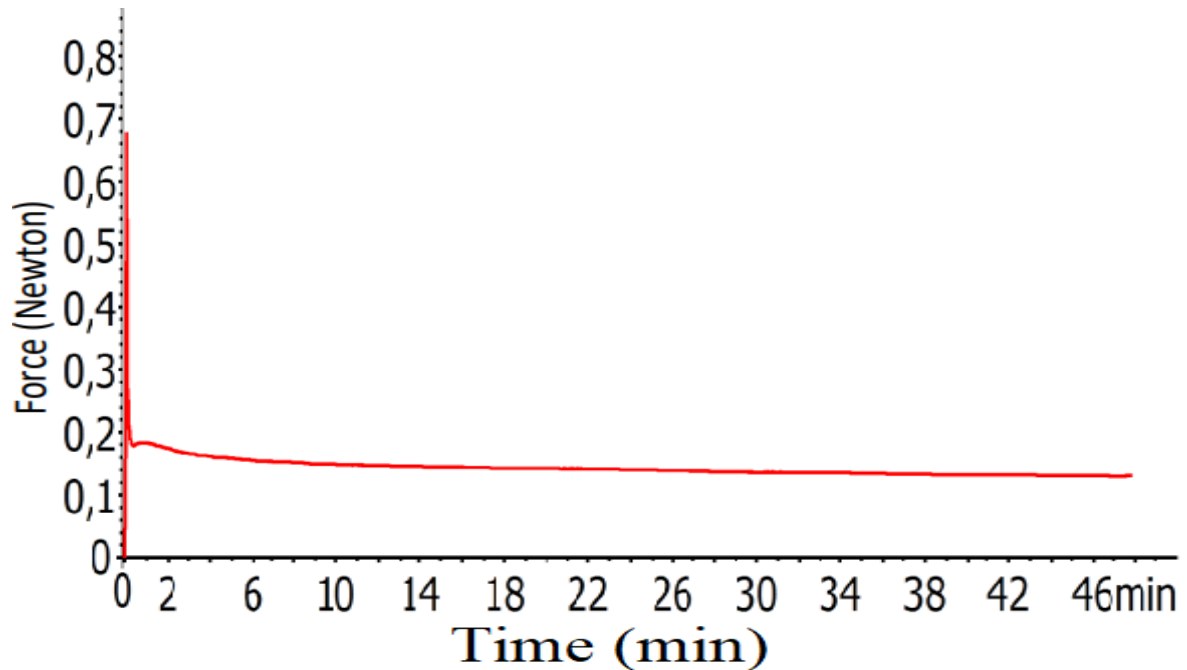


Figure 4.19: stress-relaxation of the AFRP composite



Figure 4.20: zoomed view of the AFRP composite stress-relaxation curve

4.4.3 Thermogravimetric analysis

The weight variation of pure post-cured epoxy and aramid fibers, in N₂ atmosphere, at 350 °C for 240 minutes is shown in Figure 4.21. In this graph, it can be seen that after exposure at 350 °C in N₂ atmosphere, for 240 minutes, the post-cured epoxy loses approximately 80% of its weight whereas, under the same circumstances, the aramid fibers remain mostly thermally unaffected. They lose only approximately of 4.5% of their weight and this loss is attributed to loss of humidity which was concentrated on the surface of the fibers; the aramid fibers are highly hydrophilic and this is verified from the fact that after this weight loss, after the tenth minute, the weight curve is linear at steady 95.5%.

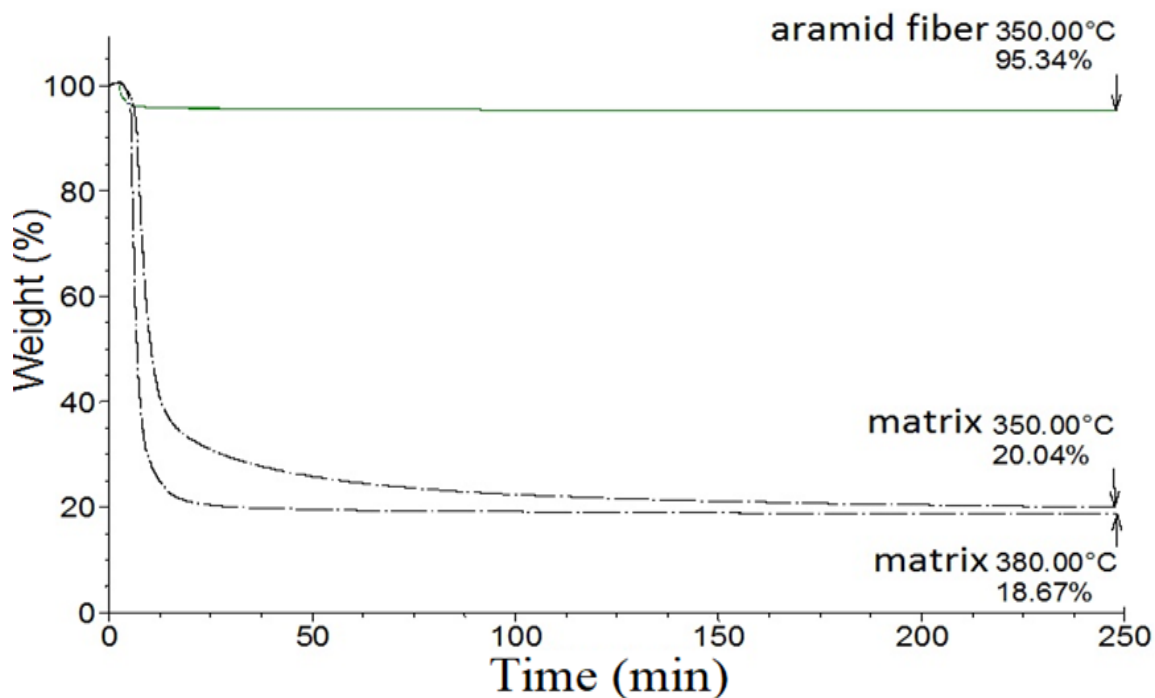


Figure 4.21: TGA results presenting the thermal stability of — aramid fibers, and — pure post-cured epoxy in exposure at 350 °C for 240 minutes in N₂ atmosphere (epoxy also at 380 °C)

So, two samples, for reliability, of the AFRP composite were TGA measured, in N₂ environment, Figure 4.22. It was found that the remaining weight of them, after exposure for 240 minutes at 350 °C, is 66.65% and 63.27%, respectively. It should be noted that the overall time on the x-axis is more than 240 minutes because the instrument measures also the time until the temperature to reach the 350 °C. Then, with the use of simple mathematics, the remaining 20% percentage

of the epoxy, in the two AFRP compounds, was withdrawal and thus $W_{f,1} = 58.32\%$ and $W_{f,2} = 54.09\%$; average $W_{f1,2} = 56.20\%$.

Then, with the use of the equation:

$$\Phi_f = \frac{1}{1 + \frac{\rho_f}{\rho_m} \left(\frac{1}{W_t} - 1 \right)} \quad (1) \quad (4.1) \quad [56]$$

Where ρ_m = density of matrix =1.16 g/cm³, ρ_f = density of reinforcing phase = 1.44 g/cm³, W_t = weight proportion of the reinforcing phase. So, finally, it was found that approximately $\Phi_f = 51\%$ and thus $\Phi_m = 49 \%$. It should be mentioned, that during the preparation of the composite laminates, the weight of the aramid fabric reinforcement was measured and then compared with the whole weight of the AFRP composite structure. It was found that the aramid fibers' fabrics consist the 54% of the whole weight of the AFRP composite. So, it is concluded that the experimentally determined $W_t = 56.20\%$ is very close to the realistic value.

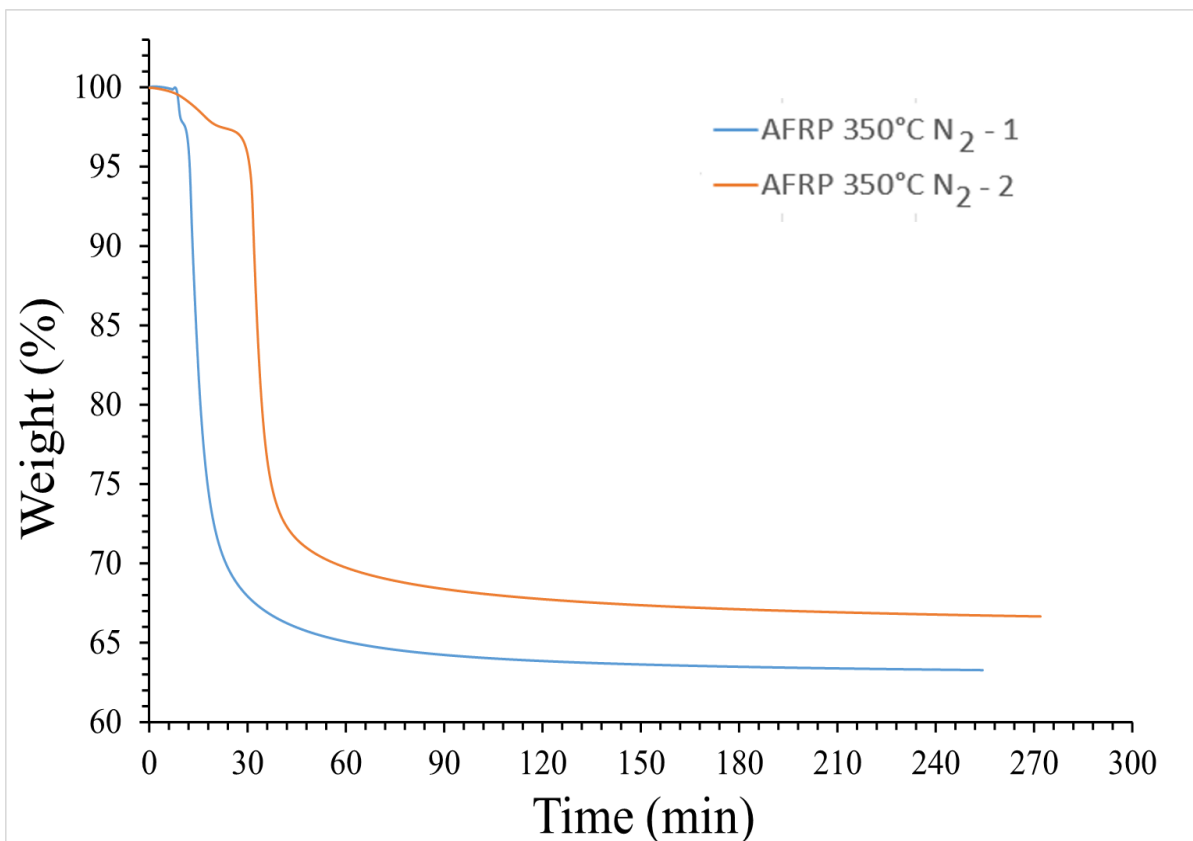


Figure 4.22: TGA graph of the AFRP composite (two samples) at 350 °C for 240 minutes under N₂ atmosphere. The difference on the time axis is because these samples were heated up to the 350 °C with different heating rates.

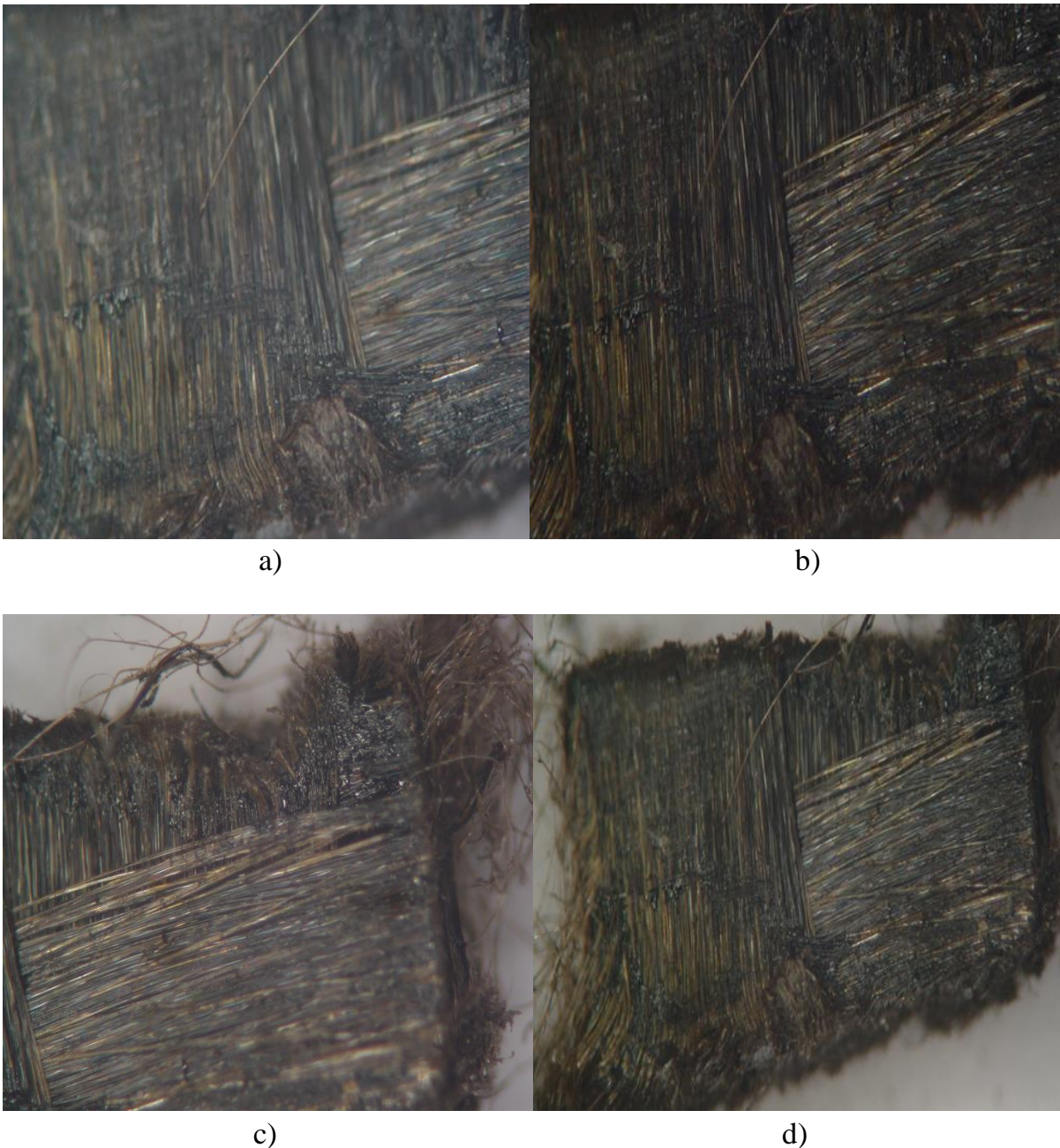


Figure 4.23: a) b) c) and d) Photos of the AFRP composite specimens under exposure for 240 minutes, at 350 °C, under N₂ atmosphere. The photos were taken with the Carl Zeiss Stemi 2000C Microscope (Jena, Germany) from the edges of the composite structure.

The TGA tests, at isothermal temperature with steps after a particular time, are of great interest because they correlate temperature with time so the weight of the materials can be precisely determined simulating real-life applications. Figure 4.24 illustrates the thermal stability of the aramid fibers, in N₂ atmosphere, under

isothermal scans at 360, 370 and 380 °C with every 60 minutes step of 10 °C. The initial 3% weight reduction is attributed to humidity due to the hydrophilic character of these fibers. In this graph, the very good thermal stability of the aramid fibers is revealed as they are slightly thermally influenced above the 370 °C.

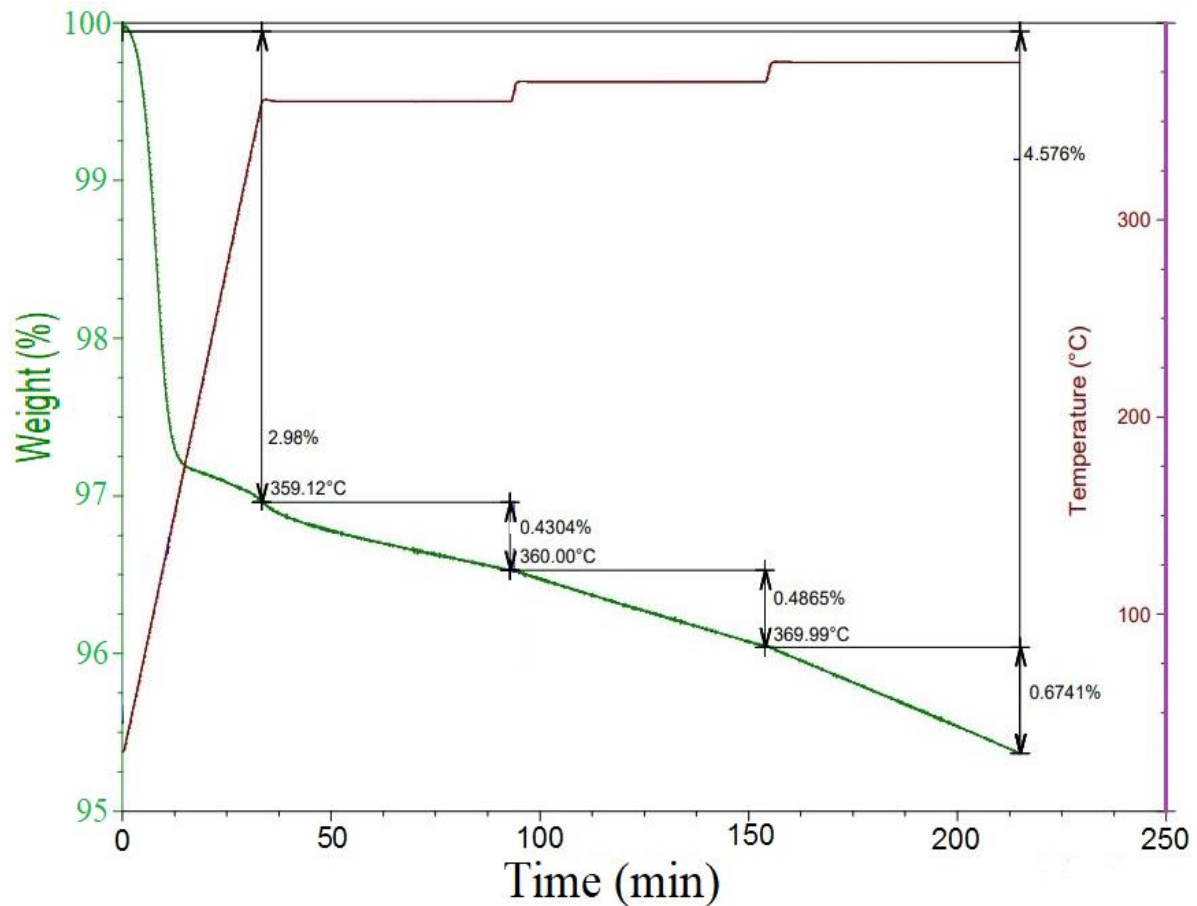


Figure 4.24: TGA results presenting the thermal stability of the aramid fibers at exposure at 360, 370 and 380 °C, in N₂ atmosphere, with every 60 minutes step of 10 °C

The figure 4.25 illustrates the decomposition of the AFRP composite, in the range 30-900 °C, in air and nitrogen atmosphere, respectively. As was expected, the high Φ_f contributes towards enabling the composite structure to achieve very good thermal resistance. Notably, under both atmospheres, the weight loss mainly occurs after the 480 °C. In the case of air atmosphere, the oxidation phenomenon leads to whole thermal degradation of the composites' weight up to the 590 °C whereas under N₂ gas, where pyrolysis takes part, resulting in 30% of the composite weight to remain, up to the final 900 °C. Moreover, in order to check

the reliability of these experiments and of the VIP production method, two samples, which were taken from different places of the AFRP composite plate, were tested in N_2 . Through this graph, the high reliability of the VIP production method is revealed. Despite the small size of the TGA specimens, each of 35 mg, both curves are very identical and concluding in the same remaining weight at 900 °C. Thus, the composites' production method is characterized as highly effective.

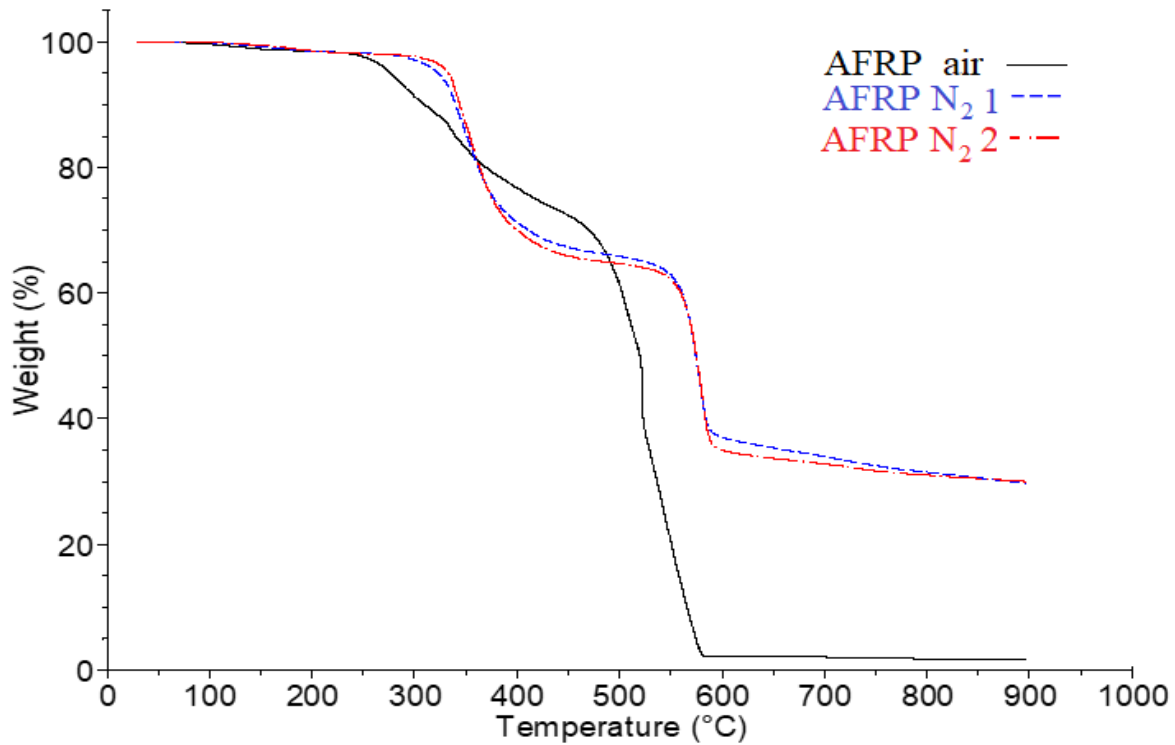


Figure 4.25: TGA results showing the weight of the AFRP composites as a function of the temperature, in air and N_2 atmosphere, respectively

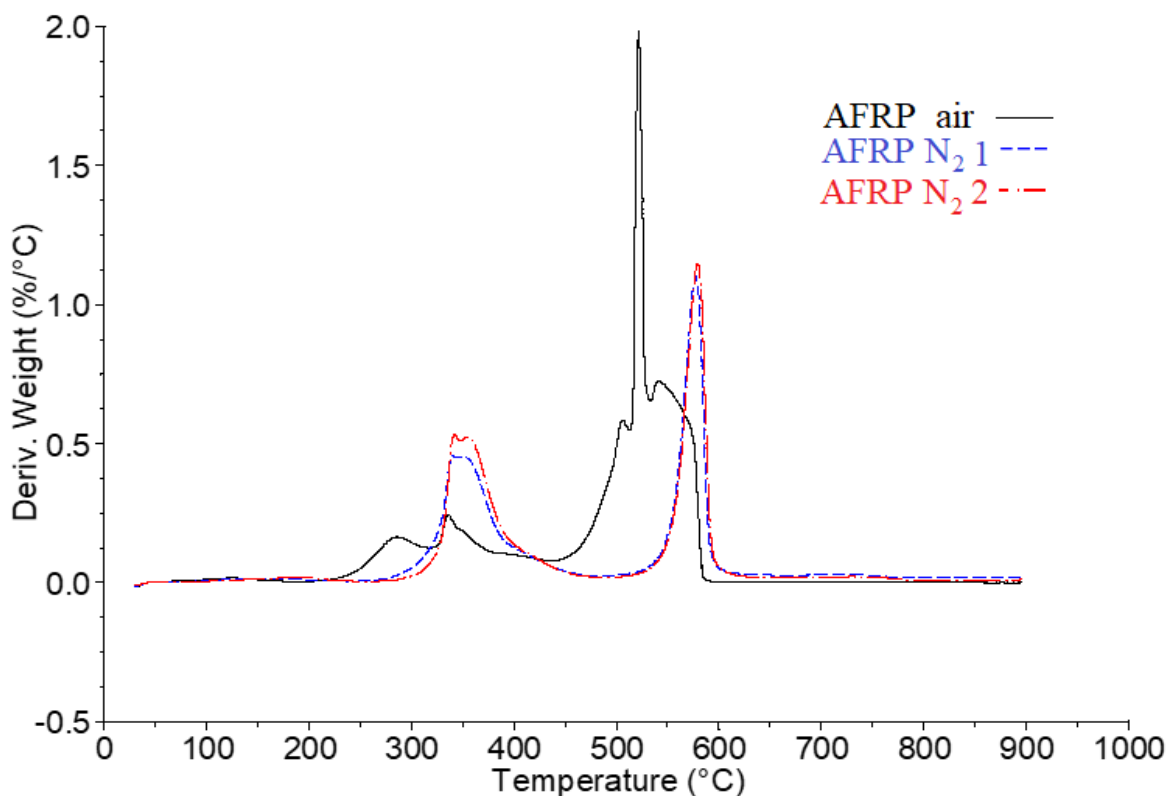


Figure 4.26: DTG (weight loss rate) curves of the AFRP composite in air and N₂ atmosphere, respectively.

The figure 4.26 depicts the corresponding DTG curves of the figure 4.25. In N₂ atmosphere, the first peak, at approximately 350 °C, is dedicated to thermal decomposition of the matrix, whereas the second peak, at about 580 °C, is a combination of thermal degradation of aramid fibers and remaining part of the matrix.

The figure 4.27 presents the thermal degradation, in the temperature range 30-900 °C, of pure cured epoxy and aramid fibers, in air or N₂ atmosphere. The first obvious observation is that, at both atmospheres, the aramid fibers have much better thermal behavior than the epoxy; the aramid fibers are mainly thermally affected above the 480 °C whereas the post-cured epoxy is highly thermally affected over the 275 °C. Moreover, both of materials, epoxy and aramid fibers, in air atmosphere, have completely thermally degraded, due to thermal oxidation, up to the 590 °C.

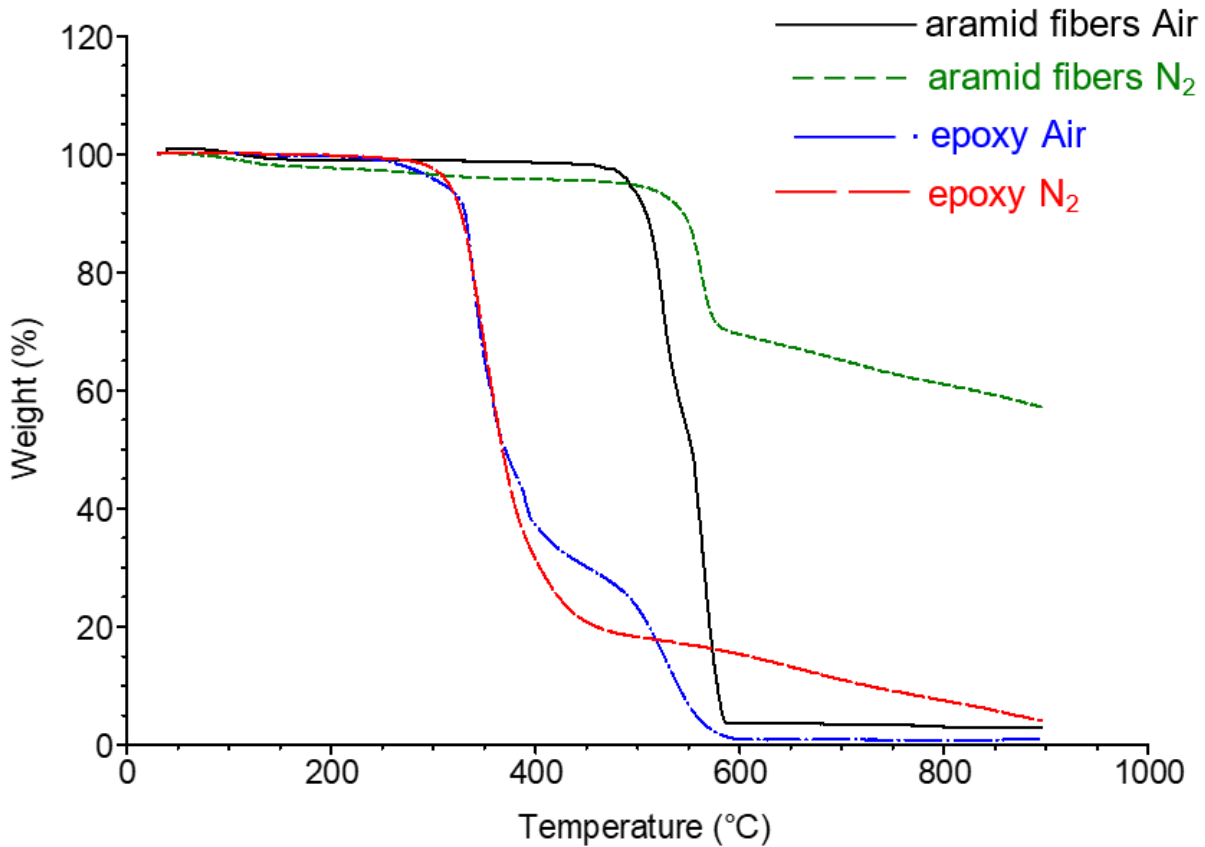


Figure 4.27: TGA results showing the weight (%) of the aramid fibers and pure post-cure epoxy matrix as a function of temperature in air and N₂ atmosphere, respectively.

4.4.4 DSC

Figure 4.28 shows the DSC curves, in the range 30-600 °C, in N₂ atmosphere, of the two heating circles and the two corresponding cooling circles, of the AFRP composite.

Based on the datasheet [60] of the manufacturer of the resin-hardener, the T_g of a fully cured neat resin (Biresin[®] CR80 and Biresin[®] CH80-2), determined according to the standard ISO 11375, is 93 °C. This standard specifies the T_g using DSC experiments but the author of this research didn't specify the T_g according to this standard. However, the T_g determined from the midpoint of the first heating is 94.67 °C, a value which cannot be compared directly with the one from the datasheet, but it needs to be noted that both, which were determined by DSC are very close.

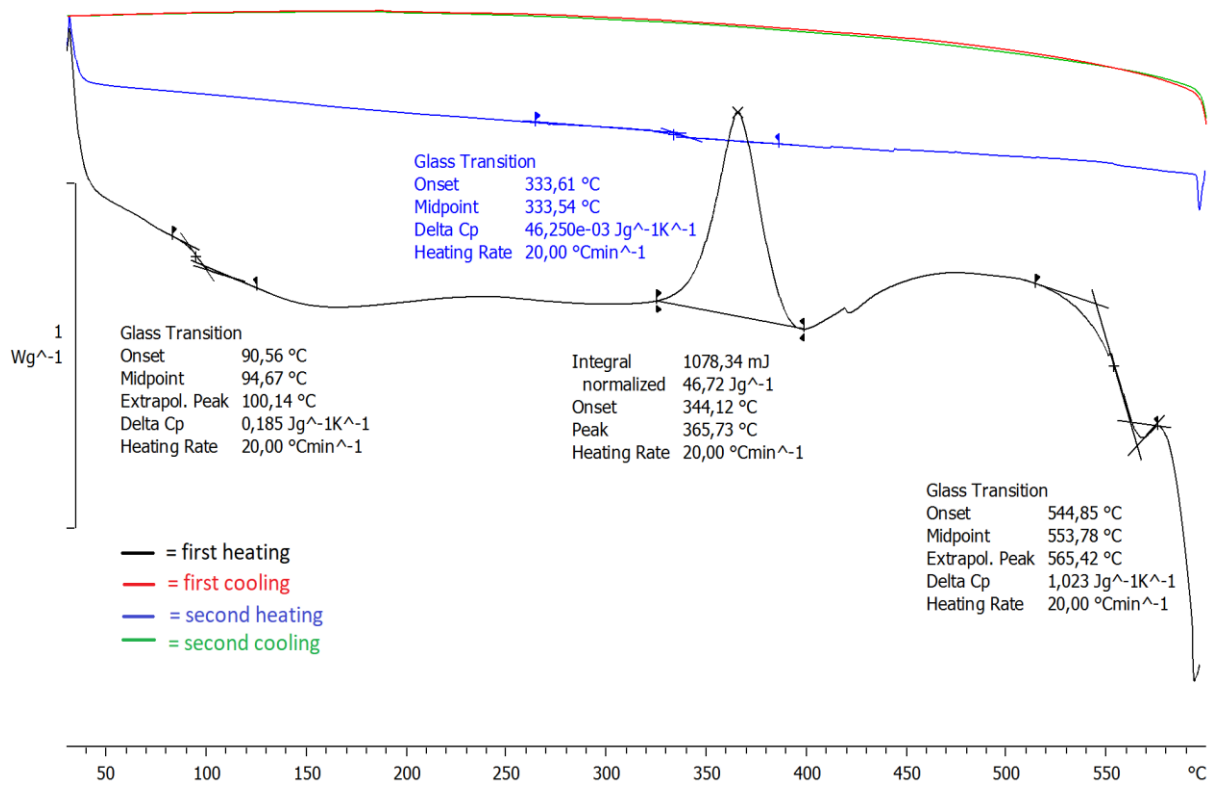


Figure 4.28: DSC curves of the AFRP composite

4.5 Results of the CFRP and ACFRP composites

4.5.1 DMA

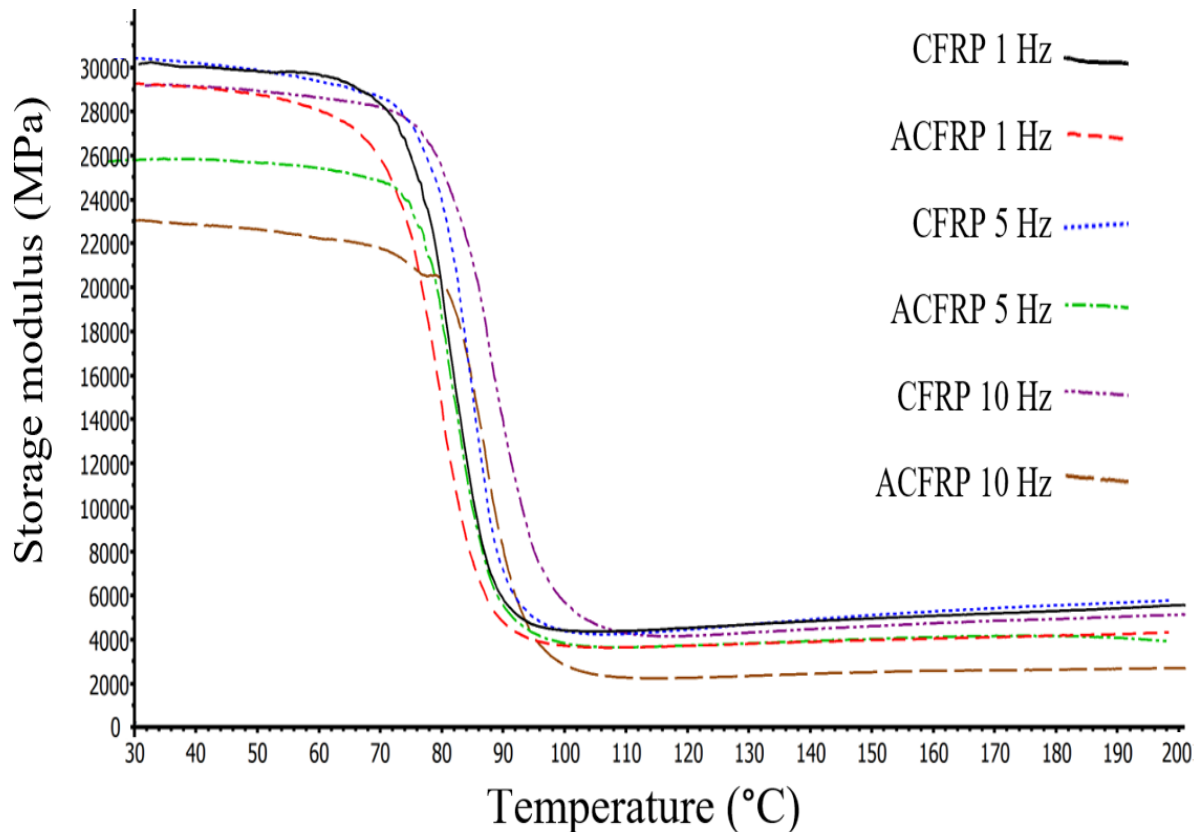


Figure 4.29: E' versus temperature of the CFRP and ACFRP composites under 1, 5 and 10 Hz

The storage modulus, of the CFRP and ACFRP composites as a function of the temperature at 1, 5 and 10 Hz, is presented in Figure 4.29. As can be seen, under all frequencies, the CFRP composite achieved higher storage modulus than the ACFRP composites; difference which was becoming greater as the frequency was increased. The storage modulus of the latter composite is reduced as the frequency is increased whereas this property of former composite remains generally unaffected from the frequency. Moreover, the abrupt reduction in the storage modulus curves in the middle transition region is observed; this sudden fall is correlated with the T_g .

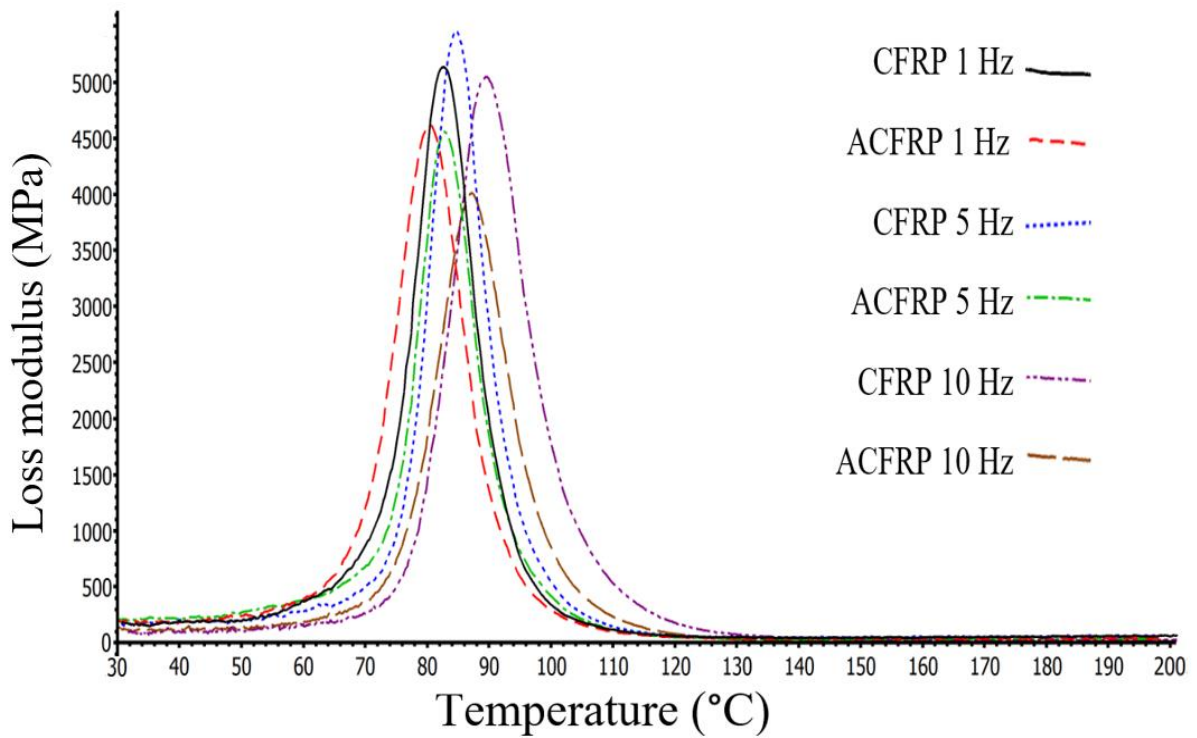


Figure 4.30: E'' versus temperature of the CFRP and ACFRP composites under 1, 5 and 10 Hz

Figure 4.30 shows the loss modulus of the CFRP and ACFRP composites. As in storage modulus experiments, the CFRP composites exhibited higher loss modulus than the ACFRP composites. From this graph, it can be observed that as the frequency is increased the reference temperature of the peaks of the loss modulus is moving to higher temperature; the frequency influences positively the T_g of the CFRP and ACFRP composites. Moreover, at low temperatures, the loss modulus curves follow a steep increase achieving peak values whereas then a steep fall is observed until almost zero values which are maintained up to the final 200 °C.

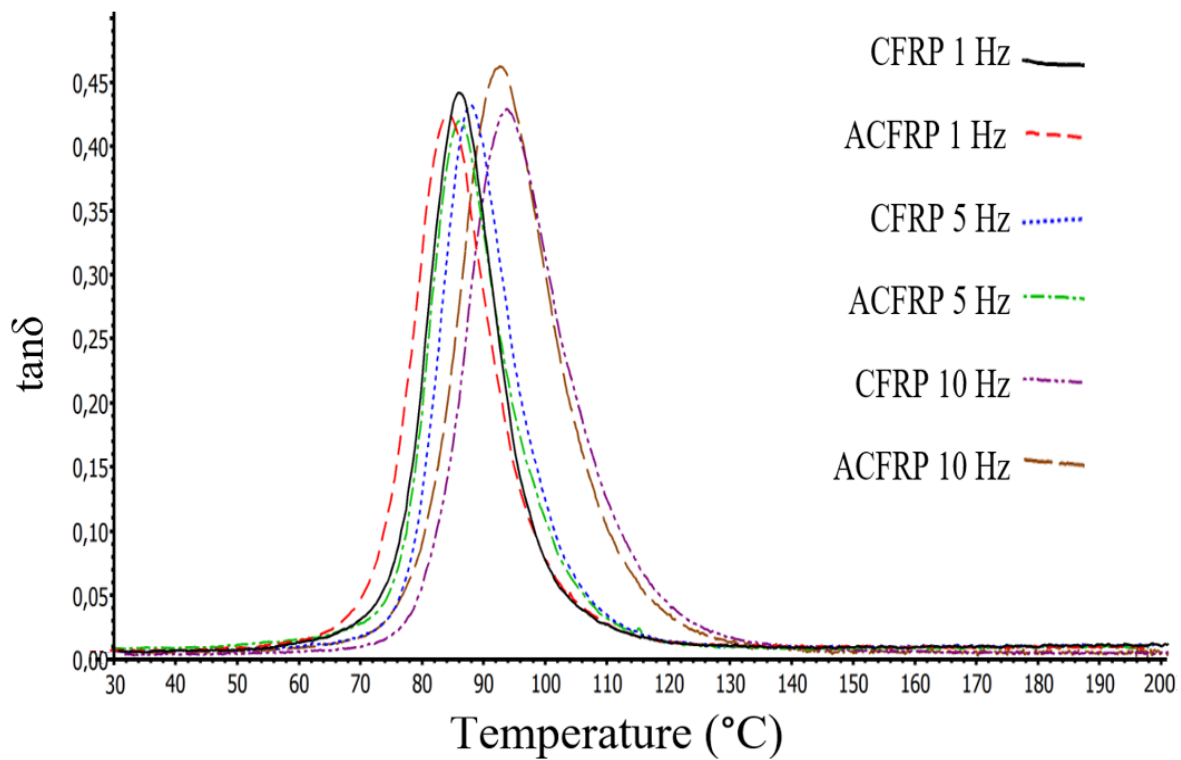


Figure 4.31: $\tan\delta$ versus temperature of the CFRP and ACFRP composites under 1, 5 or 10 Hz

The $\tan\delta$ curves of the CFRP and ACFRP composites, over the temperature 30-200 °C, at frequency 1, 5 and 10 Hz, are shown in Figure 4.31. As can be seen at low temperatures, the values are almost stable, whereas after approximately the 55 °C, they follow a step upward trend, achieving peak values, which is then followed by a steep decrease. Moreover, similar with loss modulus curves, as the frequency is increased the reference temperature of the peak point of these curves moves to higher temperatures. According to the corresponding temperatures of peak values of the $\tan\delta$ curves, it is revealed that the CFRP composite exhibits slightly better performance than the ACFRP composite.

4.5.2 T_g of the CFRP and ACFRP composites

The T_g temperatures, which were acquired from the corresponding temperatures of the peak of the loss modulus and $\tan\delta$ curves, of the CFRP and ACFRP composites are shown in Table 4.6. As can be seen, under all frequencies, the CFRP composites exhibited higher T_g than the ACFRP composites and that the T_g based on $\tan\delta$ curves is higher than the T_g determined by the loss modulus curves.

Moreover, between a comparison of these results with the data from Table 4.5, it is revealed the AFRP composites have higher T_g than the CFRP and ACFRP composites. This can be attributed to positive effect of the aramid fibers.

Table 4.6 T_g of the CFRP and ACFRP composites (based on DMA)

	T_g obtained by $\tan\delta$ peak (°C)	T_g obtained by loss modulus peak (°C)
CFRP 1 Hz	82.52	86.10
ACFRP 1 Hz	79.96	84.54
CFRP 5 Hz	84.45	87.81
ACFRP 5 Hz	82.84	85.84
CFRP 10 Hz	89.38	93.72
ACFRP 10 Hz	87.08	92.65

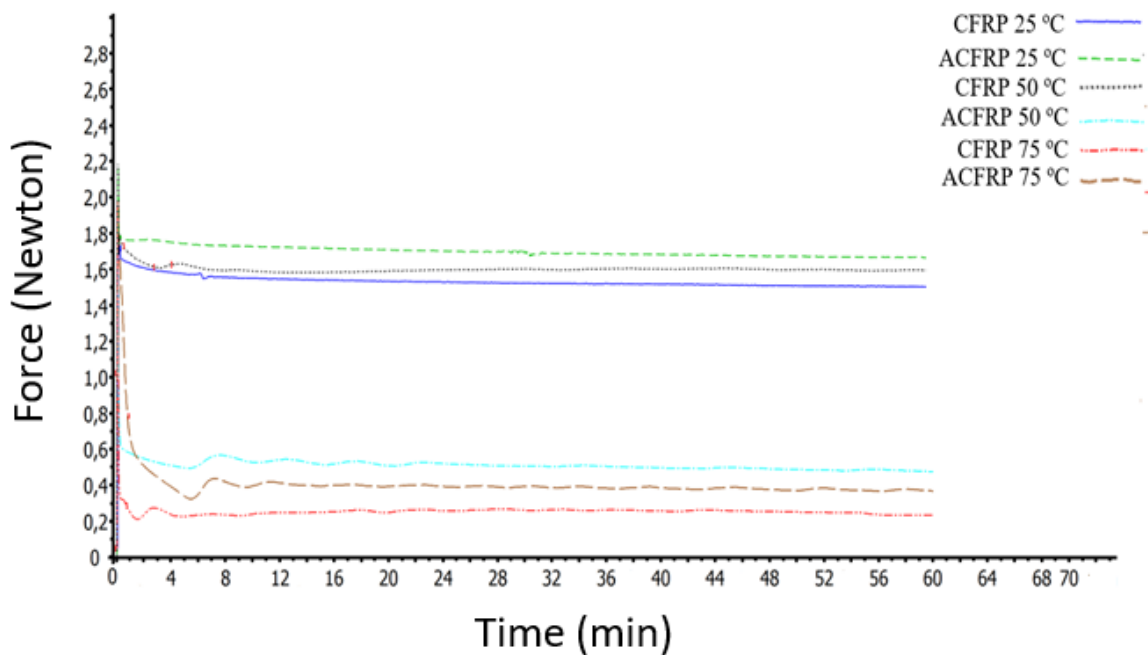


Figure 4.32: stress-relaxation curves of the CFRP and ACFRP composites at 25, 50 and 75 °C

Figure 4.32 depicts the stress-relaxation curves of CFRP and ACFRP composites at 25, 50 and 75 °C. Notably, whereas at 50 °C the former composite depicts the same stress-relaxation behavior as in 25 °C, the ACFRP composite is heavily affected at 50 °C. Moreover, both composites at 75 °C have extremely reduced their resistance in deformation forces.

4.5.3 DSC of the CFRP and ACFRP composites

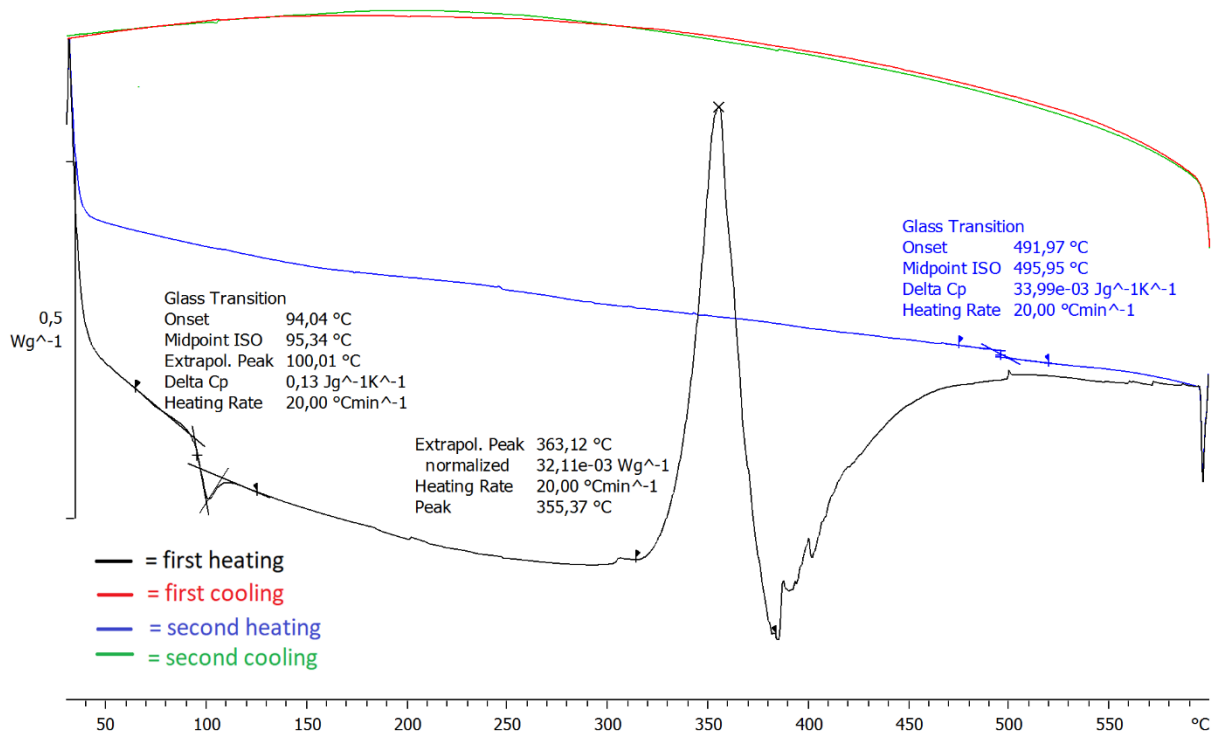


Figure 4.33: DSC curves of the CFRP composite

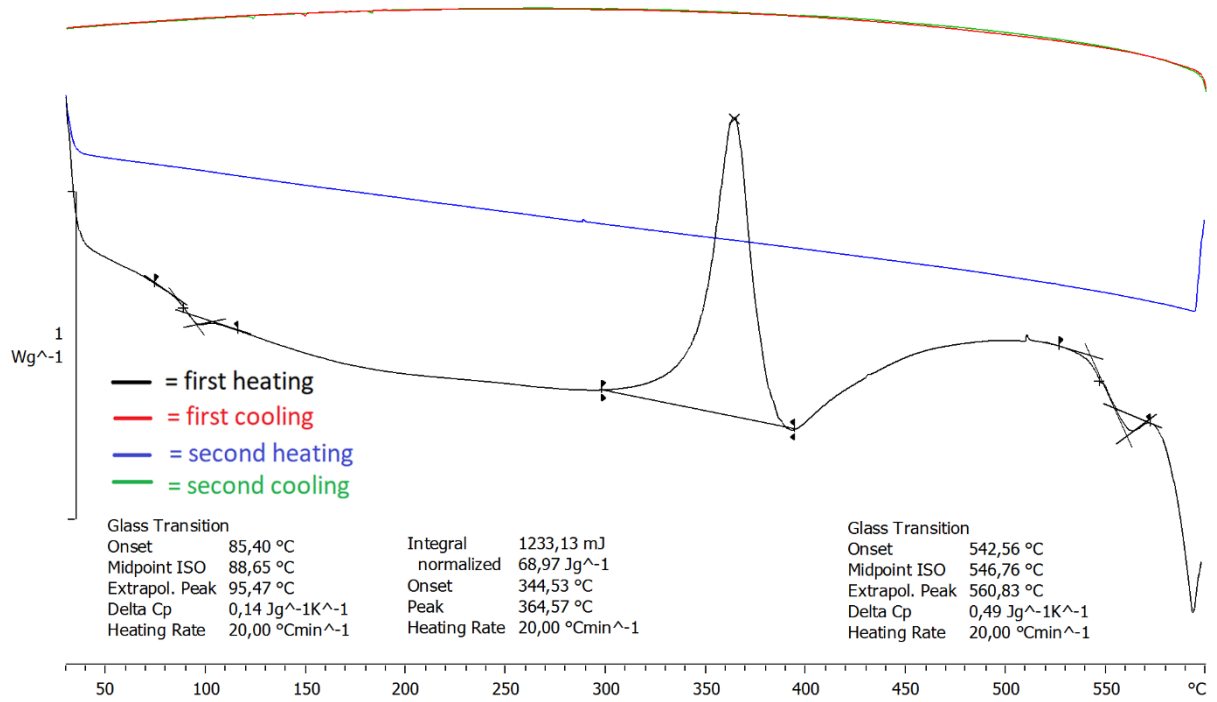


Figure 4.34: DSC curves of the ACFRP composite

The figures 4.33 and 4.34 illustrate the DSC curves of the CFRP and ACFRP composites, respectively. It can be seen that the CFRP composite achieved higher T_g than the ACFRP composites.

4.5.4 TGA of the carbon fibers, aramid fibers, CFRP and ACFRP composites

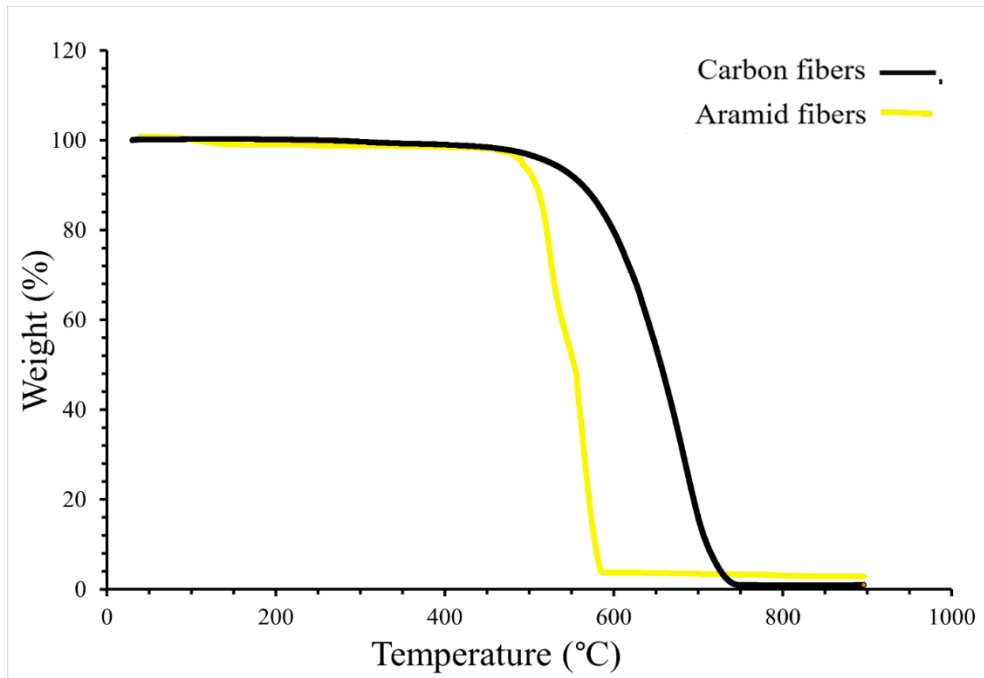


Figure 4.35: TGA results showing the weight (%) of the carbon and aramid fibers as a function of the temperature in air atmosphere

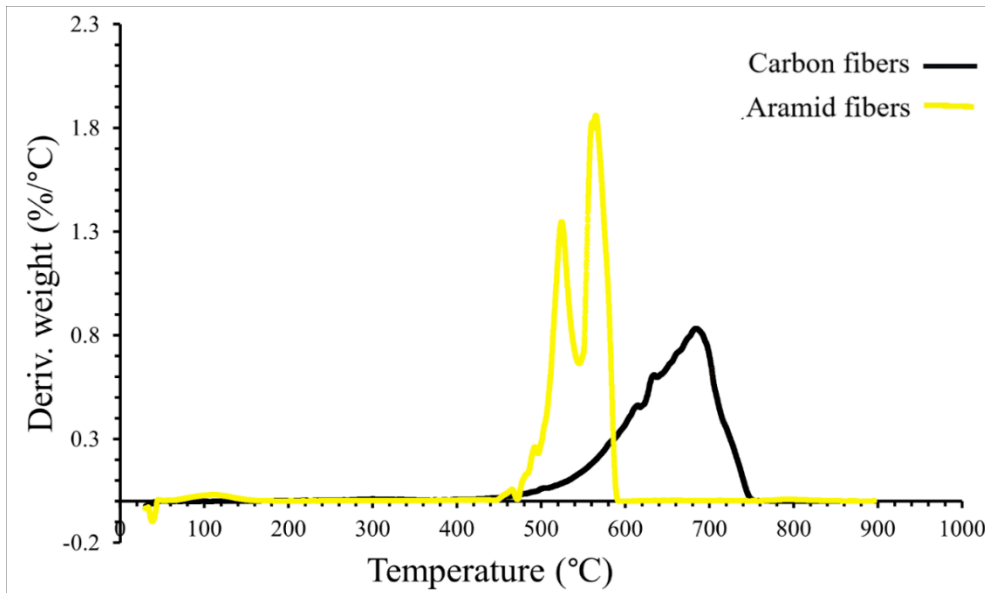


Figure 4.36: DTG (weight loss rate) of the carbon and aramid fibers as a function of the temperature in air atmosphere

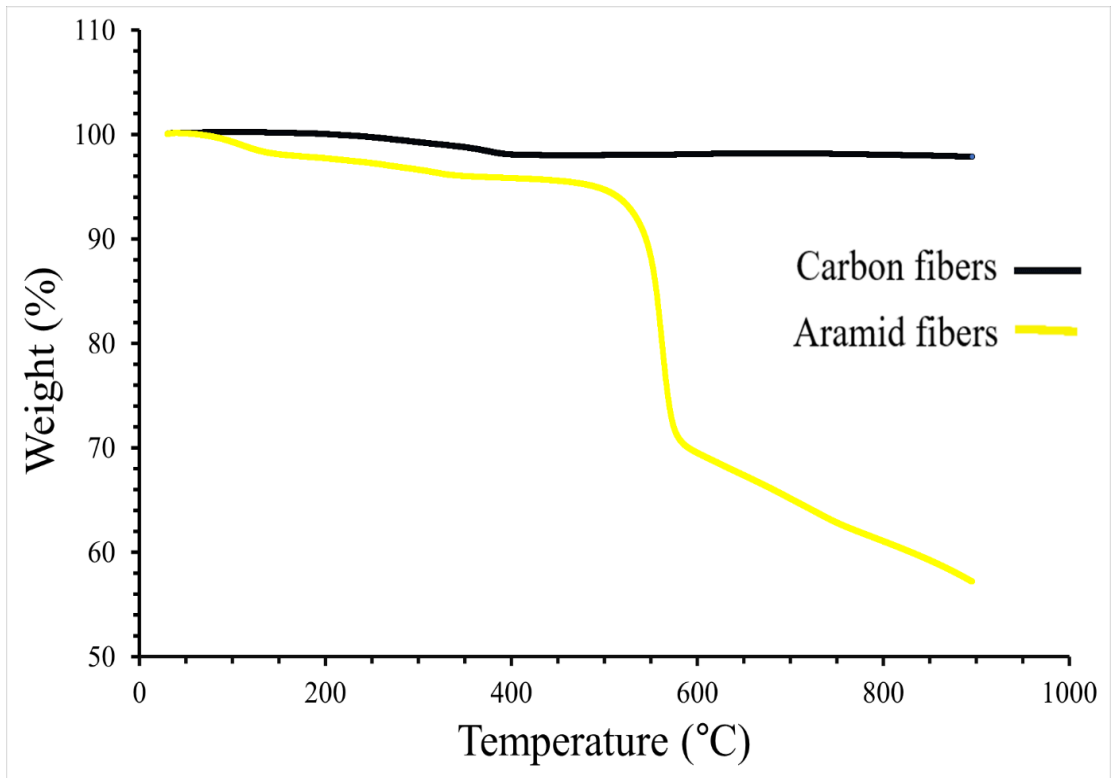


Figure 4.37: TGA results showing the weight of the carbon and aramid fibers as a function of the temperature in N_2 atmosphere

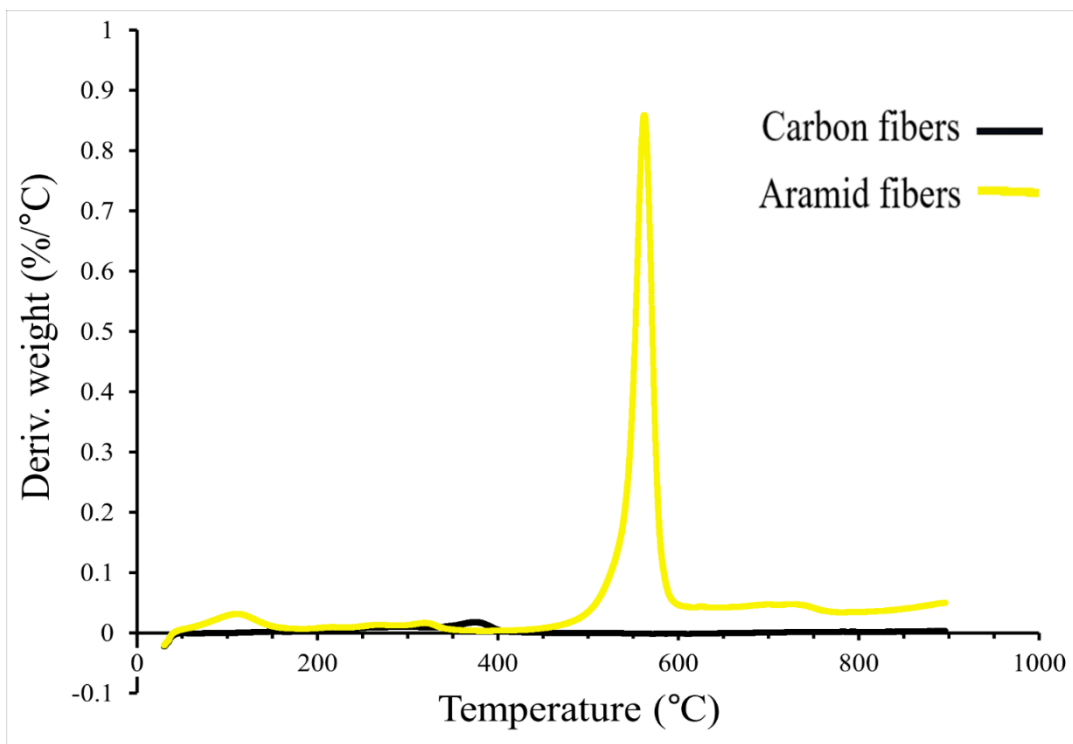


Figure 4.38: DTG (weight loss rate) curves of the carbon and aramid fibers as a function of the temperature in N_2 atmosphere

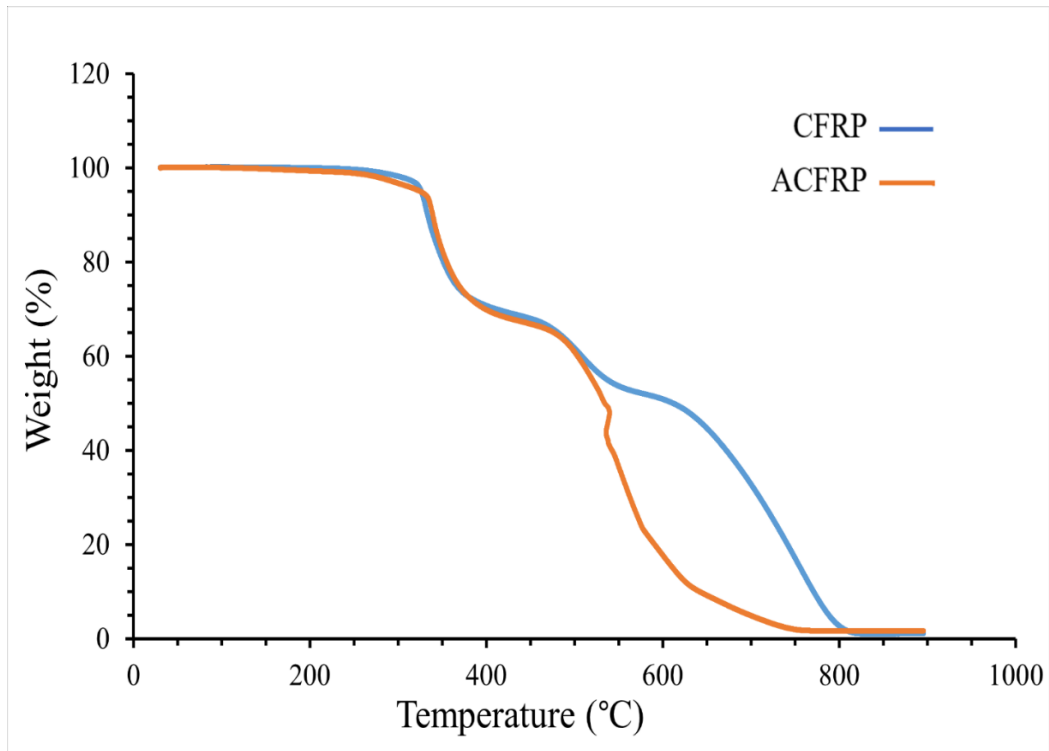


Figure 4.39: TGA results presenting the weight (%) of the CFRP and ACFRP composites as a function of the temperature in air atmosphere

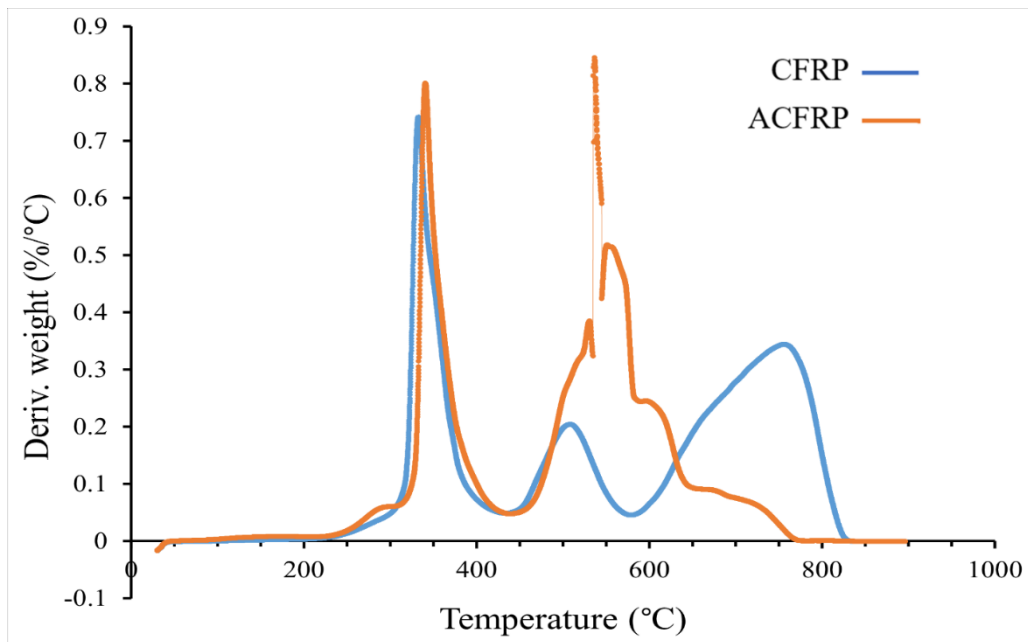


Figure 4.40: DTG (weight loss rate) curves of the CFRP and ACFRP composites as a function of the temperature in air atmosphere

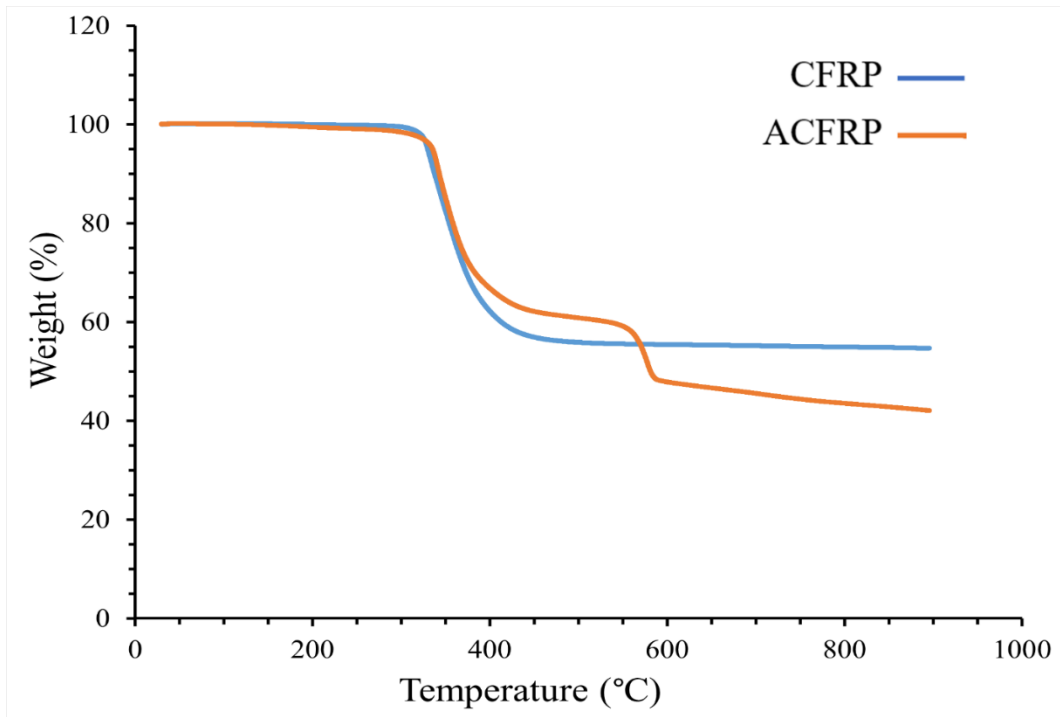


Figure 4.41: TGA results presenting the weight variation (%) of the CFRP and ACFRP composites as a function of the temperature in N_2 atmosphere

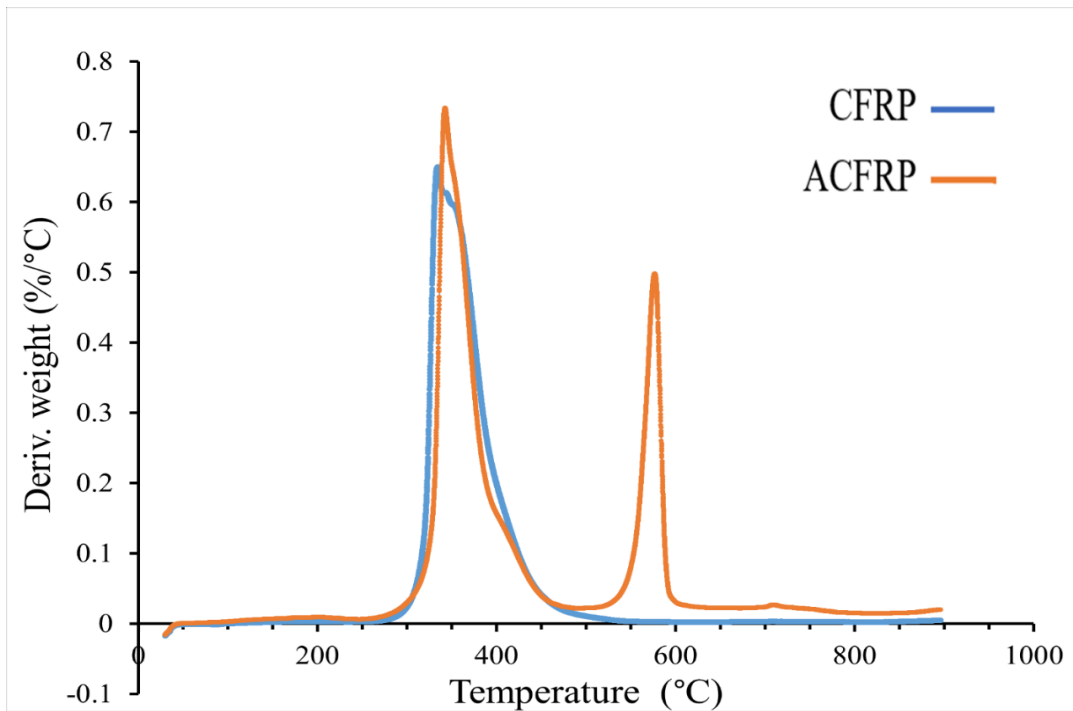


Figure 4.42: DTG (weight loss rate) of the CFRP and ACFRP composites as a function of the temperature in N_2 atmosphere

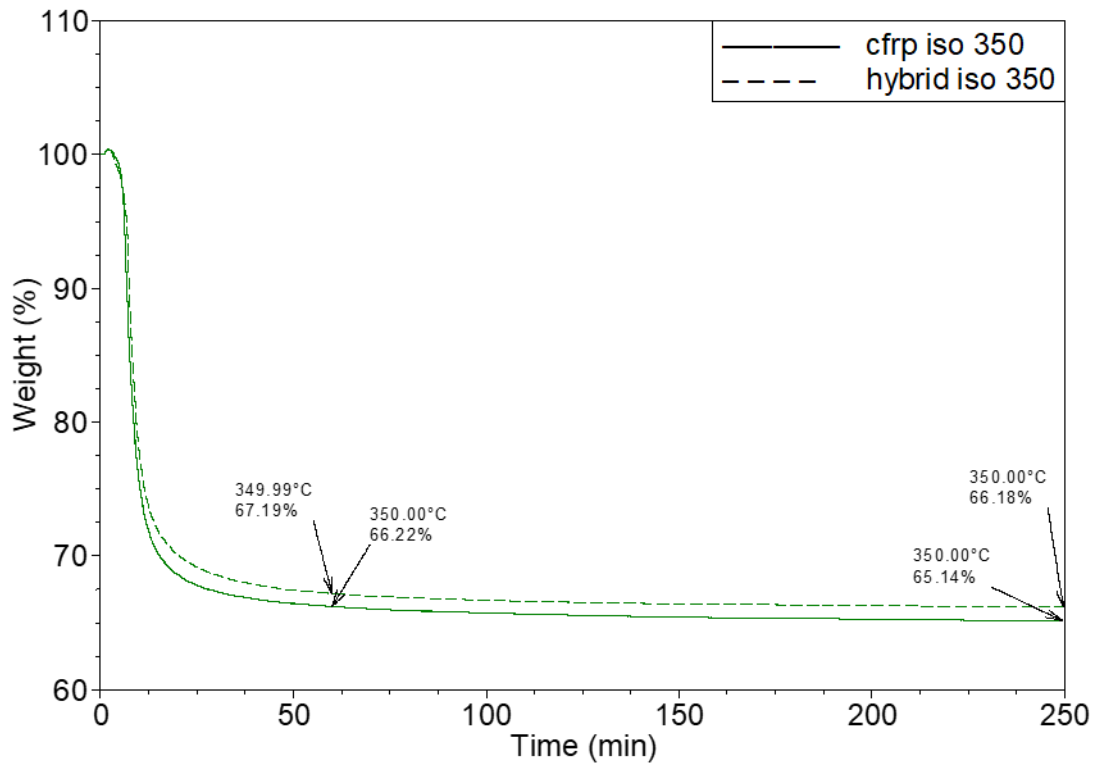


Figure 4.43: TGA results showing the thermal stability of the CFRP and ACFRP composites, at exposure at 350 °C for 240 minutes, in N₂ atmosphere

$$\Phi_f = \frac{1}{1 + \frac{\rho_f}{\rho_m} (W_t - 1)} \quad (4.3) \quad [56]$$

ρ_m = density of matrix = 1.16 g/cm³, ρ_f = density of carbon or carbon/aramid fibers = 1.79 g/cm³ or 1.44 g/cm³, respectively; For the case of the ACFRP the density was calculated $1.79 + 1.44 / 2 = 1.615$ g/cm³, W_t = weight of carbon or carbon/aramid fibers = 65.14 % or 66.18 %, respectively.

In the figure 4.43, it was found that after exposure, for 240 minutes at 350 °C, in nitrogen atmosphere, the epoxy matrix loses 80 % of its weight, so, the remaining 20 % of matrix was withdrawn;

CFRP $W_t = 56.425$ % , ACFRP $W_t = 57.725$ %

Finally, it was found:

CFRP $\Phi_f = 45.66$ %

ACFRP $\Phi_f = 49.52$ %

The difference in the Φ_f of both composites is relatively small and this characteristic in conjunction with the fact that these composites consist of fabrics which have the same weave, weight and thickness allows their properties to be compared directly.

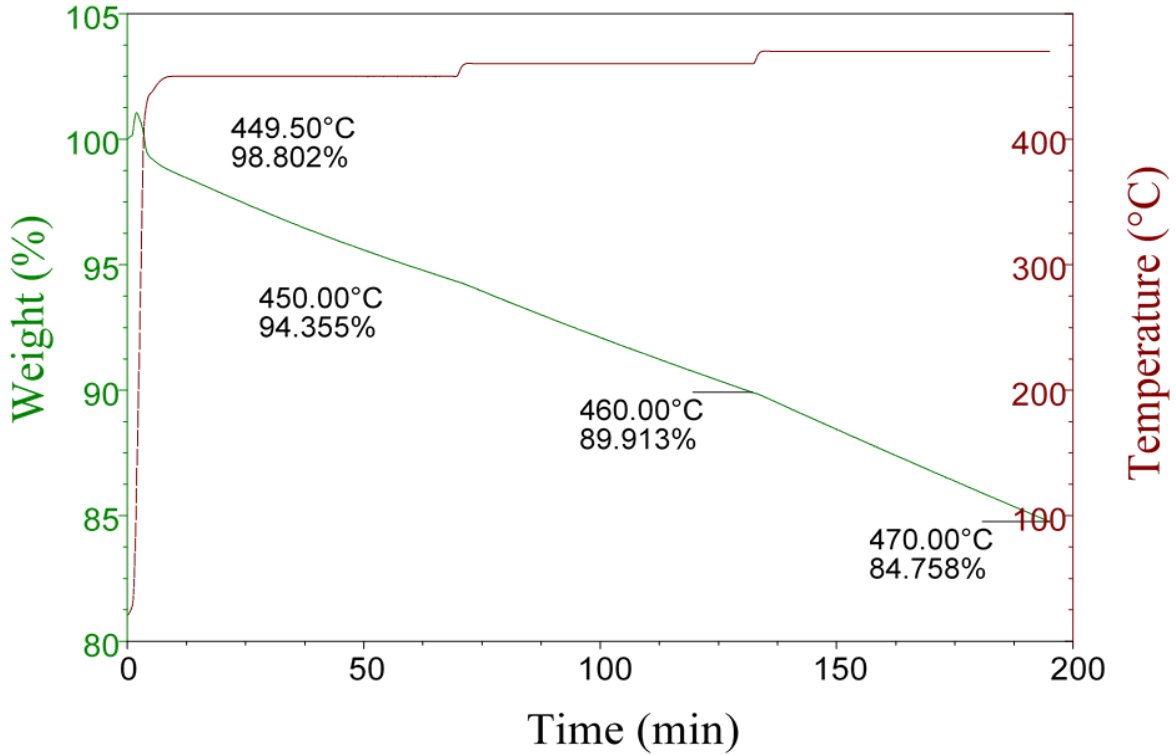


Figure 4.44: The weight (%) of carbon fibers as a function of time by TGA scans at 450, 460 and 470 °C, in air atmosphere, with every 60 minutes step of 10 °C

The figure 4.44 shows the thermal stability of the carbon fibers, in oxygen atmosphere, at 450, 460 and 470 °C. Remarkably, the carbon fibers are slightly thermally influenced at even such high temperatures.

4.5.5 Mechanical properties of the CFRP and ACFRP composites

Tables 4.7 and 4.8 depict the results of the six 3-point experiments of each composite and Figures 4.45, 4.46, 4.47 and 4.48 show these curves in detail. As can be seen, whereas the CFRP composites achieved remarkably higher flexural strength ($\sigma_{f_{max}}$) than the ACFRP composites. Nevertheless, the latter composites

demonstrated much higher young modulus than the former composite. The flexural modulus is the resistance of a material to bend under a stress which is applied perpendicular to its longitudinal side; so it is highly related with the stiffness of the materials. In detail, the flexural strength curves, of both types of composites, are straight towards lines and the materials break suddenly, showing very little plasticity. The characteristic of a material which breaks, under an applied force, but shows a little or no deformation before the breakage is described by the term brittleness. Remarkably, both composites, they break sharply after the σ_{fmax} ; the “ ΔL at breakage” is very slightly increased or is the same in comparison with the “ ΔL at σ_{fmax} ”. So, the CFRP and ACFRP composites are characterised as highly brittle materials.

Exceptionally, the six curves of each type of composite are very similar and their maximum values are in a very narrow range; the composites’ production method is characterized as highly efficient and with high reliability.

Based on the datasheet [60] of the resin producer, a fully cured neat resin, of Biresin[®] CR80 plus Biresin[®] CH80-2, has flexural strength = 125 MPa (according to ISO 178) and flexural modulus = 3100 MPa (according to ISO 178) so it is clear that the carbon and aramid fibers have highly enhanced these flexural characteristics of the epoxy matrix.

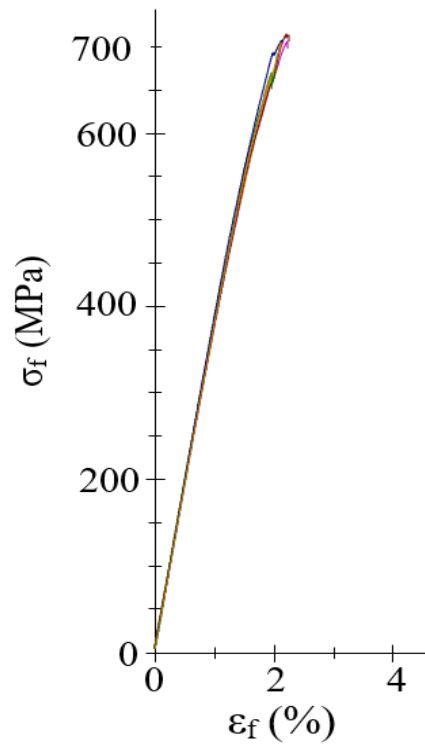


Figure 4.45: $\sigma_f - \varepsilon_f$ diagram of the six three-point bending experiments on the CFRP composite

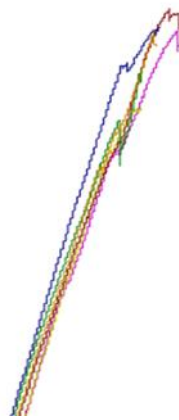


Figure 4.46: zoom view of the six $\sigma_f - \varepsilon_f$ curves of the CFRP composite

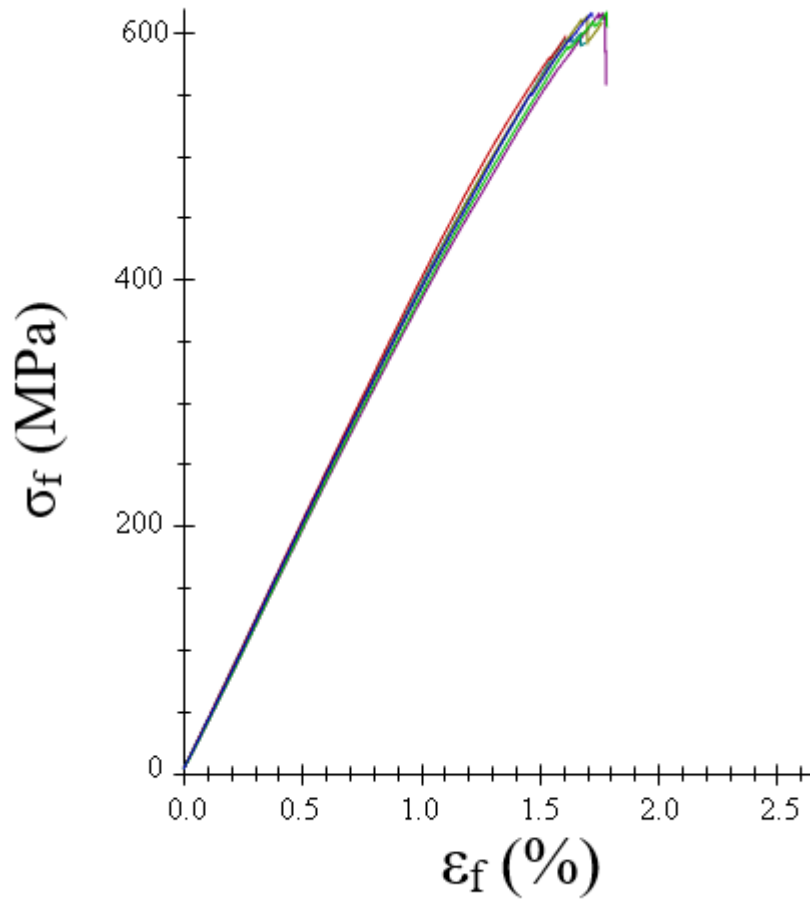


Figure 4.47: σ_f - ε_f diagram of the six three-point bending experiments on the ACFRP composite



Figure 4.48: zoom view of the six σ_f - ε_f curves of the ACFRP composite

Table 4.7 Three-point bending experimental results

sample	F at 0.2% (N)	Flexural modulus (MPa)	σ_{fmax} (MPa)	ΔL at σ_{fmax} (mm)	ΔL at fracture (mm)	Force at fracture (N)
CFRP ₁	276	37400	707	11.4	11.5	294
ACFRP ₁	271	38700	616	8.8	9	248
CFRP ₂	271	38000	675	10.5	10.6	281
ACFRP ₂	263	40100	600	8.5	8.5	263
CFRP ₃	269	38000	716	11.3	11.5	295
ACFRP ₃	263	39500	614	8.6	8.9	270
CFRP ₄	274	38400	691	10.6	10.6	287
ACFRP ₄	-	40000	598	8.1	8.1	265
CFRP ₅	289	38600	708	11	11	296
ACFRP ₅	272	38600	617	9	9	268
CFRP ₆	277	37900	706	10.9	10.9	292
ACFRP ₆	-	39400	617	8.7	8.7	272
CFRP average value	276	38050	700.5	10.95	11.01	290.83
ACFRP average value	267.25	39400	610.33	8.6	8.7	264.33

Table 4.8 (continue of Table 4.7) Work-at-force and work-at-fracture from the three-point bending experiments

sample	Work-at-force (Nmm)	Work-at-fracture (Nmm)
CFRP ₁	1900.4	1911.3
ACFRP ₁	1290.7	1330.9
CFRP ₂	1636.8	1651.6
ACFRP ₂	1219.8	1244.7
CFRP ₃	1853.4	1927.5
ACFRP ₃	1253.6	1335.7
CFRP ₄	1676.3	1677.2
ACFRP ₄	1149	1149
CFRP ₅	1829.4	1830.3
ACFRP ₅	1346.8	1348.6
CFRP ₆	1748.3	1756.1
ACFRP ₆	1276.9	1279.8
CFRP average value	1774.1	1792.3
ACFRP average value	1256.1	1281.4

4.5.6 Hardness Shore D

The table 4.9 illustrates a comparison between the CFRP and ACFRP composites Shore D hardness. The hardness indicates the magnitude of the resistance of a material in scratching, puncturing or deformation [63]. Specifically, the hardness which is based in penetration is associated with the modulus of elasticity and viscoelastic properties of the materials and it is in reverse alteration with the depth of the penetration [63].

As in the three-point bending tests, the former composite achieved higher hardness than the latter composite. Remarkably, the standard deviation of the ACFRP composite is smaller than the one of the CFRP composite. It is well known that the degree of cure of polymers influences their hardness, so the

significant small variation of the Shore D hardness of both composites indicates that these composites have been appropriately cured.

Table 4.9 Shore D hardness of the CFRP and ACFRP composites

Sample	CFRP composite	ACFRP hybrid composite
1	92.1	88.6
2	89.1	88.6
3	90.4	88.2
4	87.0	87.1
5	87.8	87.6
Average value	89.3	88.0
Maximum	92.1	88.6
Minimum	87.0	87.1
Standard deviation	2.0	0.7
Coefficient of variation	2.3	0.7

4.5.7 Conclusions regarding the CFRP, AFRP and ACFRP composites

In all cases of the TGA experiments, it was found that thermal degradation in an oxidative environment, (i.e. in air atmosphere) is much more harmful than the one due to pyrolysis (in N₂). In the TGA experiments, the very good thermal resistance of both carbon and aramid fibers was revealed. This characteristic together with the relatively high T_g of the post-cured CFRP, AFRP and ACFRP composites, in the range 80-95 °C, depending on the frequency and determination method, classify these composites as potential materials in applications where resistance in high temperatures is of great interest.

Based on the TMA creep-recovery experiments, it was revealed that the recovery of the AFRP composite structure took place immediately after the force release and that in all cases the final (plastic) deformation in the AFRP composite structure was relatively small. Relating this aspect with the overall results from the DMA experiments, it is concluded that, under the T_g, elastic behavior prevails entirely over viscous one in the AFRP composites' structure. Additionally, the creep-recovery behavior of the AFRP composite is the same at 25-50 °C, confirming hence the composite structure ability to work in this temperature range.

The exceptionally low densities of both carbon and aramid fibers, 1.77 g/cm^3 and 1.44 g/cm^3 respectively, result in a composite structure with low weight, making thus the composite highly attractive in a broad range of applications, especially in airplane industry where, nowadays, the efforts for fuel savings are of significant importance.

The results showed that a steady difference, under all frequencies and determination methods, between T_g temperatures of the CFRP and ACFRP composites; in all cases, the former composite achieved higher T_g . In terms of mechanical behavior, flexural strength, and hardness shore D, the CFRP composite demonstrated higher values than the ACFRP one. Moreover, the carbon fibers exhibited significant high thermal resistance in exposure at remarkably high temperatures, such as in 450, 460, and 470 °C in oxygen atmosphere; exceptionally, they lost approximately 5% of their weight after exposure in these temperatures for 60 minutes. According to the exhibited experiments, the overall results reveal that the hybrid CFRP composite did not manage to achieve the performance of the CFRP composite.

5. CONCLUSIONS OF THE DISSERTATION

In this dissertation synthetic fibers, namely glass, carbon and aramid as well as natural origin basalt fibers were embedded in various epoxy matrices. For the production of the composites were both used expensive production methods and materials, such as prepreg processing and more economic ways, like the hand lay-up compression moulding combined method and Vacuum Infusion Process. The purpose of the dissertation is to explore FRP composites, targeted as potential materials in a broad range of applications, from automobile parts to aircraft applications. The experimental part of this dissertation is divided in three parts.

In the first part, the GFRP and CFRP composites verified their high quality, as these achieved significant high T_g . In detail, the GFRP composites exhibited T_g in the range 111-123 °C, depending on the type of fabric/orientation of fibers and as well as on the method followed for the T_g determination: peak of $\tan\delta$ or loss modulus curves. Remarkably, DMA revealed that, in terms of storage and loss modulus, the placement of unidirectional glass fibers in the longitudinal direction of GFRP composites is much more effective than when placed in the transverse one. Moreover, the GFRP composites with slightly higher Φ_f , exhibited higher storage and loss modulus; this points out the positive effect of glass fibers in the composite structure. Based on the DMA results, the GFRP and CFRP composites are classified as optimal materials for the production of body parts of luxury cars, marine boats along with low-speed small airplanes. However, it should be mentioned that the applications of composites produced by prepreg materials need to justify their significantly high cost.

In the second experimental part, an eco-friendly reinforcement phase, basalt fibers were embedded in an epoxy matrix, in a high $\Phi_f = 53.66\%$, applying the hand lay-up compression molding method. In terms of tensile and flexural properties, the cold-cured BFRP composites displayed very good mechanical behavior, which verifies a very good interaction between basalt fibers/epoxy matrix, despite the high Φ_f . In FRP composites industry, the introduction of fibers in a polymer matrix in a high Φ_f is always a major concern, as in many cases, high fiber volume tends to form an inappropriate interfacial bond between them and the matrix; this, in turn, results in poor overall performance of the composite. Exceptionally, the hand lay-up compression molding method is qualified as highly effective in preparation of high Φ_f FRP composites. Moreover, the basalt fibers showed excellent thermal resistance, as they were not thermally affected up to the final 900 °C of the TGA experiments, pointing out their highly usefulness in applications where thermal resistance is essential. As an example, if basalt fibers are combined with a high thermal resistance polymer matrix in high Φ_f and

the formed composite is applied as structural material in the body of an airplane, in case of fire, basalt fibers will continue to offer structural support up to very high temperatures, important behavior in airplane industry. Moreover, the potential applications of basalt fibers could be in the surrounding sites of exhaust systems of cars, airplanes, and helicopters. In addition, the relative low price of basalt fibers, compared especially with the price of carbon and aramid fibers, combined with the inexpensive composites' fabrication method categorize the BFRP composites as optimal materials in low-cost applications, such as body parts of cars, motorcycles, and boats. Significantly, the natural origin of basalt fibers is another positive advantage. Specifically, these fibers will not pose the difficult problem of recycling, after their end-cycle use, like artificial fibers, such as carbon and aramid; this is a very important factor nowadays, due to the continuously increased use of FRP composites.

In the third experimental part, CFRP, AFRP and ACFRP composites were fabricated, following the VIP process. Remarkably, both carbon and aramid fiber fabrics demonstrated the same waive, weight and thickness, so the composite properties were compared with accuracy. Moreover, in this study, an effort was made to improve thermal behavior of the composites, with a relatively low cost. In particular, after curing at 23 °C for seven days, the composites were exposed to post-curing in an oven, under specific heating-cooling rates, following the resin producer suggestions. Various thermal analysis techniques were performed on the composites, so as to determine the positives and negatives of each composite structure. Notably, by TGA, an approach for determining the composite Φ_f was followed. Both the CFRP and ACFRP composites had a similar Φ_f and hence, the results section of this study was divided in two parts: thermal analysis of the AFRP composite and comparison of the CFRP and ACFRP composite properties.

Regarding the results section on the AFRP composites, their T_g was found to be in the range of 85-95 °C. T_g appears more a transition than a specific temperature whereas the T_g of the composites was specified by various ways, DMA and DSC, and under various frequencies, justifying thus such a fluctuation. Specifically, the T_g of the AFRP composites was relatively high for epoxy matrix composites, which indicates that the low-cost post-cure process has significantly improved the thermal behavior of the composites. Moreover, aramid fibers showed very good thermal resistance in TGA under N_2 atmosphere; they were very slightly thermally influenced under 60 minutes exposure in the temperature range of 350-390 °C. Also, the aramid fiber low density of 1.44 g/cm³ results in a composite with very low weight, a factor which nowadays is very important in all transport industries due to environmental concerns; low weight will eliminate the

overall weight of a vehicle, resulting hence in lower fuel consumption. Moreover, the experimentally determined T_g values are in agreement with those provided by the resin producer datasheets. It is concluded that the AFRP composites are fully and appropriately cured while the cure-post-cure process, specifically the particular heating-cooling rates which were followed are highly effective for this kind of materials.

In the second results section, a comparison between the CFRP and ACFRP composites was realized. The overall results show that the CFRP appears to have a better mechanical behavior than the ACFRP composite. Specifically, the former composite exhibited higher σ_f , ΔL at fracture and work-at-fracture, than the latter one; in these terms, the incorporation of aramid fibers did not contribute to a better performance. However, the fact that the AFRP exhibited higher E_f needs to be emphasized.

6. RELATING THE SCIENTIFIC RESULTS WITH PRACTICAL APPLICATIONS

- Regarding the first experimental part, the GFRP and CFRP composites exhibited remarkably high T_g , fact which classifies them as potential materials in high demanding applications, such as in aircraft industry, and generally wherever thermal resistance is a critical factor.
- The relatively high T_g of the post-cure AFRP composite, which is in the range of 85-95 °C and depending on the frequency and determination method, classifies these composites as potential materials in applications where resistance in high temperatures is of great interest.
- The low density of aramid fibers, 1.44 g/cm³, results in a composite with very low weight, a very important factor in all transport industries nowadays due to environmental concerns; the low weight is expected to eliminate the overall weight of a vehicle, resulting hence in lower fuel consumption.
- The excellent thermal resistance of basalt fibers, both in air and N atmosphere, makes their introduction in high performance polymer matrix, like bismaleimide or phenolic, essential, in order for a FRP composite with excellent overall thermal behavior to be formed. For sure, this composite could be target as potential material for body parts of airplanes. Moreover, the potential applications of basalt fibers could be in the surrounding sites of exhaust systems of cars, airplanes, and helicopters.
- Exceptionally, the hand lay-up compression molding method is qualified as highly effective in preparation of FRP composites with high Φ_f . Moreover, the method's low cost and simplicity classifies it as suitable for both low cost uses, such as every day and high demanding applications, for example marine and automotive industries.
- Future research on a hybrid high performance polymer matrix composite, consisted of alternately layers of carbon-aramid fiber fabrics and its comparison with pure AFRP, CFRP composites, where all of them have reinforcement phases with the same weight, weave and thickness appears an optimistic idea.

BIBLIOGRAPHY

[1] OLADELE, Isiaka Oluwole, Taiwo Fisayo OMOTOSHO and Adeolu Adesoji ADEDIRAN. Polymer-Based Composites: An Indispensable Material for Present and Future Applications. *International Journal of Polymer Science* [online]. 2020, vol. 2020, 12 pages [viewed 2021-4-17]. Article ID 8834518. Available from: <https://doi.org/10.1155/2020/8834518>

[2] MIGUEL, Jesus Cerezo and Miguel Angel Nunez DIAZ. Fiber Reinforced Polymer (FRP): A New Material Used in Façades of Tall Buildings. *Council on Tall Buildings and Urban Habitat* [online]. 2015, pp. 636-644 [viewed 2021-5-26]. Available from: <https://global.ctbuh.org/resources/papers/download/2519-fiber-reinforced-polymer-frp-a-new-material-used-in-facades-of-tall-buildings.pdf>

[3] LIAO, Kin, Carl SCHULTHEISZ, Donald L. HUNSTON and L. Catherine BRINSON. Long-term durability of fiber-reinforced polymer-matrix composite materials for infrastructure applications: A Review. *Journal of Advanced Materials* [online]. 1998, vol. 30, pp. 3-40 [viewed 24-4-2021]. Available from: https://www.researchgate.net/publication/279541055_Long-term_durability_of_fiber-reinforced_polymer-matrix_composite_materials_for_infrastructure_applications_A_review

[4] HOTA, Gangarao and Ruifeng LIANG. ADVANCED FIBER REINFORCED POLYMER COMPOSITES FOR SUSTAINABLE CIVIL INFRASTRUCTURES. *International Symposium on Innovation & Sustainability of Structures in Civil Engineering* [online]. 2011, Available from: [http://www.civil.ist.utl.pt/~cristina/RREst/Aulas_Apresentacoes/07_Bibliografia/construcao%20terra%20\(earth%20construction\)/5%20FINAL%20hota_paper_keynote.pdf](http://www.civil.ist.utl.pt/~cristina/RREst/Aulas_Apresentacoes/07_Bibliografia/construcao%20terra%20(earth%20construction)/5%20FINAL%20hota_paper_keynote.pdf)

[5] WARD, I. M. and J. SWEENEY, Mechanical properties of solid polymers. 3rd Edition, United Kingdom: John Wiley & Sons, Ltd, 2013.

[6] MURATA, H. Rheology - Theory and Application to Biomaterials. In: GOMES, Ailton De Souza ed. *Polymerization*. Rijeka: IntechOpen, 2012, pp. 403-426. DOI: 10.5772/48393. Available from: <https://www.intechopen.com/books/polymerization/rheology-theory-and-application-to-biomaterials>

[7] LIONETTO, Francesca and Alfonso MAFFEZZOLI. Monitoring the Cure State of Thermosetting Resins by Ultrasound. *Materials* [online]. 2013, vol. 6, no. 9. pp. 3783-3804 [viewed 2021-4-17], ISSN 1996-1944. DOI: 10.3390/ma6093783. Available from: <https://doi.org/10.3390/ma6093783>

[8] LEE, Joon Seok and Jong Won KIM. Impact Response of Carbon Fibre Fabric/Thermoset-Thermo-plastic Combined Polymer Composites. *Advanced Composites Letters* [online]. 2017, vol. 26, iss. 3, pp. 82-88 [viewed 2021-4-17]. DOI:10.1177/096369351702600304 Available from: <https://doi.org/10.1177/096369351702600304>

[9] PAPANICOLAOU, G. C. and S. P. ZAOUTSOS. Viscoelastic constitutive modeling of creep and stress relaxation in polymers and polymer matrix composites. In: GUEDES, Rui Miranda, ed. *Creep and Fatigue in Polymer Matrix Composites*. UK: Woodhead Publishing, 2011. pp. 3–47. ISBN 9781845696566

[10] GUDONIS, Eugenijus, Edgaras TIMINSKAS, Viktor GRIBNIAK, Gintaris KAKLAUSKAS, Aleksandr K. ARNAUTOV and Vytautas TAMULĖNAS. FRP reinforcement for concrete structures: state-of-the-art review of application and design. *Engineering Structures and Technologies* [online]. 2013, vol. 5, iss. 4. pp. 147–158 [viewed 2021-4-17]. ISSN 2029-8838. DOI: 10.3846/2029882X.2014.889274. Available from: <https://doi.org/10.3846/2029882X.2014.889274>

[11] BEDON, Chiara. Review on the use of FRP Composites for Façades and Building Skins. *American Journal of Engineering and Applied Sciences* [online]. 09/2016, vol. 9, iss. 3, pp. 713-723. DOI: 10.3844/ajeassp.2016.713.723. Available from: <https://core.ac.uk/download/pdf/53749265.pdf>

[12] RAJAK, Dipen Kumar, Durgesh D. PAGAR , Pradeep L. MENEZES and Emanoil LINUL. Fiber-Reinforced Polymer Composites: Manufacturing, Properties, and Applications. *Polymers* [online]. 2019, vol. 11, iss. 10. 1667 [viewed 2021-4-17]. Available from: <https://doi.org/10.3390/polym11101667>

[13] DIRUOCCO, Giacomo. Basalt fibers: the green material of the XXI-century, for a sustainable restoration of historical buildings. *International journal of Architecture Technology and Sustainability* [online]. 2016, vol. 1, iss. 2 [viewed 2021-4-17]. ISSN 2444-9091. Available from: <https://polipapers.upv.es/index.php/vitruvio/article/view/6984>

- [14] DHAND, Vivek, Garima MITTAL, Kyong Yop RHEE, Soo-Jin PARK and David HUI. A short review on basalt fiber reinforced polymer composites. *Composites: Part B* [online]. 2015, vol. 73. pp. 166–180 [viewed 2021-4-17]. ISSN 1359-8368. Available from: <http://dx.doi.org/10.1016/j.compositesb.2014.12.011>
- [15] SONNENSCHNEIN, Robert, Katarina GAJDOSOVA and Ivan HOLLY. FRP Composites and Their Using in the Construction of Bridges. *Procedia Engineering* [online]. 2016, vol. 161. pp. 477 – 482. [viewed 2021-4-17]. ISSN 1877-7058. DOI:10.1016/j.proeng.2016.08.665. Available from: <https://doi.org/10.1016/j.proeng.2016.08.665>
- [16] MOROVA, Nihat, Investigation of usability of basalt fibers in hot mix asphalt concrete. *Construction and Building Materials* [online]. 2013, vol. 47, pp. 175–180 [viewed 2021-4-17]. ISSN 0950-0618. Available from: <http://dx.doi.org/10.1016/j.conbuildmat.2013.04.048>
- [17] MALLICK, P.K. FIBER-REINFORCED COMPOSITES Materials, Manufacturing, and Design, Third edition, Boca Raton: CRC Press, Taylor & Francis Group, 2008. ISBN-13: 978-0-8493-4205-9.
- [18] DLAMINI, Nkululeko Muzi Patrick. *FINISHING OF BASALT FIBRES* [online]. 2011, [viewed 2021-6-17]. Diploma thesis. Technical university of Liberec, Faculty of textile engineering, Department of Textile Chemistry. Supervisor Assoc. Prof. Jakub Wiener, PhD. Available from: <https://dspace.tul.cz/handle/15240/11021>
- [19] KEVLAR® ARAMID FIBER TECHNICAL GUIDE, Copyright © 2017 DuPont, Available from: https://www.dupont.com/content/dam/dupont/amer/us/en/safety/public/documents/en/Kevlar_Technical_Guide_0319.pdf
- [20] DE NARDO, L. and S. FARÈ, 9 - Dynamico-mechanical characterization of polymer biomaterials, In: TANZI, Maria Cristina and Silvia FARÈ, ed. *Characterization of Polymeric Biomaterials*, United Kingdom: Woodhead Publishing. 2017, pp. 203-232. ISBN 978-0-08-100737-2.
- [21] WANG, Min and Chong WANG. Bulk Properties of Biomaterials and Testing Methods, In: Roger Narayan, ed. *Encyclopedia of Biomedical Engineering*. Elsevier. 2018, pp. 53-64. DOI: 10.1016/B978-0-12-801238-3.99861-1

[22] ÖZKAYA, Nihat, Dawn Leger, David Goldsheyder, Margareta Nordin. *Fundamentals of Biomechanics Equilibrium, Motion, and Deformation*, Fourth Edition, © Switzerland: Springer International Publishing, 2018. ISBN 978-3-319-44738-4.

[23] GABBOTT, Paul. *Principles and Applications of Thermal Analysis*, UK: Blackwell Publishing Ltd, 2008. ISBN-13: 978-1-4051-3171-1.

[24] EHRENSTEIN, Gottfried W. Gabriela RIEDEL and Pia TRAWIEL, *Thermal Analysis of Plastics Theory and Practice*. Munich: © Carl Hanser Verlag, 2004, ISBN 3-446-22673-7

[25] CHEREMISINOFF, Nicholas P. and Paul N. CHEREMISINOFF. *Fiberglass reinforced plastics*, United States of America: Noyes Publications, 1995, ISBN 0-8155-1389-5

[26] CAMPANA, Charlotte, Romain LÉGER, Rodolphe SONNIER, Laurent FERRY, and Patrick IENNY. Effect of post curing temperature on mechanical properties of a flax fiber reinforced epoxy composite. *Composites Part A: Applied Science and Manufacturing* [online]. 2018, vol. 107, pp. 171-179 [viewed 2021-4-17]. ISSN 1359-835X. Available from: <https://doi.org/10.1016/j.compositesa.2017.12.029>

[27] OBAID, Numaira, Mark T. KORTSCHOT and Mohini SAIN. Predicting the stress relaxation behavior of glass-fiber reinforced polypropylene composites. *Composites Science and Technology* [online]. 2018, vol. 161. pp. 85–91 [viewed 2021-4-17]. ISSN 0266-3538. Available from: <https://doi.org/10.1016/j.compscitech.2018.04.004>

[28] SPATHIS, G. and E. KONTOU. Creep failure time prediction of polymers and polymer composites. *Composites Science and Technology* [online]. 2012, vol. 72. pp. 959–964 [viewed 2021-4-17]. ISSN 0266-3538. Available from: <http://dx.doi.org/10.1016/j.compscitech.2012.03.018>

[29] LV, Mei, Fei ZHENG, Qihua WANG, Tingmei WANG and Yongmin LIANG. Friction and wear behaviors of carbon and aramid fibers reinforced polyimide composites in simulated space environment. *Tribology International* [online]. 2015, vol. 92. pp. 246–254 [viewed 2021-4-17]. ISSN 0301-679X. Available from: <http://dx.doi.org/10.1016/j.triboint.2015.06.004>

- [30] JIA, Zian, Tiantian LI, Fu-pen CHIANG and Lifeng WANG. An experimental investigation of the temperature effect on the mechanics of carbon fiber reinforced polymer composites. *Composites Science and Technology* [online]. 2018, vol. 154. pp. 53-63 [viewed 2021-4-17]. ISSN 0266-3538. Available from: <https://doi.org/10.1016/j.compscitech.2017.11.015>
- [31] ALAM, Parvez, Dimitrios MAMALIS, Colin ROBERT, Christophe FLOREANI and Conchúr M. Ó BRÁDAIGH. The fatigue of carbon fibre reinforced plastics - A review. *Composites Part B* [online]. 2019, vol. 166. pp. 555–579 [viewed 2021-4-17]. ISSN 1359-8368. Available from: <https://doi.org/10.1016/j.compositesb.2019.02.016>
- [32] ISLAM, Md.S., E. MELENDEZ-SOTO, A.G. CASTELLANOS and P. PRABHAKAR, Investigation of woven composites as potential cryogenic tank materials, *Cryogenics* [online]. 2015, vol. 72, pp. 82–89 [viewed 2021-4-17]. ISSN 0011-2275. Available from: <http://dx.doi.org/10.1016/j.cryogenics.2015.09.005>
- [33] SONG, Jun Hee. Pairing effect and tensile properties of laminated high-performance hybrid composites prepared using carbon/glass and carbon/aramid fibers, *Composites Part B* [online]. 2015, Vol. 79, pp. 61-66 [viewed 2021-4-17]. ISSN 1359-8368. Available from: <http://dx.doi.org/10.1016/j.compositesb.2015.04.015>
- [34] NUNES, Stephanie Goncalves, Wanderley Ferreira de AMORIM JR, Andrea MANES and Sandro Campos AMICO. The effect of thickness on vacuum infusion processing of aramid/epoxy composites for ballistic application. *Journal of Composite Materials* [online]. 2018, vol. 53, iss. 3, pp. 383-391 [viewed 2021-4-17]. DOI: 10.1177/0021998318785702
- [35] COSTA, Michelle Leali, Edson Cocchieri BOTELHO, Jane Maria Faulstich de PAIVA and Mirabel Cerqueira REZENDE, Characterization of Cure of Carbon/Epoxy Prepreg Used in Aerospace Field, *Materials Research* [online]. 2005, vol. 8, no. 3, pp. 317-322 [viewed 2021-4-17]. DOI: 10.1590/S1516-14392005000300016.
- [36] HOSSAIN, Mokarram, G. POSSART and Paul STEINMANN. A finite strain framework for the simulation of polymer curing. Part I: elasticity. *Computational Mechanics* [online]. 2009, vol. 44, pp. 621–630 [viewed 2021-4-17]. DOI: 10.1007/s00466-009-0397-0

[37] CHE, Demeng, Ishan SAXENA, Peidong HAN, Ping GUO and Kornel F. EHMANN. Machining of Carbon Fiber Reinforced Plastics/Polymers: A Literature Review. *Journal of Manufacturing Science and Engineering* [online]. 2014, vol. 136, iss. 3 [viewed 2019-7-16], 034001. Available from: <https://doi.org/10.1115/1.4026526>

[38] WANG, Tingting, Bo SONG, Kun QIAO, Chen DING and Li WANG. Influence of the hybrid ratio and stacking sequence on mechanical and damping properties of hybrid composites. *Polymer Composites* [online]. 2019, vol. 40, Iss. 6, pp. 2368-2380 [viewed 2021-4-17]. Available from: <https://doi.org/10.1002/pc.25096>

[39] ZAOUTSOS, S. P. and M. C. ZILIDOU. Influence of extreme low temperature conditions on the dynamic mechanical properties of carbon fiber reinforced polymers. *IOP Conference Series: Materials Science and Engineering* [online]. 2017, vol. 276, 012024 [viewed 2021-4-17]. DOI:10.1088/1757-899X/276/1/012024

[40] HAZER, Seda, Meral COBAN and Ayse AYTAC. A study on carbon fiber reinforced poly(lactic acid)/polycarbonate composites. *Journal of Applied Polymer Science* [online]. 2018, vol. 135, iss. 48, 46881 [viewed 2021-4-17]. DOI: 10.1002/APP.4688.

[41] Ronald JOVEN, Rajeswar DAS, A. Ahmed, Pooneh ROOZBEHJAVAN and B. MINAIE. Thermal properties of carbon fiber-epoxy composites with different fabric weaves. *International SAMPE Technical Conference* [online]. 2012. [viewed 2021-4-17]. Available from: https://www.researchgate.net/publication/262007032_Thermal_properties_of_carbon_fiberepoxy_composites_with_different_fabric_weaves

[42] DONG, Kai, Xiao PENG, Jiajin ZHANG, Bohong GU and Baozhong SUN. Temperature-dependent thermal expansion behaviors of carbon fiber/ epoxy plain woven composites: Experimental and numerical studies. *Composite Structures* [online]. 2017, vol. 176, pp. 329–341 [viewed 2021-4-17]. ISSN 0263-8223. Available from: <http://dx.doi.org/10.1016/j.compstruct.2017.05.036>

[43] PINCHEIRA, Gonzalo, Cristian CANALES, Carlos MEDINA, Eduardo FERNANDEZ and Paulo FLORES. Influence of aramid fibers on the mechanical behavior of a hybrid carbon–aramid–reinforced epoxy composite. *Proceedings of the Institution of Mechanical Engineers Part L. Journal of Materials: Design and*

Applications [online]. 2015, vol. 232, iss. 1, pp. 58-66 [viewed 2021-4-17]. DOI: 10.1177/1464420715612827.

[44] HASHIM, Nurain, Dayang Laila Abdul MAJID, El-Sadig MAHDI, Rizal ZAHARI and Noorfaizal YIDRIS. Effect of fiber loading directions on the low cycle fatigue of intraply carbon-Kevlar reinforced epoxy hybrid composites. *Composite Structures* [online]. 2019, vol. 212, pp. 476–483 [viewed 2021-4-17]. ISSN 0263-8223. Available from: <https://doi.org/10.1016/j.compstruct.2019.01.036>

[45] HOSSAIN, Milon, Kamrun N. KEYA, Nasrin A. Kona, Naimul ISLAM, Farjana A. KOLY, Mubarak A. KHAN, Abu Bakar SIDDIQUEE, Jumana MAHMUD and Ruhul A. KHAN. Mechanical, thermal and interfacial properties of Carbon-Kevlar reinforced epoxy composite. *Materials Engineering Research* [online]. 2019, vol. 1, no. 2, pp. 56-63 [viewed 2021-4-17]. DOI: 10.25082/MER.2019.02.004.

[46] MAHNKEN, Rolf and Christian Dammann. A three-scale framework for fibre-reinforced-polymer curing Part I: Microscopic modeling and mesoscopic effective properties. *International Journal of Solids and Structures* [online]. 2016, volumes 100–101, pp. 341-355, [viewed 2021-4-17]. ISSN 0020-7683. Available from: <https://doi.org/10.1016/j.ijsolstr.2016.09.003>

[47] NIKFOROOZ, M, J. MONTESANO, M. GOLZAR, and M.M. SHOKRIEH. Assessment of the thermomechanical performance of continuous glass fiber reinforced thermoplastic laminates. *Polymer Testing* [online]. 2018, vol. 67, pp. 457–467 [viewed 2021-4-17]. ISSN 0142-9418. Available from: <https://doi.org/10.1016/j.polymertesting.2018.02.023>

[48] MENAIL, Y, Abderrahim EL MAHI and M. ASSARAR . Effect of Fatigue Testing and Aquatic Environment on the Tensile Properties of Glass and Kevlar Fibers Reinforced Epoxy Composites. *Journal of Aeronautics and Aerospace Engineering* [online]. 2015. Vol. 4, iss. 3 [viewed 2021-4-17]. ISSN: 2168-9792. DOI: 10.4172/2168-9792.1000150

[49] NI, Nannan, Yuefang WEN, Delong HE, Xiaosu YI, Tao ZHANG and Yahong XU. High damping and high stiffness CFRP composites with aramid non-woven fabric interlayers. *Composites Science and Technology* [online]. 2015, vol. 117, pp. 92-99 [viewed 2021-4-17]. ISSN 0266-3538. Available from: <http://dx.doi.org/10.1016/j.compscitech.2015.06.002>

[50] CECEN, Volkan, Ismail H. TAVMAN, Mediha KOK and Yildirim AYDOGDU. Epoxy- and Polyester-Based Composites Reinforced with Glass, Carbon and Aramid Fabrics: Measurement of Heat Capacity and Thermal Conductivity of Composites by Differential Scanning Calorimetry. *Polymer Composites* [online]. 2009, vol. 30. iss. 9. pp. 1299-1311 [viewed 2021-4-17]. DOI: 10.1002/pc.20695.

[51] ANISKEVICH, Klara, Olesja STARKOVA, Juris JANSONS, and ANDREY ANISKEVICH. *Long-term deformability and aging of polymer matrix composites*. New York: Nova Science Publishers, Inc., 2012.

[52] CRISTEA, Mariana, Daniela IONITA and Manuela M. IFTIME. Dynamic Mechanical Analysis Investigations of PLA-Based Renewable Materials: How Are They Useful? *Materials* [online]. 2020, vol. 13, no. 22, 5302 [viewed 2021-6-19]. Available from: <https://doi.org/10.3390/ma13225302>

[53] YAO, Yin and Shaohua CHEN. The effects of fiber's surface roughness on the mechanical properties of fiber-reinforced polymer composites. *Journal of Composite Materials* [online]. 2013, vol. 47, iss. 23. pp. 2909–2923 [viewed 2021-4-17]. DOI: 10.1177/0021998312459871.

[54] FU, Shao-Yun, Xi-Qiao FENG, Bernd LAUKE and Yiu-Wing MAI. Effects of particle size, particle/matrix interface adhesion and particle loading on mechanical properties of particulate–polymer composites. *Composites: Part B* [online]. 2008, vol. 39, Iss. 6, pp. 933–961 [viewed 2021-4-17]. ISSN 1359-8368. DOI:10.1016/j.compositesb.2008.01.002.

[55] Yield Strength and Other Near-Elastic Properties, Materion Brush Performance Alloys, November 2012, Issue No. 47.

[56] BAZAN, Patrycja, Przemysław NOSAL, Barbara KOZUB and Stanisław KUCIEL. Biobased Polyethylene Hybrid Composites with Natural Fiber: Mechanical, Thermal Properties, and Micromechanics. *Materials* [online]. 2020, vol. 13, iss. 13. 2967 [viewed 2021-4-17]. DOI:10.3390/ma13132967.

[57] AL-BAHADLY, Ekhlas Aboud Osman. *The mechanical properties of natural fiber composites* [online]. January 2013 [cit. 2021-06-05]. Doctoral Thesis. Swinburne University of Technology, Faculty of Engineering. Supervisors Professor Anatoli Vakhguelt and Dr. Igor Sbarski. Available from: <https://researchbank.swinburne.edu.au/file/3787052e-f8e9-4762-bdc2-b33eeda1951b/1/Ekhl%20Aboud%20Osman%20Al-Bahadly%20Thesis.pdf>

- [58] Style 442, Technical datasheet, Engineered Cramer Composites, 05.04.2017
- [59] Style 502, Technical datasheet, Engineered Cramer Composites, 16.09.2015
- [60] Biresin[®] CR80 Composite resin system, Product Data Sheet, Version 05/2017, Sika[®]
- [61] ANDREOPOULOS, A.G. and P.A. TARANTILI. Study of the off-axis properties of composites reinforced with ultra high modulus polyethylene fibres. *European Polymer Journal* [online]. 1999, vol. 35, pp. 1123-1131 [viewed 2021-4-17]. Available from: [https://doi.org/10.1016/S0014-3057\(98\)00079-2](https://doi.org/10.1016/S0014-3057(98)00079-2)
- [62] ADVANCED COMPOSITES SOLUTIONS HIGH PERFORMANCE EPOXY AND POLYURETHANE SYSTEMS, issue May 2019, Sika[®], Available from: <https://automotive.sika.com/content/dam/dms/global-industry/8/BRO-Advanced-Resins-Composites.pdf>
- [63] VÎLCEA, Elena-Janina and Rodica-Mariana ION. DETERMINATION OF HARDNESS POLYPROPYLENE FLAME RETARDANTS REOGARD 2000[®] USING SHORE D METHODE. *The Scientific Bulletin of VALAHIA University – MATERIALS and MECHANICS* [online]. 2014, Nr. 9 [viewed 2021-4-17]. Available from: https://fsim.valahia.ro/sbmm.html/docs/2014/materials/4_Vilcea_2014.pdf

LIST OF FIGURES

Figure 1.1: a) and b) the structure of an Aluminium matrix\Silicon Carbide particulate 3% composite, as it was observed through scanning electron microscope (SEM). The silicon carbide (SiC) particulates are clearly depicted in the metal matrix.	12
Figure 1.2: Fabrication of composite plate by vacuum injection process (VIP).	17
Figure 2.1: base of orientation: unidirectional fibers in longitudinal direction (0°)	23
Figure 2.2: a) Produced GFRP and CFRP composite plates and b) materials of the vacuum bag system.....	26
Figure 2.3: GFRP composite plates.....	26
Figure 2.4: The other side of the GFRP composite plates	27
Figure 2.5: a) and b) GFRP composite on the three-point bending configuration on the instrument DMA 1 METTLER TOLEDO	28
Figure 2.6: GFRP and CFRP composites specimens after the DMA experiments	28
Figure 2.7: Storage modulus of the GFRP composites as a function of the temperature in the range 30-200 °C	29
Figure 2.8: Storage modulus of the CFRP composites as a function of the temperature in the range 30-200 °C	30
Figure 2.9: Loss modulus of the GFRP composites as a function of the temperature in the range 30-200 °C	31
Figure 2.10: Loss modulus of the CFRP composites as a function of the temperature in the range 30-200 °C	32
Figure 2.11: $\tan\delta$ of the GFRP composites as a function of the temperature in the range 30-200 °C.....	33
Figure 2.12: $\tan\delta$ of the CFRP composites as a function of the temperature in the range 30-200 °C.....	34
Figure 3.1: Preparation of the BFRP composites by the hand lay-up compression molding combined method.....	37
Figure 3.2: The produced BFRP composite plate. The compression machine pushed the excessive resin in the edges of the mold, contributing towards so as the composite structure to achieve high Φ_f . Moreover, some small white pieces on the surface of the composite plate are just cook paper from the mold.....	38
Figure 3.3: a) and b) Photos of the used Basalt fibers fabric. The photos were taken with the Carl Zeiss Stemi 2000C Microscope (Jena, Germany) from the edges of the BFRP composite structure.	38
Figure 3.4: DMA 1 METTLER TOLEDO instrument	39
Figure 3.5: BFRP sample on the single cantilever configuration	40

Figure 3.6: DMA specimens	40
Figure 3.7: (a) Tensile specimens and (b) tensile specimen on the tension grips	43
Figure 3.8: Displacement sweep test	44
Figure 3.9: Storage modulus of the BFRP composites, as a function of the temperature, at 1, 5 and 10 Hz	45
Figure 3.10: Loss modulus of the BFRP composites, as a function of the temperature, at 1, 5 and 10 Hz	46
Figure 3.11: $\tan\delta$ of the BFRP composites as a function of the temperature at 1, 5, or 10 Hz.....	47
Figure 3.12: The creep-recovery curves of the BFRP composites, at 25 °C, and under 1, 3 and 5 N	48
Figure 3.13: The effect of 25, 50 and 75 °C on the creep-recovery of the BFRP composites, under initial force of 1 Newton.....	49
Figure 3.14: Stress-relaxation curves of the BFRP composites at 25, 50 and 60 °C	50
Figure 3.15: The four $\sigma_f - \varepsilon_f$ curves of the BFRP composites.....	52
Figure 3.16: The three-point bending specimens after the experiments.....	53
Figure 3.17: $\sigma - \varepsilon$ curves of the five tension experiments.....	55
Figure 3.18: tension specimen on the grips after the breakage.....	56
Figure 3.19: TGA results showing the weight (%) and weight loss rate (DTG) of the BFRP composite as a function of the temperature in N ₂ atmosphere (first sample)	57
Figure 3.20: TGA results showing the weight (%) and weight loss rate (DTG) of the BFRP composite as a function of the temperature in N ₂ atmosphere (second sample)	58
Figure 3.21: TGA results showing the weight variation and weight loss rate (DTG) of the BFRP composite as a function of the temperature, in air atmosphere	59
Figure 3.22: TGA results presenting the weight (%) variation and weight loss rate (DTG) of the basalt fibers* in N ₂ atmosphere.	60
Figure 3.23: TGA results showing the weight (%) variation and weight loss rate (DTG) of the basalt fibers* in air atmosphere	61
Figure 4.1: Biresin [®] CR80	65
Figure 4.2: The three types of the eight-layered composites (a) CFRP, (b) AFRP and (c) hybrid ACFRP	67
Figure 4.3: Zoom on the twill 2/2 aramid fiber fabric roll.	68
Figure 4.4: post-cure temperature diagram.....	69
Figure 4.5: Preparation of the CFRP composite with the Vacuum Infusion Process. The photo was taken hours after the resin infusion.....	70
Figure 4.6: a) and b) the two sides of the CFRP composite plate.	71

Figure 4.7: The prepared CFRP, AFRP ACFRP and composite plates. The laminates were cut in the half, through mechanical cutting, so as to be put in the oven.....	72
Figure 4.8: Zoom view of the AFRP composite plate.....	73
Figure 4.9: The post-cure process of the (a) CFRP and (b) AFRP in the oven. Down of the composites plates there is a metal plate for support.....	73
Figure 4.10: Part of the DMA, TMA creep-recovery and TMA stress-relaxation specimens of the (a) CFRP, (b) ACFRP and (c) AFRP composites.	74
Figure 4.11: a) and b) TGA Q50 TA instruments	76
Figure 4.12: ACFRP composite specimen on the three-point bending configuration.....	77
Figure 4.13: ACFRP composite specimen on the three-point bending configuration.....	78
Figure 4.14: a) CFRP and b) ACFRP three-point bending specimens	78
Figure 4.15: Storage modulus of the AFRP composite in the range 30-200 °C, at 1, 5 and 10 Hz.....	79
Figure 4.16: Loss modulus of AFRP composite in the range 30-200 °C, at 1, 5, and 10 Hz.....	80
Figure 4.17: $\tan\delta$ variation of the AFRP composite in the range 30-200 °C, at 1, 5 and 10 Hz.....	81
Figure 4.18: TMA creep-recovery of the AFRP composite.....	82
Figure 4.19: stress-relaxation of the AFRP composite	83
Figure 4.20: zoomed view of the AFRP composite stress-relaxation curve	83
Figure 4.21: TGA results presenting the thermal stability of ——— aramid fibers, and ——— pure post-cured epoxy in exposure at 350 °C for 240 minutes in N ₂ atmosphere (epoxy also at 380 °C).....	84
Figure 4.22: TGA graph of the AFRP composite (two samples) at 350 °C for 240 minutes under N ₂ atmosphere. The difference on the time axis is because these samples were heated up to the 350 °C with different heating rates.....	85
Figure 4.23: a) b) c) and d) Photos of the AFRP composite specimens under exposure for 240 minutes, at 350 °C, under N ₂ atmosphere. The photos were taken with the Carl Zeiss Stemi 2000C Microscope (Jena, Germany) from the edges of the composite structure.	86
Figure 4.24: TGA results presenting the thermal stability of the aramid fibers at exposure at 360, 370 and 380 °C, in N ₂ atmosphere, with every 60 minutes step of 10 °C	87
Figure 4.25: TGA results showing the weight of the AFRP composites as a function of the temperature, in air and N ₂ atmosphere, respectively	88
Figure 4.26: DTG (weight loss rate) curves of the AFRP composite in air and N ₂ atmosphere, respectively.	89

Figure 4.27: TGA results showing the weight (%) of the aramid fibers and pure post-cure epoxy matrix as a function of temperature in air and N ₂ atmosphere, respectively.	90
Figure 4.28: DSC curves of the AFRP composite	91
Figure 4.29: E'' versus temperature of the CFRP and ACFRP composites under 1, 5 and 10 Hz	92
Figure 4.30: E' versus temperature of the CFRP and ACFRP composites under 1, 5 and 10 Hz	93
Figure 4.31: tanδ versus temperature of the CFRP and ACFRP composites under 1, 5 or 10 Hz.....	94
Figure 4.32: stress-relaxation curves of the CFRP and ACFRP composites at 25, 50 and 75 °C	95
Figure 4.33: DSC curves of the CFRP composite	96
Figure 4.34: DSC curves of the ACFRP composite	97
Figure 4.35: TGA results showing the weight (%) of the carbon and aramid fibers as a function of the temperature in air atmosphere	98
Figure 4.36: DTG (weight loss rate) of the carbon and aramid fibers as a function of the temperature in air atmosphere	98
Figure 4.37: TGA results showing the weight of the carbon and aramid fibers as a function of the temperature in N ₂ atmosphere	99
Figure 4.38: DTG (weight loss rate) curves of the carbon and aramid fibers as a function of the temperature in N ₂ atmosphere	99
Figure 4.39: TGA results presenting the weight (%) of the CFRP and ACFRP composites as a function of the temperature in air atmosphere.....	100
Figure 4.40: DTG (weight loss rate) curves of the CFRP and ACFRP composites as a function of the temperature in air atmosphere	100
Figure 4.41: TGA results presenting the weight variation (%) of the CFRP and ACFRP composites as a function of the temperature in N ₂ atmosphere	101
Figure 4.42: DTG (weight loss rate) of the CFRP and ACFRP composites as a function of the temperature in N ₂ atmosphere	101
Figure 4.43: TGA results showing the thermal stability of the CFRP and ACFRP composites, at exposure at 350 °C for 240 minutes, in N ₂ atmosphere	102
Figure 4.44: The weight (%) of carbon fibers as a function of time by TGA scans at 450, 460 and 470 °C, in air atmosphere, with every 60 minutes step of 10 °C	103
Figure 4.45: σ _f - ε _f diagram of the six three-point bending experiments on the CFRP composite	105
Figure 4.46: zoom view of the six σ _f - ε _f curves of the CFRP composite	105
Figure 4.47: σ _f - ε _f diagram of the six three-point bending experiments on the ACFRP composite.....	106

Figure 4.48: zoom view of the six $\sigma_f - \varepsilon_f$ curves of the ACFRP composite..106

LIST OF TABLES

Table 2.1 Prepared GFRP and CFRP composites.....	24
Table 2.2 T_g of the GFRP and CFRP composites.....	35
Table 3.1 T_g of the BFRP composites	47
Table 3.2 Three-point bending results	51
Table 3.3 Tensile experimental results of the BFRP composites	54
Table 3.4 Tensile experimental results of the BFRP composites (continue of Table 3.3).....	54
Table 4.1 Materials used for the fabrication of the CFRP, AFRP and hybrid ACFRP composites	66
Table 4.2 Physical data of the resin and the hardener [60].....	66
Table 4.3 Typical thermal properties of fully cured neat resin [60].....	66
Table 4.4 Typical Mechanical properties of Fully Cured Neat Resin [60]	67
Table 4.5 T_g of the AFRP composites (based on the DMA)	81
Table 4.6 T_g of the CFRP and ACFRP composites (based on DMA).....	95
Table 4.7 Three-point bending experimental results	107
Table 4.8 (continue of Table 4.7) Work-at-force and work-at-fracture from the three-point bending experiments.....	108
Table 4.9 Shore D hardness of the CFRP and ACFRP composites.....	109

LIST OF SYMBOLS, ACRONYMS AND ABBREVIATIONS

FRP	Fiber-reinforced polymer
DMA	Dynamic Mechanical Analysis
TMA	Thermomechanical Analysis
TGA	Thermogravimetric Analysis
DSC	Differential Scanning Calorimetry
T _g	Glass transition temperature
BFRP	Basalt fiber-reinforced polymer
Φ _f	Volume fraction of fibers
PMC	Polymer matrix composites
SEM	Scanning electron microscope
GFRP	Glass fiber-reinforced polymer
CFRP	Carbon fiber-reinforced polymer
AFRP	Aramid fiber-reinforced polymer
VARTM	Vacuum Assisted Resin Transfer Molding
CFRPs	Carbon fiber reinforced polymers
ANF	Aramid non-woven fabric
%	percentage in 100
GF-UD-L-34%	Unidirectional longitudinal glass fiber-reinforced polymer composite with 34% matrix
GF-UD-TR-34%	Unidirectional transverse glass fiber-reinforced polymer composite with 34% matrix
GF-UD-L-39%	Unidirectional longitudinal glass fiber-reinforced polymer composite with 39% matrix
GF-UD-TR-39%	Unidirectional transverse glass fiber-reinforced polymer composite with 39% matrix
GF-W-0°-37%	Woven at 0° (fibers at 0°/90°) glass fiber-reinforced polymer composite with 37% matrix
GF-W-45°-37%	Woven at 45° (fibers at -45°/+45°) glass fiber-reinforced polymer composite with 37% matrix
CF-UD-L-38%	Unidirectional longitudinal carbon fiber-reinforced polymer composite with 38% matrix
CF-UD-TR-38%	Unidirectional transverse carbon fiber-reinforced polymer composite with 38% matrix
CF-W-0°-38%	Woven at 0° (fibers at 0°/90°) carbon fiber-reinforced polymer composite with 38% matrix

CF-W-45°-38% Woven at 45° (fibers at -45°/+45°) carbon fiber-reinforced polymer composite with 38% matrix

E'	Elastic (storage) modulus
E''	Viscous (loss) modulus
$^{\circ}$	Degrees
Hz	Hertz
N	Newton
$^{\circ}\text{C}$	Celsius
min	Minute
$\tan\delta$	Loss factor
g/m^2	Grammar per square meter
g/cm^3	Grammar per cubic centimeter
MPa	Megapascal
h	Hour
mm	Millimeter
K/min	Kelvin per minute
mL/min	Milliliter per minute
mm/min	Millimeter per minute
μm	Micrometer
σ_{fmax}	Maximum flexural stress
δ	Deformation
ΔL	Displacement
W	Work
σ_{f}	Flexural stress
ε_{f}	Flexural strain
σ	Tensile stress
F	Force
A	Cross sectional area
E	Strain
L	Final length
L_0	Primary length
$\sigma_{0.2}$	0.2% Offset yield strength
σ_{max}	Maximum stress
E	Young modulus
DTG	Derivative Thermogravimetry
ρ_{m}	Density of matrix
ρ_{f}	Density of reinforcement
W_{t}	Weight proportion of the reinforcement phase
W_{f}	Weight of fibers
W_{m}	Weight of matrix
Φ_{m}	Volume of matrix

σ_{fiber}	Tensile strength of fibers
σ_{m}	Tensile strength of matrix
VIP	Vacuum infusion process
dtex deci-tex	Grams per 10,000 metres of yarn
mPa.s	Millipascal-second
g/ml	Gram Per Millilitre
ISO	International Organization for Standardization
kJ/m ²	Kilojoule per square meter
mg	Milligram

APPENDICES



LIST OF AUTHORS' PUBLICATIONS

1. **Karvanis Konstantinos**, Rusnáková Soňa, Krejčí Ondřej, Žaludek Milan. Preparation, Thermal Analysis, and Mechanical Properties of Basalt Fiber/Epoxy Composites. *Polymers*. 2020, 12(8):1785. Available from: <https://doi.org/10.3390/polym12081785>
2. Zaludek Milan, Rusnakova Soňa, Kubisova Milena, Bilek Ondřej, **Karvanis Konstantinos**, Fatigue life of thermoset composite materials, 2020, *IOP Conf. Ser.: Mater. Sci. Eng.* 726, 012016
3. Rusnáková Soňa, **Karvanis Konstantinos**, Košťial Pavel, Košťialová-Jančíková Zora, Zimula A. (2020) Contribution to an Electrical Transport in Montmorillonite/Polyaniline Composite. In: Öchsner A., Altenbach H. eds, *Engineering Design Applications II. Advanced Structured Materials*, vol 113. Springer, Cham.
4. Rusnáková Soňa, **Karvanis Konstantinos**, Košťial Pavel, Košťialová Jančíková Zora, Zimula A. (2020), Chosen Physical Properties of Menzolit BMC 3100. In: Öchsner A., Altenbach H. eds, *Engineering Design Applications II. Advanced Structured Materials*, vol 113. Springer, Cham.
5. **Karvanis Konstantinos**, Rusnáková Soňa, Žaludek Milan, Čapka Alexander, Preparation and Dynamic Mechanical Analysis of Glass or carbon Fiber/Polymer Composites, 2018, *IOP Conf. Ser.: Mater. Sci. Eng.* 362, 012005
6. Čapka Alexander, Rusnakova Soňa, Žaludek Milan, **Karvanis Konstantinos**. Fatigue life of al-honeycomb core composites construction, 2018, *Manufacturing Technology*, 18 (5), pp. 727-731.
7. **Konstantinos Karvanis**, Soňa Rusnáková, Ondřej Krejci, Alena Kalendová, Thermal analysis of post-cured aramid fiber/epoxy composites, *Reviews on advanced materials science*, De Gruyter Open Access, DOI:10.1515/rams-2021-0036

PROJECT PARTICIPATION

- internal grant of TBU in Zlín No. IGA/FT/2018/004
- internal grant of TBU in Zlín No. IGA/FT/2020/004
- internal grant of TBU in Zlín No. IGA/FT/2021/006

PROFESSIONAL CURRICULUM VITAE

Konstantinos Karvanis, M. Sc.

karvanisk@gmail.com

Nationality: Greek

Mechanical Engineer

Master of Science in Mechatronics

PhD studies in progress

Professional profile

Mechanical Engineer, Motorcycle Enthusiast & Racer capable of applying mechanical, thermodynamic, pneumatic, hydraulic and electrical principles to resolve engineering problems and find appropriate solutions. In search of developing skills with professional development courses. Critical thinking, decision making and complex problem-solving skills acquired through current post.

EDUCATION

- Tomas Bata University in Zlín, Czech Republic (studies in progress)
10/2016-present

Faculty of Technology, Department of production engineering

Title of PhD thesis: “Fiber reinforced polymer composites: preparation, mechanical properties and thermal analysis”

Research on polymer matrix composites with fibers as reinforcement phase.

➤ Technological Educational Institute of Western Macedonia

Kozani, Greece

10/2014-05/2016

Master of Science in Mechatronics (90 ECTS)

(department of Electrical Engineering)

Dissertation: “Production and Mechanical Properties of Al-SiC Metal Matrix Composites” Basic part of this study was the making of Al – SiC metal matrix composites many mechanical (tensile and compressive strength, impact, hardness) and other (microscopy) properties explored via experiments.

➤ Technological Educational Institute of Larissa

Larissa, Greece

2004-2011

Beng, Mechanical Engineering (240 ECTS)

Konstantinos Karvanis

Fiber reinforced polymer composites: preparation, mechanical properties and thermal analysis

Vláknny vyztužené polymerní kompozity: příprava, mechanické vlastnosti a termická analýza

Doctoral thesis

Published by: Tomas Bata University in Zlín,
nám. T. G. Masaryka 5555, 760 01 Zlín.

Typesetting by: Konstantinos Karvanis

This publication has not undergone any proofreading or editorial review.

Publication year: 2021